
ETD Archive

2008

A Hybrid Reconfigurable Solar and Wind Energy System

Sagar A. Gadkari
Cleveland State University

Follow this and additional works at: <https://engagedscholarship.csuohio.edu/etdarchive>



Part of the [Engineering Commons](#)

How does access to this work benefit you? Let us know!

Recommended Citation

Gadkari, Sagar A., "A Hybrid Reconfigurable Solar and Wind Energy System" (2008). *ETD Archive*. 101.
<https://engagedscholarship.csuohio.edu/etdarchive/101>

This Dissertation is brought to you for free and open access by EngagedScholarship@CSU. It has been accepted for inclusion in ETD Archive by an authorized administrator of EngagedScholarship@CSU. For more information, please contact library.es@csuohio.edu.

**A HYBRID RECONFIGURABLE SOLAR AND WIND ENERGY
SYSTEM**

SAGAR A GADKARI

Master of Science Industrial and Manufacturing Engineering

Cleveland State University

May, 2005

submitted in partial fulfillment of requirements for the degree

DOCTOR OF ENGINEERING

at the

CLEVELAND STATE UNIVERSITY

August, 2008

This dissertation has been approved
for the Department of Industrial and Manufacturing Engineering
and the College of Graduate Studies by

Dissertation Committee Chairperson, Dr. Taysir H. Nayfeh

Department/Date

Dr. Mounir H. Ibrahim

Department/Date

Dr. Majid Rashidi

Department/Date

Dr. M. Brian Thomas

Department/Date

Dr. Kiril A. Streletzky

Department/Date

ACKNOWLEDGEMENT

I am delighted to culminate my student life at Cleveland State working on a project with a great relevance in current times. I feel privileged of having been the part of Industrial and Space Systems Laboratory (ISSL), a team of dynamic university students led by Dr. Nayfeh with his extra-ordinary vision.

I would like to thank Dr. Nayfeh, my advisor, for his assistance, guidance and advice, which proved invaluable in the completion of this research. I thank him to encourage me all through my work and my study at Cleveland State. He has helped me grow not only as a good research student but also a good person.

Special thanks to Mr. Bernard Sater from NASA Glenn Research Center, for introducing us all to the Vertical multi-junction cells (VMJ), the most integral part of this work. I also thank him to provide us with the data on VMJ cells for our study. With his son Neil Sater, actively seeking to commercialize this phenomenal technology with Mr. Doug Wood's low cost concentrator design; I thank them both to approach us to build a prototype of the low cost concentrator made from aluminum matrix frame. I specially thank Mike, Dustin and Harry to work with me on building the prototype.

I thank Dr. Ibrahim, Dr Rashidi, Dr Thomas and Dr. Streletzky to be on my committee. I thank Dr Ibrahim for his suggestions that helped me in my work.

I am grateful to my co-workers at ISSL; Scott, Brian, Daniel, Tom, Dragos, Andy, Dave and Amanda. Special thanks to Esam, Anita and Renjun with whom I shared my work place.

In addition, I specially thank my roommates and my friends, old and new who have been with me at all times. Special thanks to all my roommates, especially Dhanda, during my stay and my friends Hemant, Neeraj, Jitu, Ranjeet, Kunal, Karthik, Navin, Samrat, Bobby, Sagar B and all others. I deeply thank Hemant for helping me with ProE learning and being with me through my work. He has also been integral to various discussions on the possibilities of this system. Finally, I feel obliged to my parents and my family for supporting me and providing inspiration.

A HYBRID RECONFIGURABLE SOLAR AND WIND ENERGY SYSTEM

SAGAR A. GADKARI

ABSTRACT

We study the feasibility of a novel hybrid solar-wind hybrid system that shares most of its infrastructure and components. During periods of clear sunny days the system will generate electricity from the sun using a parabolic concentrator. The concentrator is formed by individual mirror elements and focuses the light onto high intensity vertical multi-junction (VMJ) cells. During periods of high wind speeds and at night, the same concentrator setup will be reconfigured to channel the wind into a wind turbine which will be used to harness wind energy. In this study we report on the feasibility of this type of solar/wind hybrid energy system. The key mechanisms; optics, cooling mechanism of VMJ cells and air flow through the system were investigated using simulation tools.

The results from these simulations, along with a simple economic analysis giving the levelized cost of energy for such a system are presented. An iterative method of design refinement based on the simulation results was used to work towards a prototype design.

The levelized cost of the system achieved in the economic analysis shows the system to be a good alternative for a grid isolated site and could be used as a standalone system in regions of lower demand. The new approach to solar wind hybrid system reported herein will pave way for newer generation of hybrid systems that share common infrastructure in addition to the storage and distribution of energy.

TABLE OF CONTENTS

	Page
ABSTRACT	v
NOMENCLATURE	ixix
LIST OF TABLES	xii
LIST OF FIGURES	xiii
I INTRODUCTION	1
1.1 Background	1
1.2 The Proposed System.....	5
1.3 Research Work.....	8
1.4 Document Organization	8
II BACKGROUND	9
2.1 Solar and Wind Energy Concepts	9
2.2 Concentrator Solar Energy Systems	19
2.2.1 Concentrating Solar-Thermal (CST) energy systems	19
2.2.2 Concentrator Solar PV (CPV) Systems	22
2.3 Vertical Multi-junction Cells (VMJ)	24
2.4 Simulation Software.....	33
2.4.1 LightTools 5.40.....	33

2.4.2	CFdesign V9	41
2.5	Economic Analysis	49
III	LITERATURE REVIEW.....	51
3.1	Upgrading the conventional wind turbine.....	51
3.2	Diffuser Augmented wind turbines.....	53
3.3	Global Multistage turbines.....	54
3.4	New Generation Solar Concentrators	56
IV	PROBLEM FORMULATION.....	58
4.1	Optics Calculations	59
4.2	Heat Transfer Calculations	63
4.3	Wind energy calculations.....	70
4.4	Economic calculations	72
V	RESEARCH METHODOLOGY	74
5.1	3D Model of the system.....	78
5.2	Optics Simulations Methodology	82
5.3	Heat Transfer Simulations Methodology.....	87
5.4	Airflow Simulations Methodology	99
VI	RESULTS.....	104
6.1	Optics simulation results.....	105

6.2	Heat Transfer Simulation Results	114
6.3	Airflow Simulation results	125
6.4	Economic calculation results	136
6.5	Prototype system model	139
VII	CONCLUSIONS	145
VIII	FUTURE RESEARCH	149
	REFERENCE	151
	APPENDICES	154
A.	Solar Concentrator at CSU	155
B.	One Dish Per Village (ODPV)	156
C.	CFDesign Code validation	157

NOMENCLATURE

CSP: Concentrated Solar Power

CST: Concentrated Solar Thermal

CPV: Concentrated Photovoltaics

VMJ: Vertical Multi-junction

HT: Heat Transfer

DAWT: Diffuser Augmented Wind turbines

CLFR: Compact Linear Fresnel Reflector

SA : Surface Area

A_p : Solar receiver area (m^2)

α : absorptivity of the absorber with respect to the solar spectrum

C : concentration factor

E_s : Radiation density of the direct solar radiation (W/m^2)

ε : emissivity of the absorber with respect to the black body radiation

σ : Stefan-Boltzmann constant , $5.67 \cdot 10^{-8} W/m^2 K^4$

U_{air} : Heat loss coefficient due to convection of air. ($W/m^2 K$)

T_{abs} : Temperature of the solar receiver

T_a : Ambient temperature (K)

Q : Total heat incident on the area (W)
 U_{overall} : Overall heat transfer coefficient ($\text{W/m}^2 \text{ } ^\circ\text{K}$)
 A : Heat transfer area of the surface (m^2)
 T_f : Steady state temperature attained at the heat transfer surface ($^\circ\text{K}$)
 T_∞ : Temperature of the cooling fluid ($^\circ\text{K}$)
 $U_{\text{conductive}}$: Conductive heat transfer coefficient
 $U_{\text{convective}}$: Convective heat transfer coefficient
 T_w : Thickness of copper plate in the direction of conduction (m)
 K_{cu} : Thermal conductivity of copper ($\text{W/m}^\circ\text{K}$)
 h : Heat transfer coefficient of water flow through the pipe ($\text{W/m}^2 \text{ } ^\circ\text{K}$)
 Nu_{Dh} : Nusselt number based on the hydraulic diameter
 D_h : Hydraulic diameter
 K_{water} : Thermal conductivity of water ($\text{W/m } ^\circ\text{K}$)
 f : friction coefficient
 Re : Reynolds number for the fluid flow
 U_{av} : inlet bulk velocity (m/s)
 ν : Kinematic viscosity of fluid (m^2/s)
 Pr : Prandtl Number
 μ : Dynamic viscosity of fluid (N-s/m^2)
 C_p : Specific heat ($\text{J/kg}^\circ\text{K}$)
 ρ : density of fluid (kg/m^3)
 A_c : Area of cross-section of the inlet (m^2)

\dot{m} : mass flow rate of the cooling fluid

\dot{M} : mass flow rate over the rotor with area A_{rotor} .

velocity : velocity of air in the wind tunnel onto the turbine rotor

A_{rotor} : area swept by the rotor

LCOE : Levelized Cost of Energy

LCC : Levelized Cost of Capital

LRR: Levelized annual revenue required

O&M : Operation and maintenance cost

LAE : Levelized annual expenses

FCR : Fixed charge rate

CRF : Capital recovery factor

LIST OF TABLES

Table	Page
TABLE I: Optical calculation parameters	62
TABLE II: Constants and values used for theoretical model calculations.....	68
TABLE III: Solar irradiation results	106
TABLE IV: Annual capacity of the system	137
TABLE V: System costs.....	138

LIST OF FIGURES

Figure	Page
Figure 1: World consumption for electricity generation [1]	4
Figure 2: Solar energy mode of operation of the proposed system	6
Figure 3: Wind energy mode of operation of the proposed system	7
Figure 4: Solar Insolation map of United States [2].....	12
Figure 5: Efficiencies of solar cells and timeline of development [2]	15
Figure 6: Wind resource in United States [nrel 4].....	18
Figure 7: Solar dish systems.....	20
Figure 8: Parabolic trough system.....	20
Figure 9: Central receiver system.....	21
Figure 10: Schematic drawing of VMJ cell.....	25
Figure 11: Schematic of VMJ fabrication technique.....	26
Figure 12: IV curves for VMJ cell [range 100 to 2500 suns@ AM1.5 intensities] ...	28
Figure 13: Efficiency vs. Temperature for Concentrator Photocells.....	32
Figure 14: Geometry of aim sphere.....	35
Figure 15: Simulation setup in LightTools.....	39
Figure 16: Chart views in LightTools	40

Figure 17:	Upfront CFD platform	42
Figure 18:	CFdesign Task Dialog menu.....	45
Figure 19:	Multistage turbine	55
Figure 20:	Results for Multistage turbine.....	55
Figure 21:	CLFR schematic.....	57
Figure 22:	Cooling system schematic.....	65
Figure 23:	Final temperature T_f from the theoretical model of HT design	69
Figure 24:	Concept refinement Approach	75
Figure 25:	Schematic of the concept system	79
Figure 26:	Skeleton model in ProE	81
Figure 27:	Vane assembly imported in LightTools	83
Figure 28:	Components for simulation in LightTools.....	84
Figure 29:	Schematic of experimental setup in LightTools	85
Figure 30:	Heat transfer mechanism assembly.....	88
Figure 31:	Three receiver designs used for HT simulations.....	89
Figure 32:	Exporting model from ProE.....	90
Figure 33:	Imported model in ProE.....	91
Figure 34:	Meshed model in CFdesign	92
Figure 35:	Assigning boundary conditions in CFdesign	93

Figure 36:	Assigning materials in CFdesign	94
Figure 37:	Simulation properties in CFdesign.....	95
Figure 38:	Analyze tab in CFdesign.....	97
Figure 39:	Results task dialogues in CFdesign.....	98
Figure 40:	Model exported to CFdesign.....	100
Figure 41:	Turbine modeled in ProE	101
Figure 42:	Simulation model with turbine.....	102
Figure 43:	Irradiation of AM0 and AM1.5.....	106
Figure 44:	Results for receiver distance 3.05m-3.175m.....	108
Figure 45:	Results for receiver distance 3.2m-3.325m.....	109
Figure 46:	Results verifying tracking system accuracy.....	112
Figure 47:	Temperature profile with water as working fluid (Design 1)	115
Figure 48:	Comparison of theoretical and simulation temperature values HT model (H ₂ O)	116
Figure 49:	Temperature profile with ammonia as working fluid (Design 1)	117
Figure 50:	Comparison of theoretical and simulation temperature values HT model (NH ₃)	118
Figure 51:	Temperature profiles using water with design 2.....	120
Figure 52:	Temperature profile using ammonia with design 2	121
Figure 53:	Temperature profile with design 3 using water	123

Figure 54:	Results of effect of vanes on air flow	126
Figure 55:	Results from first generation model simulation [concentrating mode] ..	127
Figure 56:	Results from first generation model simulation [diffuser mode]	129
Figure 57:	Results with turbine [concentrating mode]	131
Figure 58:	Velocity profile in tunnel cut plane [concentrating mode]	132
Figure 59:	Results with turbine [diffuser mode]	133
Figure 60:	Velocity profile in tunnel cut plane [diffuser mode]	134
Figure 61:	Comparison of bare turbine with the concept system	135
Figure 62:	Prototype model design.....	140
Figure 63:	System design options.....	144
Figure 64:	Concentrator solar thermal system.....	144

CHAPTER I

INTRODUCTION

1.1 Background

Currently in a global economy, there is an ever increasing need for energy security. All the shareholders (nations) are in pursuit of energy independence to maintain their path of progress. With developing nations like China, Brazil and India growing at an alarming rate, there will always be an increasing demand of oil, and as such would strain the oil supply. With the natural resource of oil and gas fast depleting, and the ill-effects of their use on the climatic cycle visible, it has compelled us to investigate other sources of energy and has also changed the mindset of the consumer towards the

consumption of energy. Altering fuel budget, using public transport systems to work, car pooling, energy conservation and energy awareness are a few trends indicators of change in lifestyle. As more of the effects of the energy crisis become visible, like the rise in inflation and climate change, governments in many countries have now become more aware of the benefits of alternative energy and encouraging renewable energy technologies.

Renewable energy sources can meet many times the present world energy demand, so that their potential is enormous. They can enhance diversity in energy supply markets, secure long-term sustainable energy supplies, and reduce local and global atmospheric emissions. They can also provide commercially attractive options to meet specific needs for energy services (particularly in developing countries and rural areas), create new employment opportunities, and offer possibilities for local manufacturing of equipment. Although there are many renewable technologies commercially available, often most are still at an early stage of development and not technically mature. They demand continuing research, development, and demonstration efforts. In addition, few renewable energy technologies can compete with conventional fuels on cost, except in some niche markets. But substantial cost reductions can be achieved for most renewables, closing gaps and making them more competitive. That will require further technology development and market deployment—and boosting production capacities to mass production.

Renewable energy sources have been important for humans since the beginning of civilization. For centuries and in many ways, biomass has been used for

heating, cooking, steam generation, and power generation—and hydropower and wind energy, for movement and later for electricity production. Renewable energy sources generally depend on energy flows through the Earth's ecosystem from the insolation of the sun and the geothermal energy of the Earth. One can distinguish:

- Biomass energy (plant growth driven by solar radiation).
- Wind energy (moving air masses driven by solar energy).
- Solar energy (as for heating and electricity production).
- Hydropower.
- Marine energy (such as wave energy, marine current energy, and energy from tidal barrages).
- Geothermal energy (from heat stored in rock by the natural heat flow of the Earth).

The renewable energy sources find a small share in the electricity generation sector. Figure 1 shows the global distribution of various sources to generate electricity in the world today. It shows that that a high percentage of electricity generation needs are currently being satisfied by natural resources like coal, natural gas and petroleum. With increasing demand, the natural resources are fast depleting and hence renewable energy sources can reduce the high dependence on these resources.

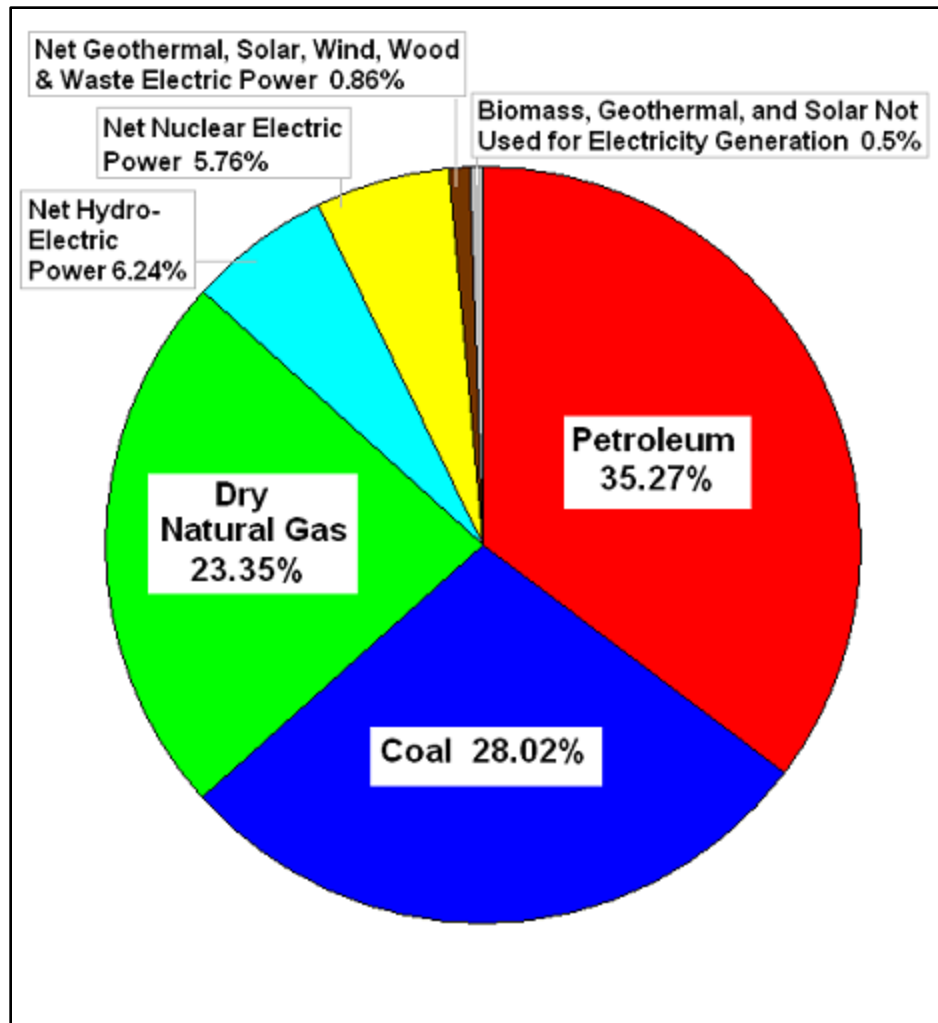


Figure 1: World consumption for electricity generation [1]

With all the global environmental concerns and the ever increasing need for energy, coupled with a steady progress in renewable energy technologies are opening up new opportunities. The following section takes a brief look at the novel solar/wind hybrid energy system proposed in this study.

1.2 The Proposed System

The proposed reconfigurable Solar/Wind hybrid energy system

The proposed hybrid system will generate electricity from solar and wind sources. During periods of clear sunny days, the solar concentrator along with the high intensity VMJ cells will be used to harness solar energy, and during periods of high wind speeds and at night, the concentrator will be reconfigured to function as a wind collector to harness wind energy.

Figure 2 shows the diagram of the concept system in the solar energy mode. A parabolic concentrator will be formed using the individual mirror elements (vanes). The concentrator will reflect the sun rays onto an array of VMJ cells. The efficiency of the VMJ cells is about 25% and is used to convert the sun's energy into electrical energy. The remaining 75% of incident energy is lost in heat and reflection. The heat removal process helps improve the efficiency of the VMJ's and increases their longevity. The VMJ's will be cooled using a heat exchange mechanism. A tracking system will be used to track the sun when operating in the solar energy mode and will be used to rotate the concentrator normal to the direction of the wind when operating in wind energy mode. The individual vanes will be actuated by an electromechanical system. The vanes will be in position to form a parabolic shape, to concentrate sun in solar energy mode.

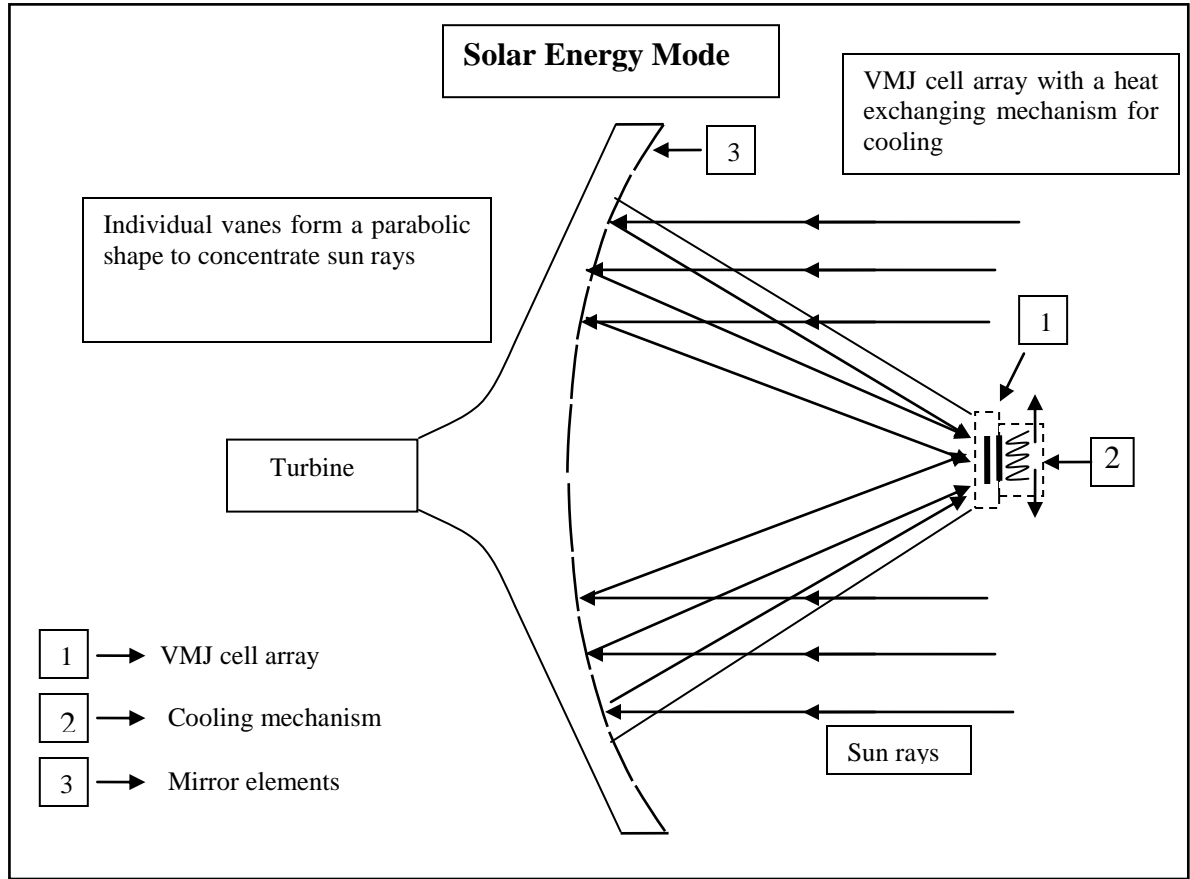


Figure 2: Solar energy mode of operation of the proposed system

In the wind energy mode, the rotated vanes will reduce the obstruction for air flow, and the concentrator will act as a wind collection device. The collected wind is then funneled into a wind tunnel. The funneling effect will result in a much higher working speed. Since the power generated by wind energy is directly proportional to the cube of wind speeds, the proposed system can harness wind energy from lower ambient wind speeds. Figure 3 shows the schematic of the system in the wind energy mode.

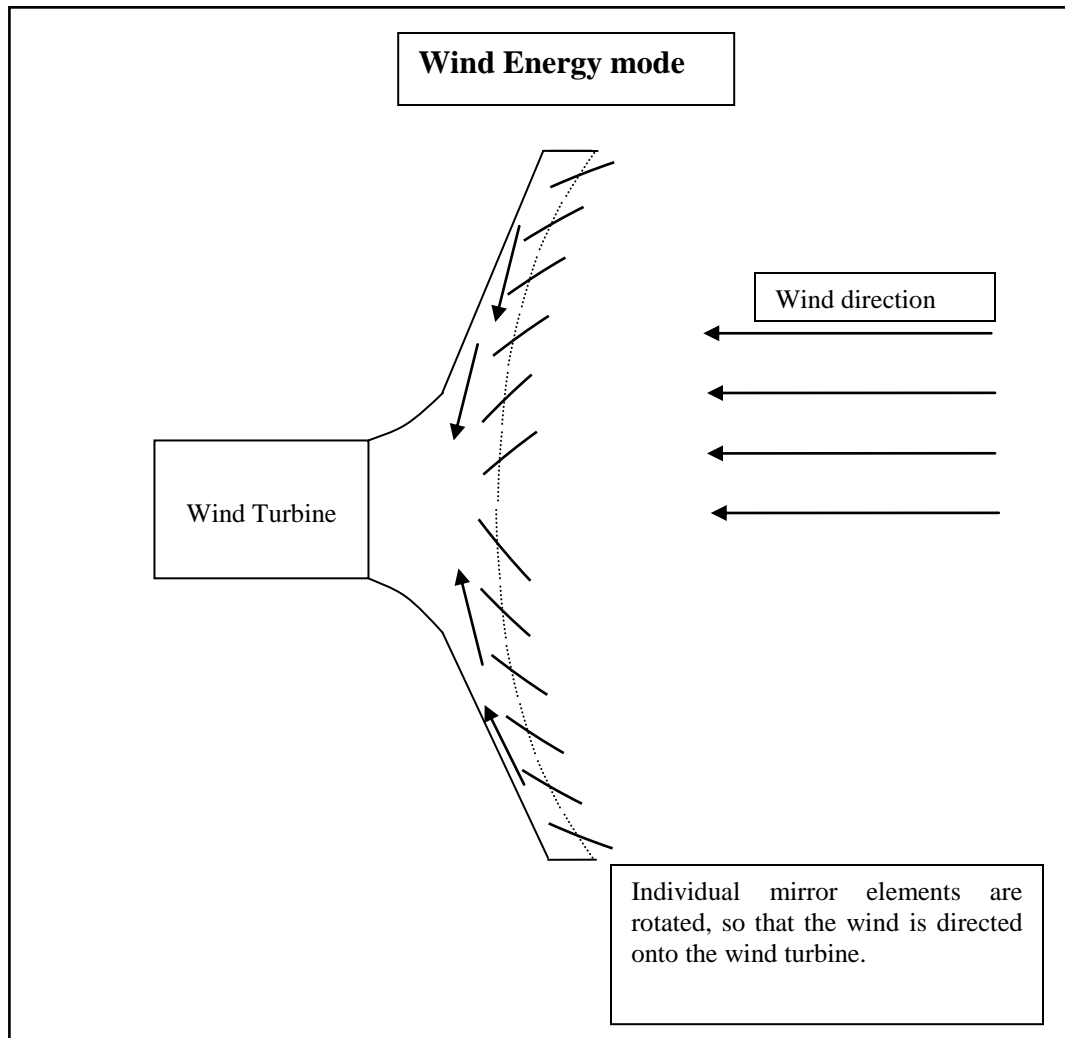


Figure 3: Wind energy mode of operation of the proposed system

1.3 Research Work

In this work we study the feasibility of a novel design of hybrid solar and wind power generation system. The feasibility of the concept system is presented in this work using 3D modeling and simulation techniques. From the concept stage, to making necessary changes in design based on the results obtained from the simulation analysis, the work refines and validates a proof of concept system.

1.4 Document Organization

In chapter two we go through a few topics necessary in understanding this work and the system in general. Chapter three is a literature review of the work close to that being researched here. Chapter four presents the formulation of theoretical concepts studied in this work. Chapter five shows the research methodology adopted while analyzing the various mechanisms of the system. Chapter six reports the findings from the work. Finally, we conclude the document by presenting remarks and suggestion for future work to be done in chapters seven and eight.

CHAPTER II

BACKGROUND

2.1 Solar and Wind Energy Concepts

Air Mass

The sun is continually releasing an enormous amount of radiant energy into the solar system. The Earth receives a tiny fraction of this energy; yet, an average of 1367 watts (W) reaches each square meter (m^2) of the outer edge of the Earth's atmosphere. The atmosphere absorbs and reflects some of this radiation, including most X-rays and ultraviolet rays.

The energy loss depends on the thickness of the atmosphere that the sun's energy must pass through. The radiation that reaches sea level at high noon in a clear sky is 1000 W/m^2 and is described as "air mass 1" (or AM1) radiation. As the sun moves lower in the sky, the light passes through a greater thickness (or longer path) of air, losing more energy. Because the sun is overhead for only a short time, the air mass is normally greater than one—that is, the available energy is less than 1000 W/m^2 . Scientists have given a name to the standard spectrum of sunlight at the Earth's surface: AM1.5G (where G stands for "global" and includes both direct and diffuse radiation, described next) or AM1.5D (which includes direct radiation only). The number "1.5" indicates that the length of the path of light through the atmosphere is 1.5 times that of the shorter path when the sun is directly overhead [2].

The standard of AM1.5 is used for the northern hemisphere. At this standard the solar radiation of 850 W/m^2 reaches the surface at high noon. The exact air mass function varies from site to site and the data can be found on the Department of Energy website. The solar radiation reaching the earth's surface is also described as 1 sun concentration. Hence, with an air mass function of AM1.5, the one sun concentration radiation is about 850 W/m^2 or 0.085 W/cm^2 . The concentration ratio's are very important while discussing the concentrating solar systems and have been used throughout this work.

Direct and Diffuse Light

The Earth's atmosphere and cloud cover absorbs, reflects, and scatters part of the solar radiation entering the atmosphere. Nonetheless, an enormous amount of the sun's energy reaches the Earth's surface and can therefore be used to produce electricity by using the photovoltaic effect. Some of this radiation is direct and some is diffuse, and the distinction is important because some PV systems (flat-plate systems) can use both forms of light, but concentrator systems can only use direct light.

- **Direct light** - consists of radiation that arrives from the sun, without reflecting off clouds, dust, the ground, or other objects. Scientists also talk about direct-normal radiation, referring to the portion of sunlight that comes directly from the sun and strikes the plane of a PV module at a 90-degree angle.
- **Diffuse light** - is sunlight that is reflected off clouds, the ground, or other objects. It obviously takes a longer path than a direct light ray to reach a module. Diffuse light cannot be focused with the optics of a concentrator PV system.

Insolation

The actual amount of sunlight falling on a specific geographical location is known as insolation—or "incident solar radiation." Insolation values for a specific site are sometimes difficult to obtain. Weather stations that measure solar radiation components are located far apart and may not carry specific insolation data for a given site. Furthermore, the information most generally available is the average daily total—or global—radiation on a horizontal surface. When sunlight reaches the Earth, it is

distributed unevenly in different regions. Not surprisingly, the areas near the Equator receive more solar radiation than anywhere else on the Earth. Sunlight varies with the seasons, as the rotational axis of the Earth shifts to lengthen and to shorten the dark or light days with the changing seasons. The quantity of sunlight reaching any region is also affected by the time of day, the climate (especially the cloud cover, which scatters the sun's rays), and the air pollution in that region. Likewise, these climatic factors all affect the amount of solar energy that is available to PV systems. Shown in Figure 4 is the average radiation received on a horizontal surface across the continental United States in the month of June. Units are in kWh/m^2 .

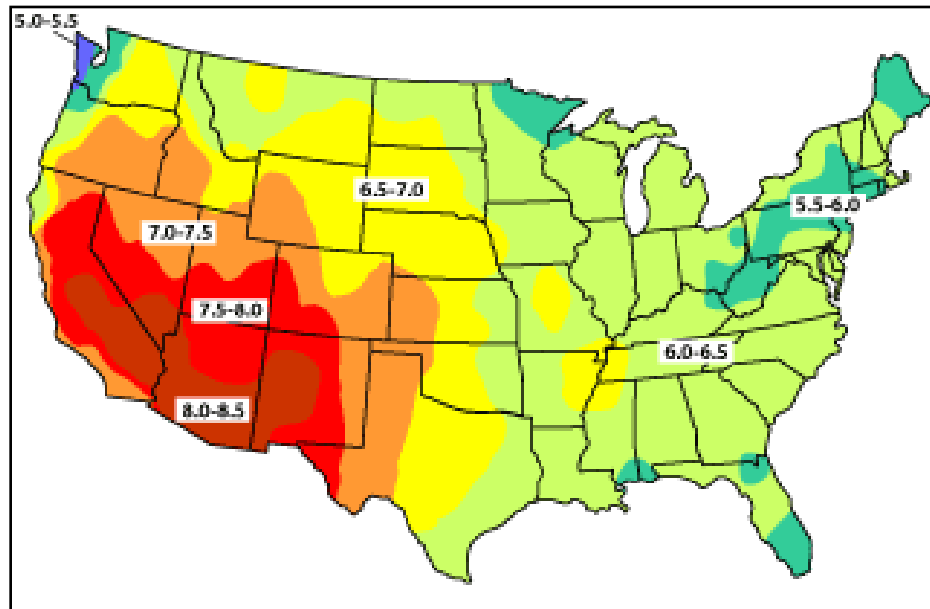


Figure 4: Solar Insolation map of United States [2]

Types of solar energy systems

Solar energy is harnessed primarily by using two methods; solar-thermal process and solar-Photovoltaic (solar-PV) process. The Solar thermal process converts solar energy into heat energy. This heat energy can be used in various forms to heat water for daily usage, generate steam, dry crops etc. The solar-PV process converts solar energy into electric energy using photovoltaics. The solar thermal systems are predominantly concentrator based systems. They concentrate the energy of sun onto a single point (solar load) by using reflecting materials and harness solar energy. The concentrator solar energy systems are described in the next section. Solar-PV systems most widely used are the flat panel systems. We briefly describe the flat panel systems here.

The most common array design uses flat-plate PV modules or panels. These panels can either be fixed in place or allowed to track the movement of the sun. They respond to sunlight that is either direct or diffuse. Even in clear skies, the diffuse component of sunlight accounts for between 10% and 20% of the total solar radiation on a horizontal surface. On partly sunny days, up to 50% of that radiation is diffuse. And on cloudy days, 100% of the radiation is diffuse.

The simplest PV array consists of flat-plate PV panels in a fixed position. The advantages of fixed arrays are that they lack moving parts, there is virtually no need for extra equipment, and they are relatively lightweight. These features make them suitable for many locations, including most residential roofs. Because the panels are fixed in place, their orientation to the sun is usually at an angle that practically speaking is less than optimal. Therefore, less energy per unit area of array is collected compared with

that from a tracking array. However, this drawback must be balanced against the higher cost of the tracking system.

Solar cell efficiency

The performance of a solar or photovoltaic (PV) cell is measured in terms of its efficiency at converting sunlight into electricity [2]. There are a variety of solar cell materials available, which vary in conversion efficiency. A solar cell consists of semiconductor materials. Silicon remains the most popular material for solar cells. The types of solar cells are classified as; crystalline, polycrystalline, amorphous thin films, and multi-junction concentrator cells. Various new materials like Ge, As, In, Se are being used in solar cells today due to their spectral responses. Figure 5 shows the efficiencies achieved and the timeline of development of solar cells over the past three decades.

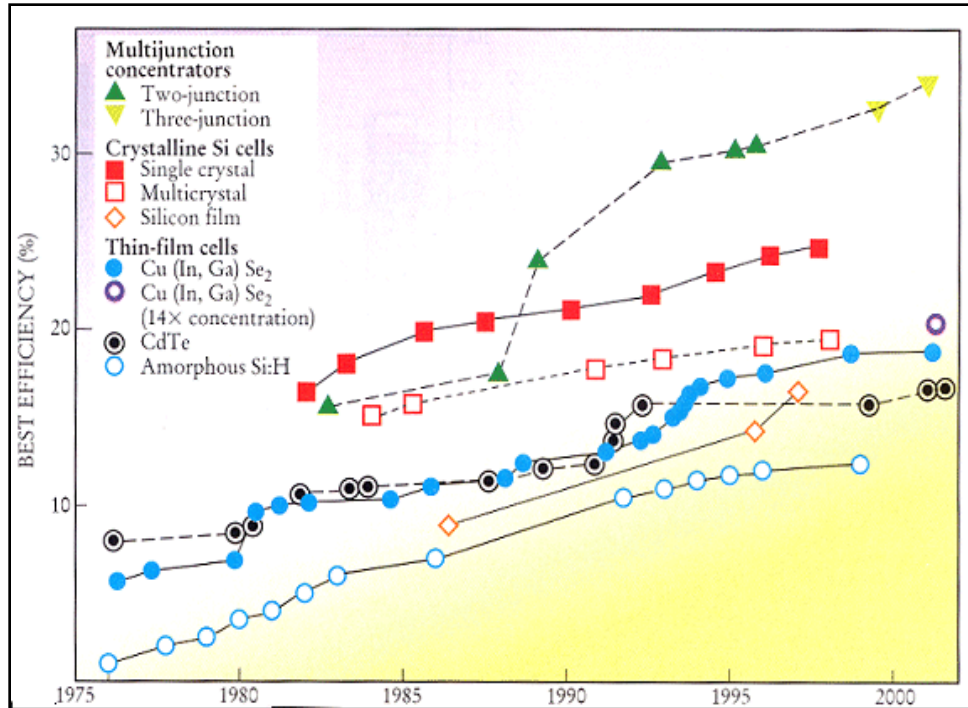


Figure 5: Efficiencies of solar cells and timeline of development [2]

Wind Energy systems

Like the weather in general, the wind can be unpredictable. It varies from location to location, and from moment to moment. Wind speed is the rate at which air flows past a point above the earth's surface. Because it is invisible, it is not easily measured without special instruments. Wind velocity is affected by the trees, buildings, hills and valleys around us. Wind is a diffuse energy source that cannot be easily contained or stored for use elsewhere or at another time. The wind flows over the airfoil shaped blades causing lift, like the effect on airplane wings, causing them to turn. The blades are connected to a drive shaft that turns an electric generator to produce electricity. To be economically practical, a wind turbine should experience year-round average wind

speeds of at least 12 mph. A careful and precise wind survey should be made before buying a wind system. There are two types of wind energy systems

- **Horizontal Axis Wind turbine:** in which the axis of rotation is horizontal with respect to the ground. The rotation is roughly parallel to the wind stream. The most common types of wind turbines are horizontal axis. The wind mills are posted around 30 to 50 meters above the ground where the wind speeds are high. Various designs of horizontal axis turbines can be found in literature. They vary from single blades to multiple blade design.
- **Vertical Axis Wind turbine:** in which the axis of rotation is vertical to the ground. The rotation is roughly perpendicular to the wind stream. The most common type of vertical axis turbines is Darius turbines. The vertical axis turbines are less efficient and hence they are not widely used. The most common ones are the giant horizontal axis turbines.

Wind turbine efficiency

Wind turbines extract energy by slowing down the wind. For a wind turbine to be 100% efficient it would need to stop 100% of the wind - but then the rotor would have to be a solid disk and it would not turn and no kinetic energy would be converted. On the other extreme, if we had a wind turbine with just one rotor blade, most of the wind passing through the area swept by the turbine blade would miss the blade completely and so the kinetic energy would be kept by the wind. The theoretical maximum power

efficiency of any design of wind turbine is 0.59 (i.e. no more than 59% of the energy carried by the wind can be extracted by a wind turbine). This is the Betz limit.

Once we factor in the engineering requirements of a wind turbine - strength and durability in particular - the real world limit is well below the Betz Limit with values of 0.35-0.45 common even in the best designed wind turbines. Also taking into account other inefficiencies in a complete wind turbine system - e.g. the generator, bearings and power transmission and so on - only 20-30% of the power of the wind is ever actually converted into usable electricity.

Wind Resource evaluation

Wind resource evaluation [3] is a critical element in projecting turbine performance at a given site. The energy available in a wind stream is proportional to the cube of its speed, which means that doubling the wind speed increases the available energy by a factor of eight. Furthermore, the wind resource itself is seldom a steady, consistent flow. It varies with the time of day, season, height above ground, and type of terrain. Proper siting in windy locations, away from large obstructions, enhances a wind turbine's performance.

In general, annual average wind speeds of 5 meters per second (11 miles per hour) are required for grid-connected applications. Annual average wind speeds of 3 to 4 m/s (7-9

mph) may be adequate for non-connected electrical and mechanical applications such as battery charging and water pumping.

Wind Power Density is a useful way to evaluate the wind resource available at a potential site. The wind power density, measured in watts per square meter, indicates how much energy is available at the site for conversion by a wind turbine. Figure 6 shows the wind resource in the United States. The inset shows the wind power density values.

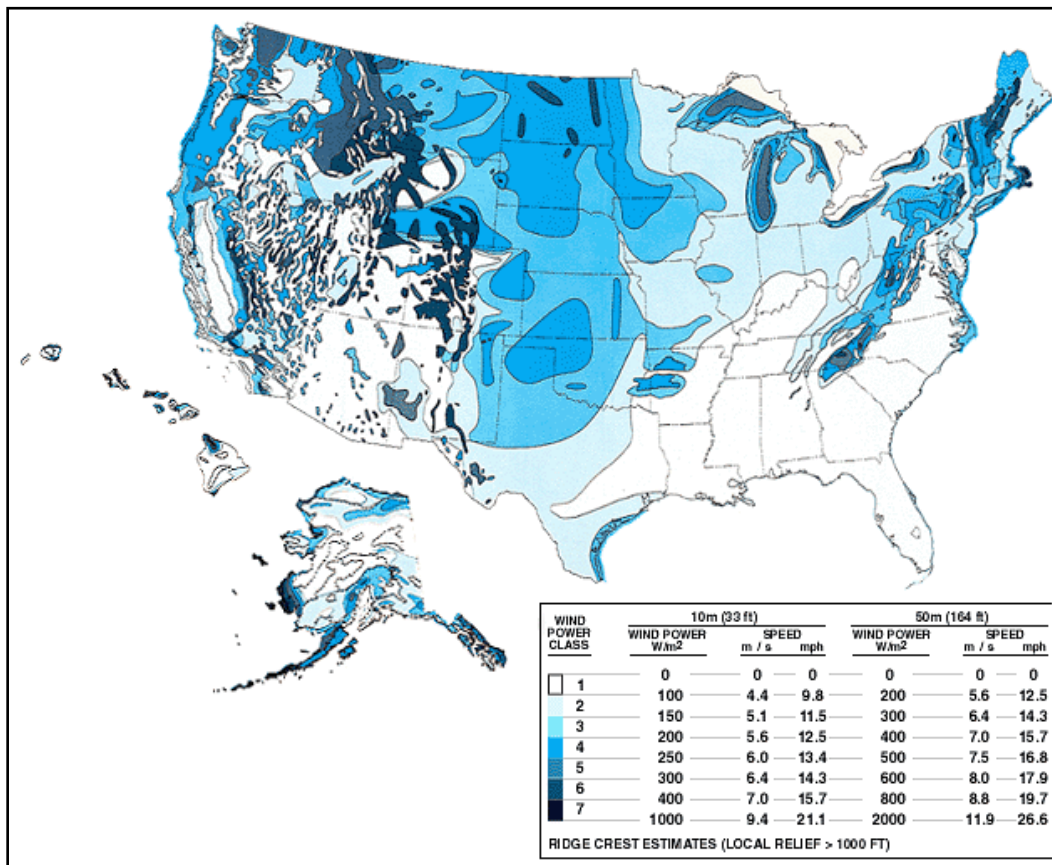


Figure 6: Wind resource in United States [4]

2.2 Concentrator Solar Energy Systems

Concentrated solar power (CSP) uses the solar-thermal method and has been used widely for power generation. With concentrating technology, newer high efficiency high concentrator PV (HCPV) cells have been developed that use less area of silicon cells to produce higher energy output. We now look at the concentrator solar energy systems available.

2.2.1 Concentrating Solar-Thermal (CST) energy systems

Concentrating solar-thermal power plants produce electric power by converting the sun's energy into high-temperature heat using various mirror configurations [2]. The heat is then channeled through a conventional generator. The plants consist of two parts: one that collects solar energy and converts it to heat, and another that converts heat energy to electricity.

Parabolic Solar dishes

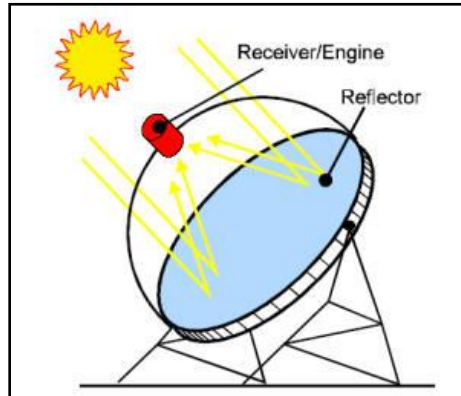


Figure 7: Solar dish systems

Parabolic dish systems consist of a parabolic-shaped point focus concentrator in the form of a dish that reflects solar radiation onto a receiver mounted at the focal point. These concentrators are mounted on a structure with a two-axis tracking system to follow the sun. The collected heat is typically utilized directly by a heat engine mounted on the receiver moving with the dish structure.

Parabolic troughs

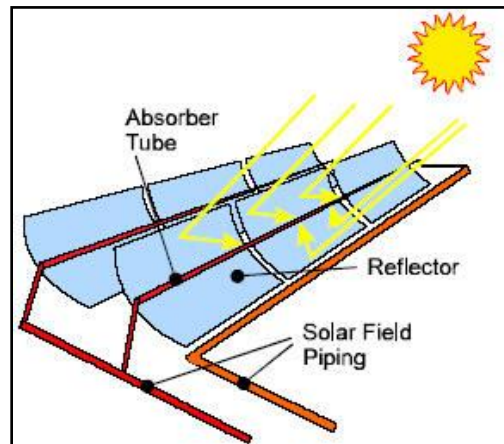


Figure 8: Parabolic trough system

The sun's energy is concentrated by parabolically curved, trough-shaped reflectors onto a receiver pipe running along the inside of the curved surface. This energy heats oil flowing through the pipe and the heat energy is then used to generate electricity in a conventional steam generator. A collector field comprises many troughs in parallel rows aligned on a north-south axis. This configuration enables the single-axis troughs to track the sun from east to west during the day to ensure that the sun is continuously focused on the receiver pipes.

Central Receivers – Solar towers

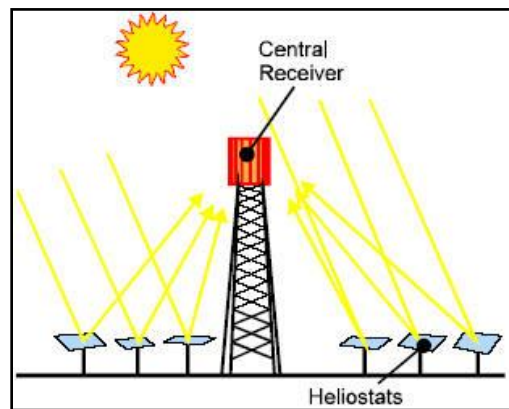


Figure 9: Central receiver system

The technology utilizes many large, sun-tracking mirrors (heliostats) to focus sunlight on a receiver at the top of a tower. A heat transfer fluid heated in the receiver is used to generate steam, which, in turn, is used in a conventional turbine-generator to

produce electricity. Early power towers utilized steam as the heat transfer fluid. Current US designs utilize molten nitrate salt because of its superior heat transfer and energy storage capabilities. Current European designs use air as heat transfer medium because of its high temperature and it is easy to handle.

2.2.2 Concentrator Solar PV (CPV) Systems

The primary reason for using concentrators is to be able to use less solar cell material in a PV system. PV cells are the most expensive components of a PV system, on a per-area basis. A concentrator makes use of relatively inexpensive materials such as plastic lenses and metal housings to capture the solar energy shining on a fairly large area and focus that energy onto a smaller area of solar cells. Unlike the standard one sun solar cells, these cells are specially designed to be able to withstand the high intensity light from the concentrating optics. One measure of the effectiveness of this approach is the concentration ratio—in other words, how much concentration the cell is receiving.

Concentrator systems lower the cost of solar energy. Under 500-sun concentration, for example, one square centimeter of solar cell area produces the same electricity as 500 cm^2 would without concentration. The use of concentration, therefore,

enables the replacement of the more expensive semiconductor area with cheaper materials (e.g., lenses or mirrors)

Advantages of concentrator PV systems

- Concentrator systems increase the power output while reducing the size or number of cells needed.
- Solar cell's efficiency increases under concentrated light. The increase depends largely on the design of the solar cell and the material used to make it.

Disadvantages of concentrated PV

- Achieving higher concentration ratios expensive tracking mechanisms and more precise controls than those of flat-plate systems with stationary structures.
- High concentration ratios also introduce a heat problem [5]. When excess radiation is concentrated, so is the amount of heat produced. Cell efficiencies decrease as temperatures increase, and higher temperatures also threaten the long-term stability of solar cells. In a concentrator system, therefore, the solar cells must be kept cool.

2.3 Vertical Multi-junction Cells (VMJ)

The high cost of silicon based and/or triple junction type photocells leads to a new generation of photocells which are suited for high intensity light [6]. The high quality silicon based VMJ cells were first introduced by NASA in the mid 1970s on an experimental basis mainly for solar concentrator applications in space. The technology continued to evolve with further refinements of the cell technology and the manufacturing processes. Currently, high quality silicon VMJ cells are produced by PhotoVOLT, Inc. (original inventor at NASA) have an operational efficiency of 25% @ solar intensities of 1000-2500 suns (100-250 Watts/cm²) depending on the quality of the heat rejection system used. Other types of VMJ cells has been recently introduced and are being used for solar concentration applications such as the triple junction cells developed by Spectrolab, a division of the Boeing Co. and the cells used by The sol3g Third Generation Solar Systems.

The VMJ cell produced by PhotoVOLT Inc. shown schematically in Figure 10 is an integrally bonded series-connected array of miniature silicon vertical junction unit cells [6]. (Because of its unique orientation to illumination it has also been descriptively referred to as an “edge-illumination” multi-junction cell.)

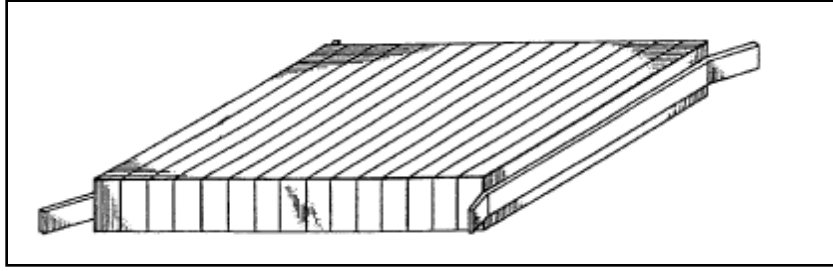


Figure 10: Schematic drawing of VMJ cell

[Courtesy: PhotoVlt Inc.]

The VMJ cell fabrication steps [6], shown in Figure 11, are relatively simple: For an example, 40 diffused $p^{+}nn^{+}$ silicon wafers of 250 microns thickness are metalized, stacked and alloyed together to form a multi-layer stack that is 1 cm high. This stack of diffused wafers, when appropriately cut, will yield around 1000 VMJ cells of 1 cm x 1 cm x .05 cm size, each containing 40 series connected unit cells for high voltage operation. The exposed silicon surfaces are etched to remove saw damage and passivated with an anti-reflection coating applied to the illuminated side. Finally electrical leads are attached to the end contacts. For clarity an edge-illuminated vertical junction $p^{+}nn^{+}$ unit cell is also shown schematically. A key feature of the VMJ cell is its design simplicity. During wafer processing a single high temperature diffusion forms both $p^{+}n$ and nn^{+} junctions and no photolithography is involved. One optimized diffused wafer design is suitable for all intensities and for fabrication of a wide range of finished cell sizes. Thus its manufacture lends itself to a high volume production capability within the present industrial sector at low manufacturing cost.

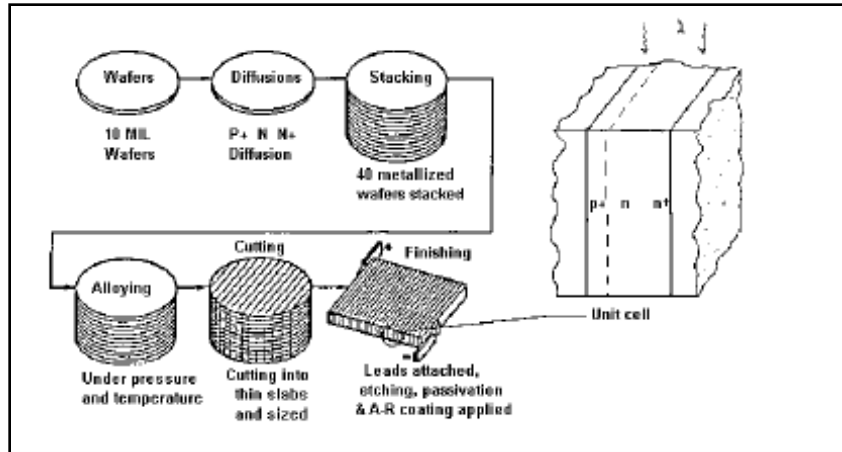


Figure 11: Schematic of VMJ fabrication technique

[Courtesy: PhotoVolt Inc.]

Working of VMJ cells

The cells are illuminated on their edge and the charge carrier wires are placed on the side, extremely close to the edge. As such, the narrow surface (edge) that is exposed to the light is fully illuminated. In addition, since the wires are placed extremely close to the surface of the edge, the free electrons have a very short distance to travel to reach the conduction wire. The extremely short path serves to dramatically reduce the resistance heating due to the flow of electrons in the semiconductor material. Furthermore, because the distances are extremely short, the time required to move the free electrons to the wires is on the order of micro-nano seconds. The combination of these factors allows the on-edge photocells to receive and to convert extremely high intensity light without saturating the Photovoltaic process. And unlike the conventional cells, heat generation due to the electron current flow to the conductor wires is extremely low. The individual cells are called junction and are grouped together in series much like

a sliced loaf of bread to form a multi junction array with the wires imbedded between the junctions, thus the term Vertical Multi-Junction Photocells (VMJ cells). Typically, the individual junctions are 7-10 mills thick (deep) and are 8 mills wide. The length of the junctions is on the order of one to a few centimeters. The level of power generated by the individual junctions is a function of the light intensity, uniformity and junction's temperature.

High voltage silicon vertical multi-junction (VMJ) solar cells are ideally suited for providing efficient operation at solar intensities exceeding 1000 suns AM1.5. Solar concentrators are a promising approach for lowering photovoltaic (PV) power cost in the near term. PV concentrators provide performance advantages since higher cell efficiencies are possible and sun tracking increases the total power delivered over time.

The design features and the characteristics of VMJ cells provide an ideal match for the concentrator systems. Figure 12 shows I-V characteristics of VMJ taken at Flash testing facility at NASA GRC. It is observed from the graph that even at high concentration ratios the VMJ cells show a uniform current output at about 24 volts.

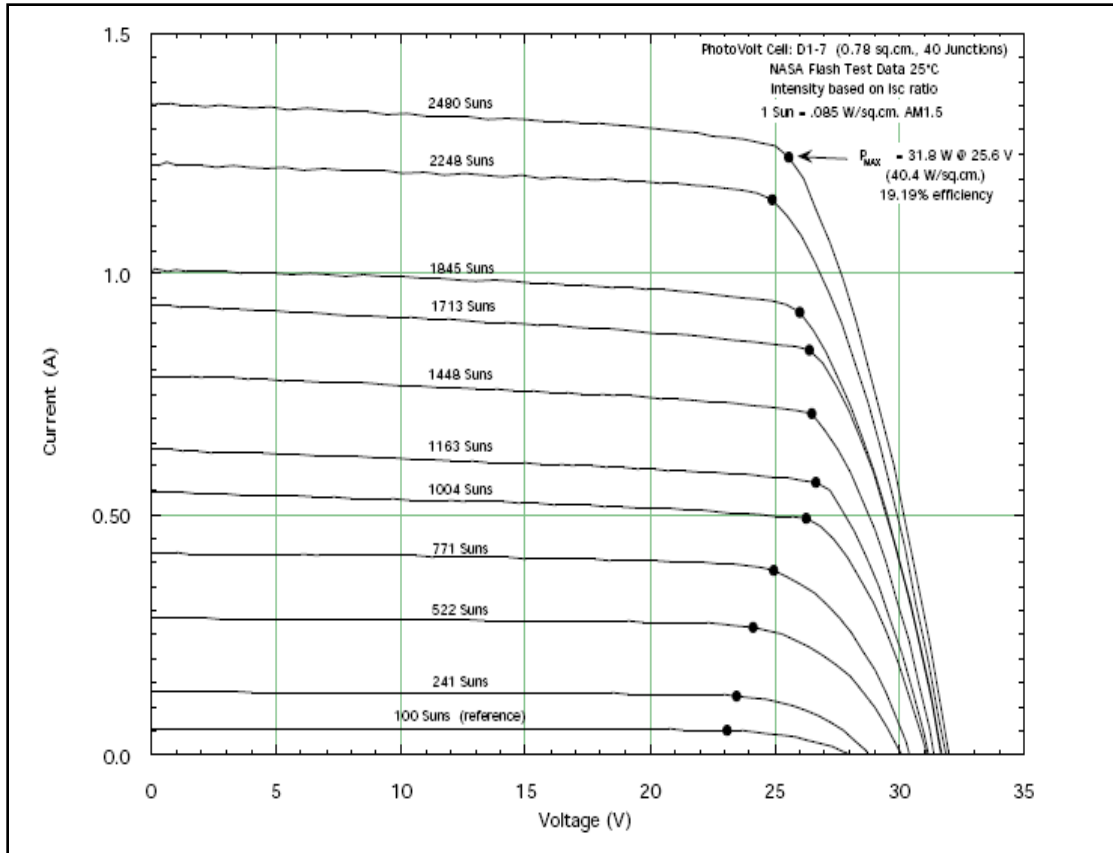


Figure 12: IV curves for VMJ cell [range 100 to 2500 suns@ AM1.5 intensities]

[Courtesy: PhotoVOLT Inc.]

Advantages of VMJ cells

- **Edge-illumination** - eliminates the need for front and/or back contacts. There are no sheet resistivity components of the series resistance and generated current carriers crossing unit cell junctions are immediately collected by their adjacent vertical contacts. There is equal collection probability for excess carriers generated at any depth, which gives improved spectral responses for both the short and long wavelengths.

- **Series-connection** – provides a high voltage, low current operation with a better compatibility to most power processing loads and a high tolerance to series resistance values within the electrical system. It gives very high reversed voltage breakdown immunity, which reduces the need for adding by-pass diode protection.
- **Low series resistance at high intensities** – is assured by effective photoconductivity modulation throughout the bulk region of unit cells, giving an almost linear decrease in series resistance with increasing intensity.
- **Structural design** – provides an extremely rugged configuration electrically, mechanically and thermally. It permits high packing densities with easy interconnecting of electrical output leads in high power density systems.

The VMJ's used in this research are 1 cm^2 in size and have efficiency of about 20% for solar intensities of more than 1000 sun concentrations. At 20% efficiency, each cell provides an output of 20 watt/cm^2 of power for 100 W/cm^2 input.

Thermal Characteristics of Multi-junction Cells

The nominal efficiency of solar cells is quoted at 25°C , above which and depending on the type of the semiconductor materials used, the efficiency of conventional one sun cells decrease considerably with increases in temperature. This in part is due to the electric charge carriers (wires) being deposited on the surface and being typically sparse in order to avoid masking large portions of the active photovoltaic area of

the array. As such, the freed electrons travel relatively long distances (generating heat in the process) before reaching the conduction wires and may recombine with a hole in an electron-hole annihilation process before reaching the conduction wires. This results in the generation of considerable amounts of heat. In addition, further increases in the temperature results in an increase in the vibration level of the free electrons and as such exacerbate the problem and results in further reduction in efficiency. Because of these factors, flat solar array panels are restricted in operation to one sun or approximately 1000 Watts/m² above which the arrays lose efficiency rapidly and in turn result in a runaway heat generation process which may result in permanent damage.

Multi-junction cells are designed to operate under extremely high intensity solar energy ranging from 100-2500 suns (10-250 Watts/cm²). As such, large amounts of heat will be absorbed and/or generated within the individual cells. Therefore, it's important that the temperature of the cells be maintained as low as possible. This will require transferring substantial amounts of heat out of the cells and into a heat exchanger for rejection.

In some cases, it may be necessary to operate the cells at high temperatures at a reduced efficiency; however, the designer must avoid catastrophic failures by insuring that the temperature is maintained below the melting point of the electrical contacts and thermal bonding materials although silicon and other types of semiconductor materials are rugged and are able to withstand high temperatures (600 °C +).

Both types of multi-junction cells, silicon and triple junction, are currently in use successfully with several types and brands of solar concentrator systems on the market.

Depending on the design and the operating environment of these systems, heat rejection systems may be passive such as the passive radiators or may be active systems, using water cooling and/or other types of heat transfer fluids.

The efficiency vs. temperature performance have been determined theoretically and validated experimentally for most of the common semi conductor photovoltaic materials. In the case of Silicon based and the Triple Junction based, one-sun photocells, the efficiency constants are:

$$\Delta E_{\text{Silicon}} = -0.0032\%/^{\circ}\text{C of the efficiency at } 25^{\circ}\text{C}$$

And

$$\Delta E_{\text{Triple Junction}} = -0.0062\% \text{ of the efficiency at } 25^{\circ}\text{C}$$

A summary of the efficiency vs. temperature for Triple Junction and Silicon based VMJ concentrator cell is presented below in Figure 13. The adverse effects of temperature rise for triple junction cells are observed from the graph. With increase in temperature the efficiencies of the triple junction cells drops sharply as compared to silicon based VMJ cells.

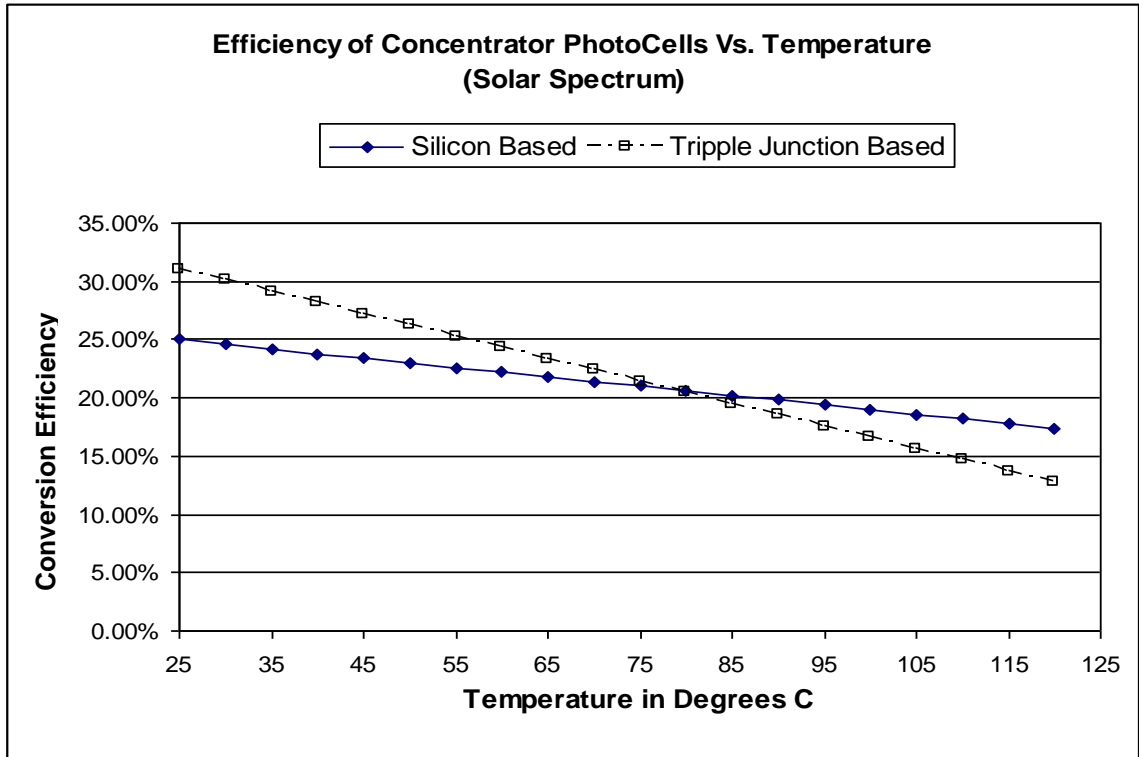


Figure 13: Efficiency vs. Temperature for Concentrator Photocells

2.4 Simulation Software

2.4.1 LightTools 5.40

Background: Illumination module in LightTools

We used illumination module in the software to simulate the incident solar power and the power densities achieved at the VMJ receiver. The LightTools illumination module is an optical add-on module to the LightTools core module. It uses inherent non-sequential ray trace and element based modeling to help simulate complete illumination systems, including the sources, the optics and the mechanical structure. The common elements of an illumination module are as follows [7].

1. Light Sources

An illumination system has at least one light source. The module allows us to specify an unlimited number of sources. These sources can be point sources, 3D surface emitting sources, or 3D volume emitting sources. Surface emitting sources can have spatial distributions that are uniform or user-defined, and can have angular distributions that are uniform, Lambertian or user defined. We can view and modify the sources dimensions, total power, type of power units and ray traceability. We can specify whether the power source is measured over the entire sphere surrounding the source or over the region defined by the aim sphere. Each source has a total power associated with it, expressed in

watts or lumens. It is the power emitted by the source into the whole sphere surrounding source or emitted into an annular cone described by the aim sphere or emitted toward the aim area. The best way to visualize the aim sphere is to imagine a globe with a +Z axis going through the North Pole. Figure 14 shows the geometry of aim sphere. The ray directions are specified by two angles associated with aim sphere; the upper angle and the lower angle. The source emits into only the annular cone between the upper and lower angles. The default angle for the upper cone is 0° , and the default angle for the lower angle is 180° , which lets the source emit into the entire sphere surrounding the source. To create a collimated light source, as we have in our experiments, we make both the upper and lower angles 0° . The types of units used for the power of the source are radiometric or photometric. We use radiometric power in our study. The light sources can be placed anywhere in the working model, with reference to the global UCS.

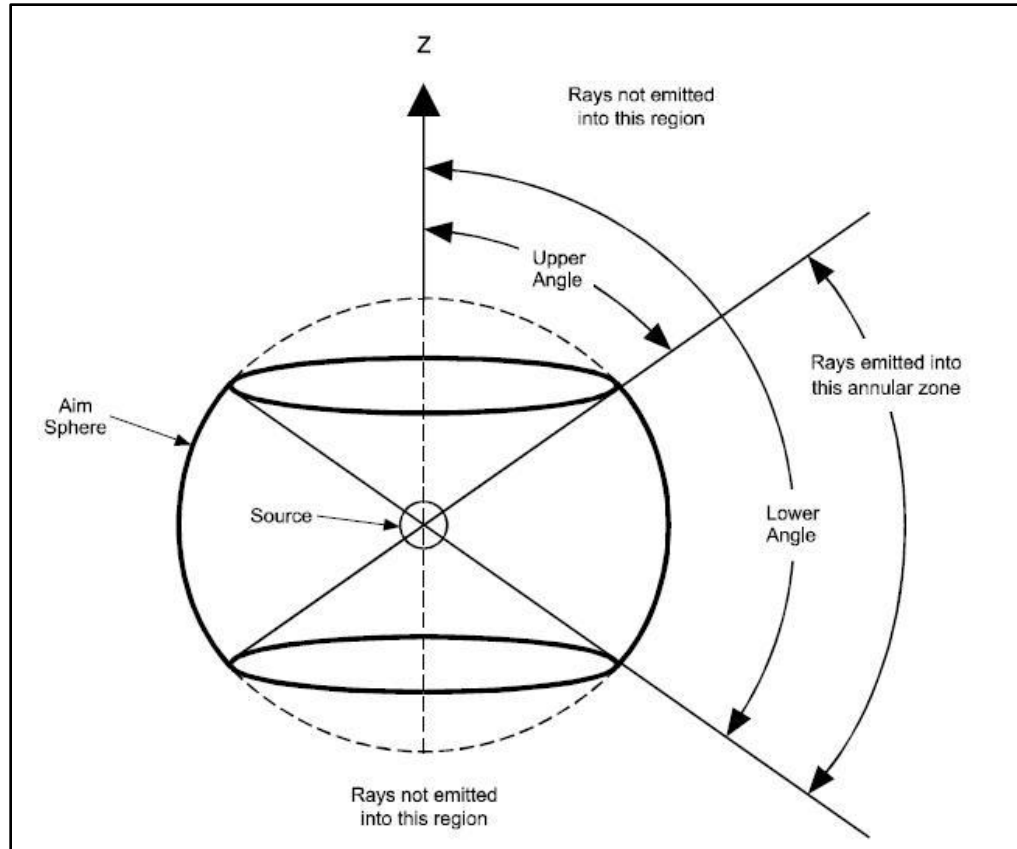


Figure 14: Geometry of aim sphere

2. Receivers

All illumination systems have at least one surface at which the illuminance is of interest. The types of surface receivers available in LightTools are; surface receivers, far field receivers and infinite far field receivers. In our simulations we use surface receivers. Surface receivers are placed on any surface where we want to observe the illumination output. Surface receivers are not of any specific size. They are simply designated on a surface. We can place them on any surface of the 3D model. Surface receivers are effectively rectangular. These surfaces generate the irradiance output (W/m^2) from the simulation. The irradiance output describes the spatial variation of the irradiance on the

receiver surface. In our analysis we use two receivers; one on the dummy surface at the concentrator vanes and second on the VMJ receiver surface collecting the focused light rays.

The illumination data is analyzed using the mesh on the receiver surface. A mesh is grid of cells which store the information of the ray coordinates. The number of cells in the mesh determines the resolution of the data. The software provides an auto meshing option in which a default mesh is on the receiver surface. The actual number used depends on the error estimate which is at a default value of around 5%. LightTools adjusts the mesh size (the number of cells) to the largest number of cells within the specifies bounds so that the error estimate for the cell with the maximum intensity or luminance is less than the error estimate target.

3. Surface Properties

The basic building block of LightTools is called a primitive. It can be a simple geometric solid such as a cube, sphere or cylinder. One can also create additional primitives like lenses and mirrors. Also 3D models can be imported into the software. The LightTools core module allows us to specify the surface properties separately for each surface of any 3D solid object. These properties include the refractive mode (refract, TIR, reflect etc) as well as surface treatments (diffraction, scattering, etc.). For optical objects, these properties can be specified separately for different zones on the surfaces.

4. Monte Carlo Ray trace

The illumination analysis is based on a Monte Carlo ray trace. This method traces the desired number of rays (which can be thousands or even millions of rays) from randomly selected points on the surface, or within the volume of the source (or sources) and into randomly selected angles in space. The selection of starting points and ray direction is based on probabilistic functions that describe emissive characteristics of light sources. Each ray starts with a specific amount of power determined by each source's characteristics; this power is then modified by the various surfaces hit by the ray in its path through the system. The rays are then collected on the specified receiver surfaces for statistical analysis and graphical display.

The ray tracing used in the illumination analysis is non-sequential. This means rays follow the laws of optics, rather than a preset order of surfaces, and thus represent the physical reality of the system. In addition to the optics in the system, the rays interact with the mechanical structure, where they are absorbed, reflected, or scattered. Since Monte Carlo rays are random in nature, it takes many rays to converge to accurate illumination distributions. To get accurate answers, it is not unusual to require hundreds of thousands or even millions of rays. Depending on the complexity of the model (and the speed and memory of the computer), this can require from several minutes to many hours to complete a simulation run. If the ray data are not saved at the receivers, the amount of memory required will be significantly smaller, and the time of the run will be shorter.

5. Running the Simulation

Once we have defined the illumination sources, specified their characteristics and placed receivers, we are ready to run an illumination simulation. Before running the analysis we view the information of the simulation parameters in the simulation properties dialog box. In this box we can define the number of rays to trace, the update info, the number of rays traced, ray report and ray preview settings. The default value is 1000 rays. It represents the total number of rays traced during the simulation. It is the number of rays emitted from the source in the directions specified by the aim entities and not necessarily the number of rays collected by the receiver. Figure 15 below shows one such simulation setup window.

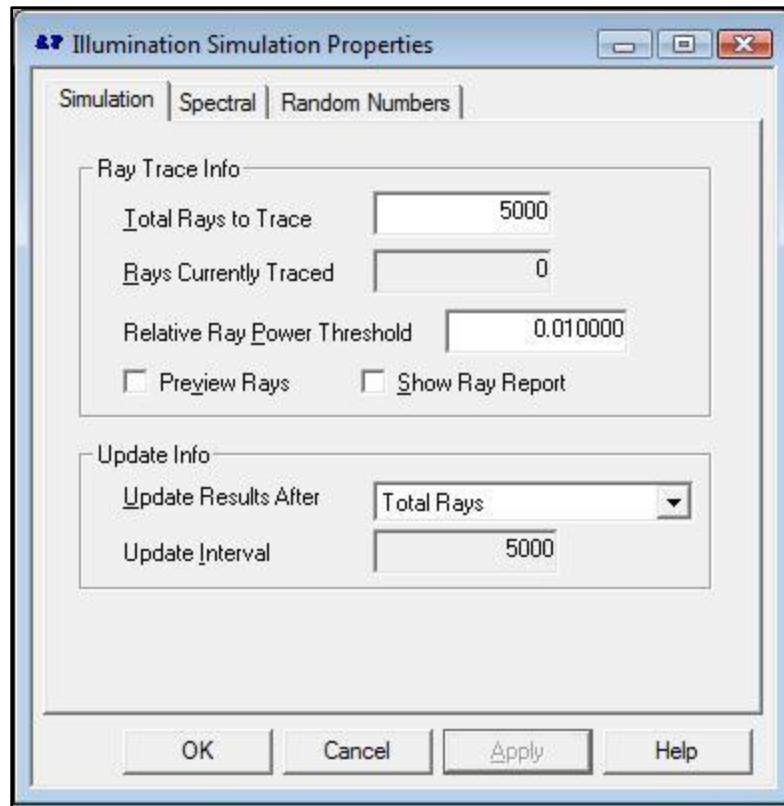


Figure 15: Simulation setup in LightTools

6. Viewing Results

The illuminance analysis applies only to the surface receivers; it does not apply to far field receivers. The output is power/area incident upon the surface receiver. It is the measure of the spatial distribution of the illuminance over the receiver surface. The units of illuminance are watts/area. The output can be viewed with a series of graphical charts. The chart views for illumination data are line chart, raster chart, surface chart and scatter chart. We have used these charts to review our simulations. Figure 16 shows the charts available to review results.

Line chart: It shows a cross-section of the illumination data in two directions.

Raster chart: It shows a pseudo-color output of the illumination distribution across the receiver.

Surface chart: It shows a perspective plot of the illuminance or intensity data over the receiver surface.

Scatter chart: It shows the ray intersection points on the receiver.

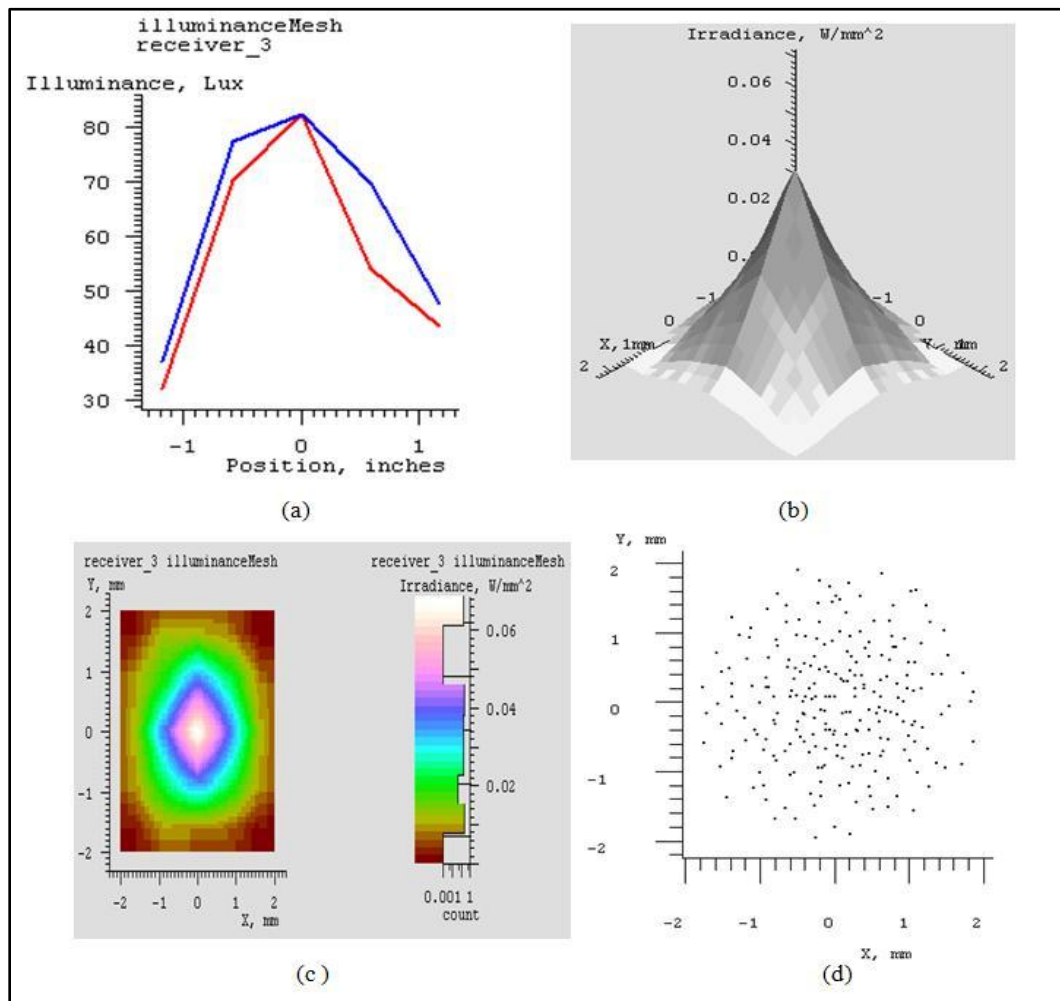


Figure 16: Chart views in LightTools

2.4.2 CFdesign V9

CFdesign is a design tool, and incorporates many features that make flow analysis a valuable and practical part of the product design process [8]. CFdesign is developed for multi-faceted product development teams using MCAD tools such as Pro/Engineer, CATIA, Autodesk Inventor, Solid Edge, Unigraphics, Solid Works, and many others. Powered by proprietary numerical techniques and leading-edge computational methods, CFdesign features a true associative relationship with components and assemblies, and automatically applies the optimal mesh required for accurate fluid and thermal simulations. CFdesign is built upon the Upfront CFD Solution Platform. The platform is shown in Figure 17.

The most significant aspect of this framework in CFdesign is that the process is repeatable- multiple design iterations can be analyzed, compared, and communicated with those in the design chain efficiently and effectively



Figure 17: Upfront CFD platform

CAD Integration

Starting in the CAD system, the component or assembly model you build is all CFdesign needs to deliver a reliable fluid flow and heat transfer simulation. A direct link to the major geometry engines eliminates the need for IGES, STEP, or STL. Make a change to the model in your CAD system, and the change will be a part of the CFdesign analysis.

Mesh Generation

CFdesign employs finite element mesh generation with numerous intelligent algorithms to make the process automatic and transparent. By using automatic, unstructured meshing, CFdesign quickly meshes complicated (real world) geometry without forcing

the user to become an expert in the application of mesh generation tools. Assignment of the mesh distribution to geometry is automatic, and is based on a highly detailed geometric interrogation of the geometry.

Simulation Scope

CFdesign solves the mathematical equations for heat and momentum transfer in a moving fluid. The finite element method is used to *discretize* the flow domain, thereby transforming the governing partial differential equations into a set of algebraic equations whose solution represent an approximation to the exact (and most often unattainable) analytical solution.

Simulation Speed

The intuitive user interface in CFdesign makes setting up the simulation very easy. Using engineering language, the user simply applies the material and operating conditions that are needed. Combined with many intelligent algorithms, analysis set-up is fast and easy for users with no CFD experience.

Design Review

Results are displayed at every step of the calculation. The user can interact with the model, and view results real-time using cutting planes, iso surfaces, xy plots, and

particle traces. Because CFdesign is a design tool, it is very important that results from multiple analyses be viewed, compared, and contrasted easily. The Design Review Center makes it easy to get a true apples-to-apples comparison between all of the analyses in your project.

Project Collaboration

Sharing results with other members of the design supply chain is easy using the Dynamic Image, a part of the Design Review Center.

Task Dialog menu

The task dialog menu bar follows a natural progression in setting up the simulation. Once the geometry is in CFdesign, this task bar helps us set up, analyze and review our simulation. The task bar on the side of the simulation screen has the icons shown in Figure 18. We take a brief look at the various menu options in the task dialog that help us set up the simulation.

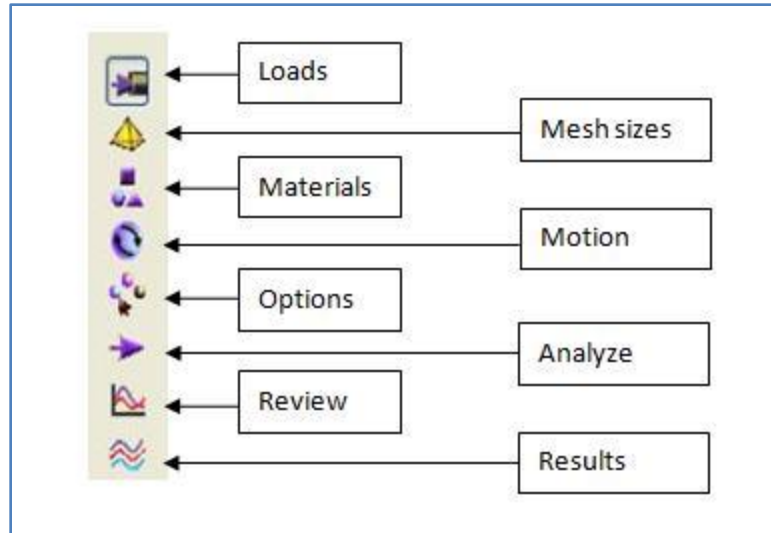


Figure 18: CFdesign Task Dialog menu

Loads

Boundary conditions and initial conditions are applied with the Loads Command Dialog. Items such as velocity, pressure, and temperature are applied to the surfaces of a model in 3D models (to edges in 2D models). We select the units for each boundary and initial condition type. Transient (time-dependent) boundary conditions are also applied and defined in the Loads task.

Mesh Sizes

A mesh has to be constructed which divides the entire geometry into small pieces, or elements. Each element has four nodes, one at each corner. The finite element equations are then solved at each node in the model. This dialog provides tools to automatically define a mesh as well as identify potential problem areas within the

geometry.

Materials

The physical material of each part is assigned with this dialog. A materials database including various fluids and solids is available within the software, and the entries are selected from the name drop menu. Materials can be modified and added to the materials database by clicking on the Create/Edit Material button.

Motion

The definition and specification of solid motion are controlled with this dialog. Several types of engineering motions are supported: linear, angular, combined linear-angular, orbital, nutating, sliding vane, and free motion. All can be defined through user-input, and most can be flow-driven. A Motion Editor is accessed by clicking the Create/Edit Motion button. This dialog allows specification of non-geometric-dependent quantities such as velocity, displacement, or driving or resistive forces.

Options

The physics to be solved in an analysis are set in the Options dialog. The defaults are good for many analyses--flow, incompressible, no heat transfer--but are easily changed if necessary. The Turbulence button allows the user to change the

turbulence model.

Analyze

After the analysis is set up, use this dialog to start the calculation. We set the Analysis mode to steady state (the default) or transient. The results and summary output intervals are also set. Stop the analysis by clicking the Stop button (which replaces the Go button during the analysis).

Review

This dialog contains numerous functions. Before the analysis, it is used to set up monitor points (points in space on which convergence can be monitored). After the analysis is complete, the summary and status files are accessible from the notes tab. These files contain information about the results as well as the analysis. The results tab lists all saved results (and time) steps, and provides a way to include them in an animation. The animate tab animates the results sets made active in the results tab.

Results

The results dialog contains the post-processing functionality. The cutting plane, a 2D slice through the model on which color results and/or vectors are shown, is the primary tool, and is the basis for particle traces, XY plots, and bulk data output. The Iso Surface is a surface of constant value, and is a great way of visualizing flow

and temperature distributions.

Steps for simulation in CFdesign

Following are the steps used to setup the simulation

1. The model to be analyzed is created in ProE. We create the geometry with the guidelines provided by CFdesign. The geometry (design) is imported from ProE into CFdesign. Once the geometry is in CFdesign, the fluid volume is automatically created.
2. We set the analysis units in CFdesign to the once consistent to ProE.
3. Using the Loads task dialog box we apply the boundary conditions to the model.
4. Using the Mesh task dialog, mesh is applied to the volume. We then refine the mesh if needed for the surfaces. We also look for any defects in the geometry, which cannot be meshed.
5. In the materials tab, we apply the materials to the various volumes of fluid. If needed custom materials are created and applied.
6. If the simulation has motion elements we apply motion to the parts.
7. In the options dialog box we define the physics that will be governing the analysis.

8. In the analyze task box, we enter the number of iterations the simulation needs to run. We then hit the “Go” button to start the analysis.
9. We can then review the progress of the simulation with the options available in the Results and Review tabs.

2.5 Economic Analysis

There have been studies involving complex economic analysis which include the social aspects, more comprehensive subsidy analysis and various components addressing the externalities. However, in this study we present a simple economic analysis calculating a levelized cost of energy of our concept system.

In this calculation [9] of cost of energy, the sum of annual fixed costs (mostly capital costs) and annual variable (operating) costs is divided by the annual energy output of the source to give the (average) cost per unit of the energy output. The annual fixed costs are assumed to be distributed uniformly (levelized) over the depreciation lifetime of the equipment and include the interest or equity return required from the initial investment. Variable costs, such as fuel costs and other operational costs, are also assumed to be levelized according to the time value of money over the years. As applied to the conventionally generated electricity, cost of energy is often limited to the power plants and does not then include the costs of transmission and distribution. As such they

are said to be the “busbar” costs of generating plant, meaning they stop at the interconnection point of the conductor to the outside.

The levelized cost of energy (LCOE) method of representing (unit) energy costs is standard in the utility industries for both electric energy (\$/KW-hr) and heat energy (\$/MBTU). This helps in conducting direct comparison between the costs of competing new energy sources and facilitates direct comparisons with the prices of existing sources in the energy markets. Other methods of energy cost analysis are in use, such as life cycle payback and discounted cash flow analysis. But these are more suitable for individual financial decision making, rather than broad market comparison. The outcomes from these various methods are similar as one would not expect a favorable payback from a technology that is clearly not cost competitive in its energy market. The payback period method, however, is able to include regional or other situational factors for a particular case, where the investment decision is being made with marginally competitive conditions and discern an advantage for investment. Most studies of new technologies therefore use levelized cost of energy and we do the same for the system presented in our work [17].

CHAPTER III

LITERATURE REVIEW

Review of the literature indicates that there has been no prior art that combines solar and wind energy as a hybrid system in a way that is proposed in this work. The following literature review was also instrumental in making design changes and in analysis and in finalizing the proposed system design.

3.1 Upgrading the conventional wind turbine

Grassmann [10] and his associates has put forth a theory based on which they claimed that loss in the efficiency of the turbine was because of the air flow which is slowed down and widened. By creating a field of low pressure behind the turbine, this

effect and the corresponding loss in efficiency can be avoided. In order to maintain this low pressure field, the air passing near, but not through the turbine needs to do work. Based on these considerations they made a model of a wind turbine with a wing around it. In [11] they present various fluidodynamical calculations in order to study the resulting increase in power and in order to estimate what the geometrical size of such an apparatus would need to be and whether it could be of advantage compared to conventional devices from an economic point of view. They modeled a turbine with a wing structure surrounding the turbine itself. They were able to predict that that wind energy generated was increased by a factor of two. They claim that the shapes they selected were arbitrary and needed to be optimized further. Grassmann in [12] presented a discussion on the physics of shrouded turbines. Based on his analysis he put forth the idea of partially static turbines, which consists of a rotating propeller and a static element (wing which he used in [10]) to extract energy from an external flow of fluid, which does not pass through the propeller itself. Grassmann validates that the Betz limit can be exceeded by placing a static wing device surrounding the turbine to extract more energy from the wind. In [12] he demonstrates this by a prototype turbine with wing structure surrounding it. In their work they claim the increase in power measured from the device is 55% more for large wind velocities and 100% for small wind speeds. In their experiments they use non optimized propeller blades for the turbine and predicted better results with a more optimized design.

3.2 Diffuser Augmented wind turbines

With the large wind turbine being mostly located away from the point of use, there has been a need for smaller wind turbine for distributed generation for the populated areas. The problem in these areas though, has been low wind speeds, and inability to have giant structures in populated areas. Also the traditional wind turbines with smaller diameters are limited by the power densities at these low wind speed areas. Hence, researchers adopted the diffuser augmented wind turbines to accelerate the wind by using a diffuser around smaller wind turbines. Significant research is being carried out to develop these turbines for installing them on building tops. Hansen [13] and Matsushima [14] in two separate works present the improved effects a diffuser had on the output power of small wind turbine systems. The effect the diffuser's shape had on the wind speed was analyzed by simulation and showed that the wind speed in the diffuser was greatly influenced by the length and expansion angle of the diffuser, and maximum wind speed increased 1.7 times with the selection of the appropriate diffuser shape. They conducted field tests using a real examination device with a diffuser and confirmed that the output power of the wind power generator increased by up to 2.4 times compared to that of a conventional turbine. Moreover, it was confirmed that the diffuser was especially useful where the wind direction was constant. The limitation of transient wind conditions that affect the efficiency of this type of a system will be greatly reduced in our proposed system.

Abe in [15] carried out experimental and numerical investigations of the flow fields for a small wind turbine with a flanged diffuser. They were able to validate that the Betz limit could be exceeded with a diffuser around the turbine. The power coefficient of the diffuser-shrouded wind turbine was about four times as high as that of the bare turbine. Also they mention a notable feature of the diffuser turbine wherein there was a rapid destruction of vortices behind the wind turbine as compared to bare turbine. Bussel [16] revisited the notion of all the wind acceleration theories and experiments and validates that although a much higher power output as claimed by various researchers was not demonstrated, a maximum of 3 times the power coefficient of a regular turbine had been achieved.

3.3 Global Multistage turbines

Ghosh D. and Ghosh S., in [17], have patented a novel idea of a multistage turbine in which multiple stages of stators and rotors accelerate air flow through a tunnel. As wind flow enters the turbine; it accelerates based on area reduction creating a laminar steady flow. They perform a detailed CFD analysis on the system. CFD results show a well designed balance system providing consistent torque in each stage, with high power output. There is increase in velocity through the turbine. They found no secondary flow between the blades and no stagnation was evident in the turbine region. On the contrary, the flow fields follow the profile of the stators and rotor indicative of streamline flow. Figure 19 below shows their proposed system. The comprehensive CFD simulations

showed higher power output from a smaller size turbine. These results have also been shown in Figure 20.

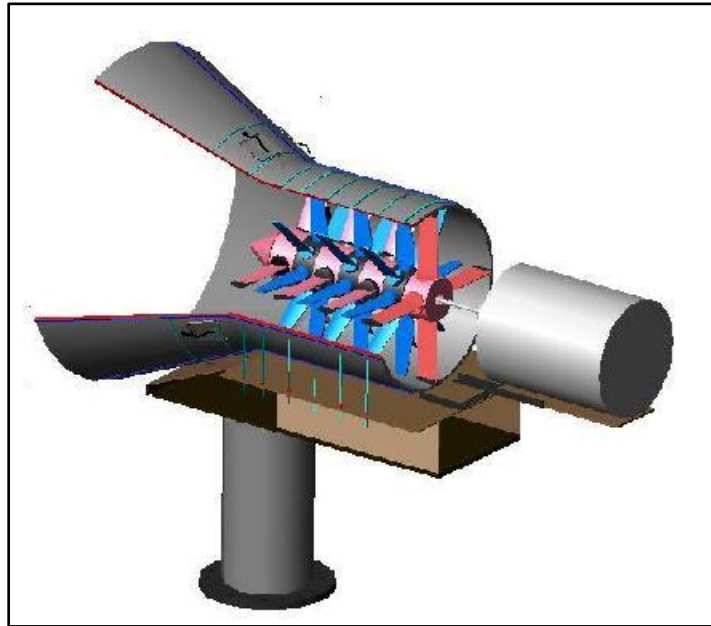


Figure 19: Multistage turbine

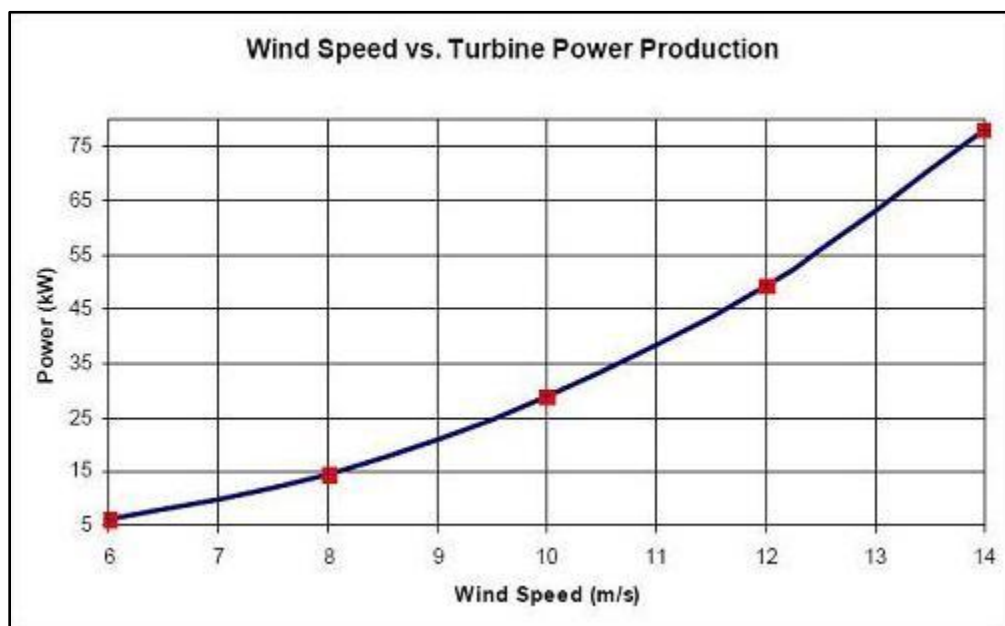


Figure 20: Results for Multistage turbine

3.4 New Generation Solar Concentrators

Dough Wood [18] puts forth the idea of using flat glass mirrors and an aluminum matrix design and creating accurate parabolic concentrator. In his design aluminum rods were interconnected to form a parabolic shape. Flat glass mirrors are then placed on the top part of this matrix frame and a concentrator dish is formed. A uniform flux greater than 1000 suns suitable for high-intensity photovoltaic cells and heating systems can be generated using this concentrator. The advantage of this idea was using less expensive materials to form the solar dish. The materials could be assembled with minimal assistance. In another effort by PhotoVolt Inc., VMJ cells were tested outdoors using this dish and efficiencies around 20% were achieved. The idea has been currently under commercialization by two separate groups. While one of the groups pursues a solar thermal approach the other is pursuing solar-PV effort.

Compact linear Fresnel Reflector (CLFR) is a technology which uses flat mirrors to track the sun and concentrate on a solar-thermal receiver. A secondary heat recovery system then uses this heat to run steam turbines to generate electricity. Compact Linear Fresnel Reflector (CLFR) [19] solar collector and steam generation system, was originally conceived in the early 1990s at Sydney University. It was first commercialized by Solar Heat and Power Pty Ltd. in 2004 in Australia and is now being refined around the world. It is mostly used in utility scale solar thermal power generation system. Ausra, a California based company has been working on rapid commercialization of the

technology. Figure 18 shows a schematic of the CLFR technology. The individual mirrors are rotated around their axes to focus on a thermal receiver.

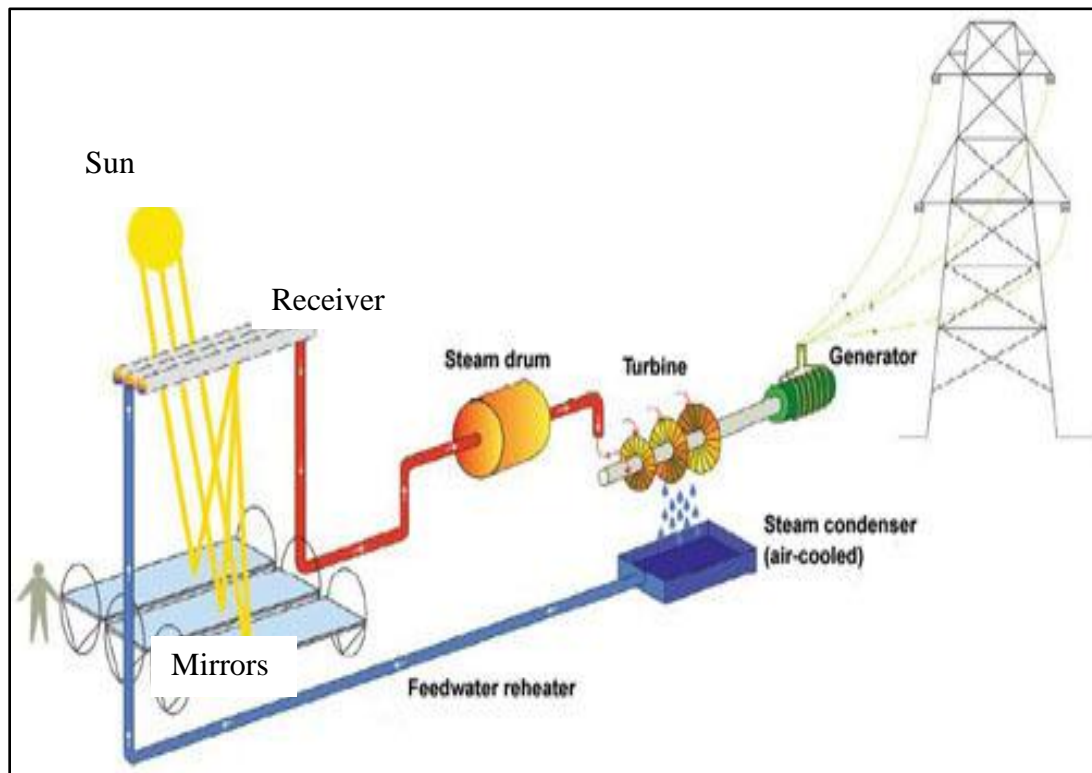


Figure 21: CLFR schematic

CHAPTER IV

PROBLEM FORMULATION

In this chapter a theoretical background to the simulations used to validate the system is presented. The theory in context to our research work related to optical, heat transfer, airflow and economic analysis is described in the following sections. We now look at these individual formulations in detail.

4.1 Optics Calculations

The first of our calculation derives the power generated from our system based on the concentration ratio achieved and the efficiency of the solar cell. The second calculation shows the estimated heat that needs to be rejected from the solar cells receiver.

Concentrated PV power calculations

The total vane area modeled in our design was 10 m^2 . To get the power available from the system we assume AM1.5 solar radiation, which is about 850 W/m^2 and is an average solar radiation for the northern hemisphere at 30° latitude [2]. Most of the southwestern states of Texas, New Mexico, Southern California, and Arizona which have a huge potential of using solar resources are located around this latitude. The VMJ cells efficiency is assumed to be about 20% [6]. The concentration ratio achieved by the system is about 1000 suns. This is because the 10 m^2 concentrator area focuses the light rays onto an area of 100 cm^2 of the receiver surface where the VMJ cells are mounted. Each VMJ sell is about 1 cm^2 . We use these values to calculate the power output of the system.

Solar radiation:	AM1.5 (850 W/m^2)
Concentrator area:	10 m^2
Total Solar Cells area:	100 cm^2 (each cell $1\text{cm} \times 1\text{cm}$)

Concentration Ratio:	1000 suns
Incident Power on Cells:	85 W/cm ²
Concentrator cell:	VMJ (20% eff. @ 1000suns)
No. of Solar Cells:	100
Concentrator efficiency:	0.9
Power Generated per hr:	$85 \times 100 \times 0.2 \times 0.9 =$ <i>1.530 KW</i>

This is the power generated at the receiver by the VMJ cells. We take into consideration the efficiency of the storage system. We use 85% as the efficiency for that. This gives us the power generated in the solar energy mode of ***1.30KW***. In section 6.1 we present the results for the concentration levels achieved at the receiver.

Power flux at the receiver calculations

The device that is used in solar concentrators for the conversion of concentrated solar radiation to energy is the receiver. It is designed to absorb the concentrated solar radiation and to transfer as much energy as possible to the receiver. The receiver can be a heat transfer fluid for solar thermal conversion or high temperature concentrator cells for solar electric conversion. There are various losses at the receiver. There are losses from the fact, that it emits thermal radiation to the environment, because it has an elevated temperature, and there are convective as well and conductive losses [20].

In our system we use solar electric conversion, using VMJ cells. The cells are a 20% efficient and convert part of this total energy into electricity. The rest is available as heat energy and needs to be rejected by cooling mechanism of the solar cells. The heat to be rejected by the receiver can be calculated as Q

$$Q = A_p (\alpha * C * E_s - \epsilon * \sigma * T_{abs}^4 - U_{air} * (T_{abs} - T_a)) \quad (eqn 4.1)$$

Where,

A_p is the receiver area (m^2), 100 cm^2

α is the average absorptivity of the absorber with respect to the solar spectrum, 0.7 for silicon

C is the concentration factor, 1000 suns

E_s is the radiation density of the direct solar radiation (W/m^2), 850 W/m^2 @ AM1.5

ϵ is the average emissivity of the absorber with respect to the black body radiation at the absorber temperature, 0.7 for silicon.

σ stands for the Stefan-Boltzmann constant = $5.67 * 10^{-8} \text{ W/m}^2 \text{ K}^4$

U_{air} is the heat loss coefficient due to convection and conduction. ($W/m^2 K$)

T_{abs} is the temperature of the receiver and T_a is the ambient temperature (K)

Q is the power in Watts

The thermal radiation input from the ambient (with the ambient temperature) to the receiver is neglected.

With an area of 100 cm^2 , the temperature at the receiver is dependent on a number of factors. The absorptivity coefficient α for silicon 250 micron thick is 0.7 [21]. For most materials the absorptivity and emissivity are the same [21]. The convective heat transfer coefficient, U_{air} , of air is $50 \text{ W/m}^2\text{K}$.

For 1000 concentration ratio (C) the temperatures reported to be achieved have ranged from 600°C to 800°C . However, due to the convective and conductive losses and due to the actual placement of the receiver around the focus, the temperatures (T_{abs}) at the absorber (receiver) reported to have been attained are about 400°C to 500°C [22]. In solar thermal systems, this energy is used for generating steam, which can then drive the steam turbines to generate electricity. In our work, this high temperature is detrimental for the efficiency of the VMJ cells, due to their loss in efficiencies with rise in temperature. This efficiency drop of the VMJ cells was explained earlier in section 2.3.

From equation 4.1 we can get the power flux (W/m^2 or W/cm^2) that is incident on the receiver surface and not available for electricity conversion. This heat needs to be rejected from the receiver to keep the VMJ cells at operating temperatures. The values used in the formula and the power values obtained are shown in Table I.

TABLE I: OPTICAL CALCULATION PARAMETERS

Parameter	Value
A_p	0.01 m^2
α	0.7

E_s	850 W/m^2
C	1000
ε	0.7
U_{air}	50 W/m K
σ	$5.67 \cdot 10^{-8} \text{ W/m}^2 \text{ K}^4$
T_{abs}	450° C
T_a	25° C
Q	558256.9741 Watts
<i>Power flux</i>	55.82 W/cm^2

The value obtained from the theoretical analysis shows the flux that is available at the receiver surface. In our system where we have VMJ cells the thermal energy needs to be rejected, so that the cells can perform efficiently. The available heat can also be used for secondary recovery of heat. This value of heat power is used as a basis for simulating our heat rejection system.

4.2 Heat Transfer Calculations

In this section we present formulae used to calculate the heat transfer from the fluid to cool the VMJ cells. The cells will be mounted onto a receiver which will be cooled by the fluid flowing through the heat exchanging mechanism. Although the final receiver design will need a more comprehensive study of the heat exchanger to be used or

designed, we present here a preliminary analysis based on the models found in literature [23]. These formulations used are for analyzing internal heat transfer process for flow through pipes. In our model be approximate the entire heat exchanging mechanism to be a rectangular channel of fluid column flowing over a receiver plate on which, heat flux is incident. The dimensions for the heat exchanger components used in these formulations are consistent with the ones used in the CFD analysis of the model in CFdesign. The cooling plate is 20cm by 20cm rectangular area. The rectangular duct is of 16cm by 6cm of inlet area. We present the formulae used for analyzing forced convective heat transfer for flow through pipes in turbulent regime. It is the closest approximation to our model. In our design, the flow of water is through a rectangular channel, cooling the VMJ receiver. This is an approximation to a real life scenario of water flow through pipes over the receiver. The basic convective heat transfer equation [23] is as follows:

$$Q = U_{overall} * A_{rec} * (T_{rec} - T_{\infty}) \quad (eqn\ 4.2)$$

Where,

Q = Total heat incident on the area (W)

$U_{overall}$ = Overall heat transfer coefficient ($W/m^2 \text{ } ^\circ K$)

A_{rec} = Heat transfer area of the receiver surface (m^2)

T_{rec} = Steady state temperature attained at the heat transfer surface ($^\circ K$)

T_{∞} = Temperature of the cooling fluid ($^\circ K$)

In our design, we have conductive heat transfer taking place from the side of incident heat flux to the inner wall of the pipe and a convective heat transfer between the fluid and receiver surface. These two modes of heat transfer can be observed from the schematic of the cooling mechanism shown in Figure 19. There is conduction taking place through the thickness of the copper plate and convection taking place between the copper plate and the fluid flowing through the pipe.

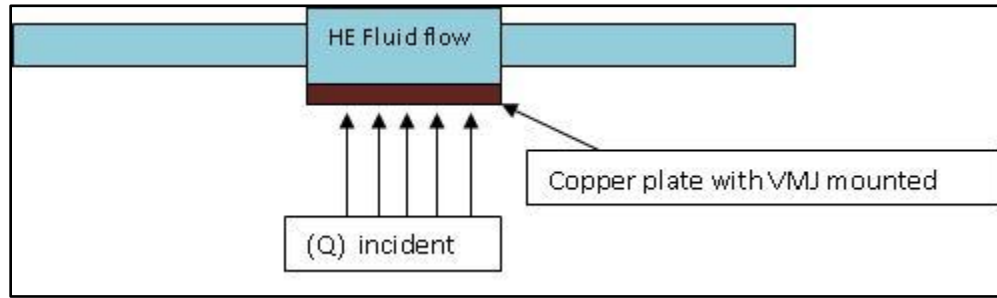


Figure 22: Cooling system schematic

Thus, the overall heat transfer coefficient is:

$$U_{\text{overall}} = U_{\text{conductive}} + U_{\text{convective}}$$

$$U_{\text{overall}} = \frac{1}{\frac{tw}{Kcu} + \frac{1}{h}} \quad (\text{eqn 4.3})$$

Where,

U_{overall} = Overall heat transfer coefficient

$U_{\text{conductive}}$ = Conductive heat transfer coefficient

$U_{\text{convective}}$ = Convective heat transfer coefficient

$t_w =$	Thickness of copper plate in the direction of conduction (m)
$K_{cu} =$	Thermal conductivity of copper (W/m ^{°K})
$h =$	Heat transfer coefficient of water flow through the pipe (W/m ² °K)

The heat transfer coefficient of fluids depends on the type of flow (turbulent or laminar), viscosity of the fluid and its velocity. Over years there have been various theories have been proposed and methods adopted to find these values. In [23] we find a detailed compilation of these methodologies. These methods use various dimensionless numbers that characterize the flow to find the approximate solution to the problem. We list the formulae for turbulent flow through a pipe mentioned in [23] that we use to calculate the heat transfer through the system. These formulations are have an error of 20-30% associated with them.

$$h = \frac{(Nu_{Dh} * K_{water})}{D_h} \quad (\text{eqn 4.4})$$

$$Nu_{Dh} = \frac{\frac{f}{8} * (Re - 1000) * Pr}{1 + 12.7 * \sqrt{\frac{f}{8}} * (Pr^{\frac{2}{3}} - 1)} \quad (\text{eqn 4.5})$$

$$f = \frac{1}{(1.82 * \log_{10} Re - 1.64)^2} \quad (\text{eqn 4.6})$$

$$Re = \frac{U_{av} * D_h}{\nu} \quad (\text{eqn 4.7})$$

$$Pr = \frac{C_p * \mu}{K_{water}} \quad (\text{eqn 4.8})$$

$$\dot{m} = \rho * A_c * U_{av} \quad (\text{eqn 4.9})$$

Where,

Nu_{Dh} = Nusselt number based on the hydraulic diameter

D_h = Hydraulic diameter. For rectangular pipes $D_h = 2ab/(a+b)$, a and b being the sides of rectangular cross-section at fluid entry.

K_{water} = Thermal conductivity of water (W/m °K)

f = friction coefficient

Re = Reynolds number for the fluid flow

U_{av} = inlet bulk velocity (m/s)

ν = Kinematic viscosity of fluid (m²/s)

Pr = Prandtl Number

μ = Dynamic viscosity of fluid (N-s/m²)

C_p = Specific heat (J/kg°K)

ρ = density of fluid (kg/m³)

A_c = Area of cross-section of the inlet (m²)

\dot{m} = mass flow rate of the cooling fluid

Using the heat flux incident to be 55 W/cm^2 and the formulations presented above we plot the temperatures attained at various flow rates of cooling fluid. We perform the heat transfer simulations in CFdesign and they are presented in section 6.2

We use these formulations (eqn's 4.2 to 4.9) to predict the temperatures for various flow rates of water and ammonia. The total heat transfer surface is a copper plate with an area (A) of 0.08 m^2 . The copper plate thickness (T_w) is 2mm. The thermal conductivity (K_{cu}) of copper is 380 W/mK . The rectangular cross-section of the pipe has sides of 0.16m and 0.06m. Hence the hydraulic diameter (D_h) is 0.08727m. We list the constants and other properties of water and ammonia used for the calculation in Table II below. The kinetic and dynamic viscosities of the fluids are temperature dependent properties. In the table the properties are at 25°C temperature. These values are consistent with the model designed in ProE and used while setting up the simulation in CFdesign.

TABLE II: CONSTANTS AND VALUES USED FOR THEORETICAL MODEL CALCULATIONS

	Water @25 °C	Ammonia @25 °C
Thermal conductivity (W/mK)	0.59	0.521
Kinematic viscosity (ν) (m^2/s)	1E-6	3.6E-7
Dynamic viscosity (μ) (N-s/ m^2)	9.0E-4	2.2E-4
Density (ρ) (kg/m^3)	998	611.75
Specific heat capacity (C_p) (J/Kg $^\circ\text{C}$)	4068	4798

The total heat input on the copper surface used is 11000W. Of the 400 cm² (20cm by 20cm) surface area of the receiver, we assume that the area of 200 cm² around the center of the plate will be the region of interest where the VMJ cells are mounted. The total area of VMJ cells will be about 100cm² – 100 cells of 1cm² each. We use the total heat input equal to 11000W. This is the value obtained from the power flux calculations from Section 4.1 (55 W/cm²) multiplied by the area of interest (200cm²). We now plot the final temperatures achieved at various mass flow rates for water and ammonia entering at a temperature of 25°C. Figure 23 below shows the plot for the steady state temperature (T_f) that can be achieved for various flow rates using the equations listed in this section.

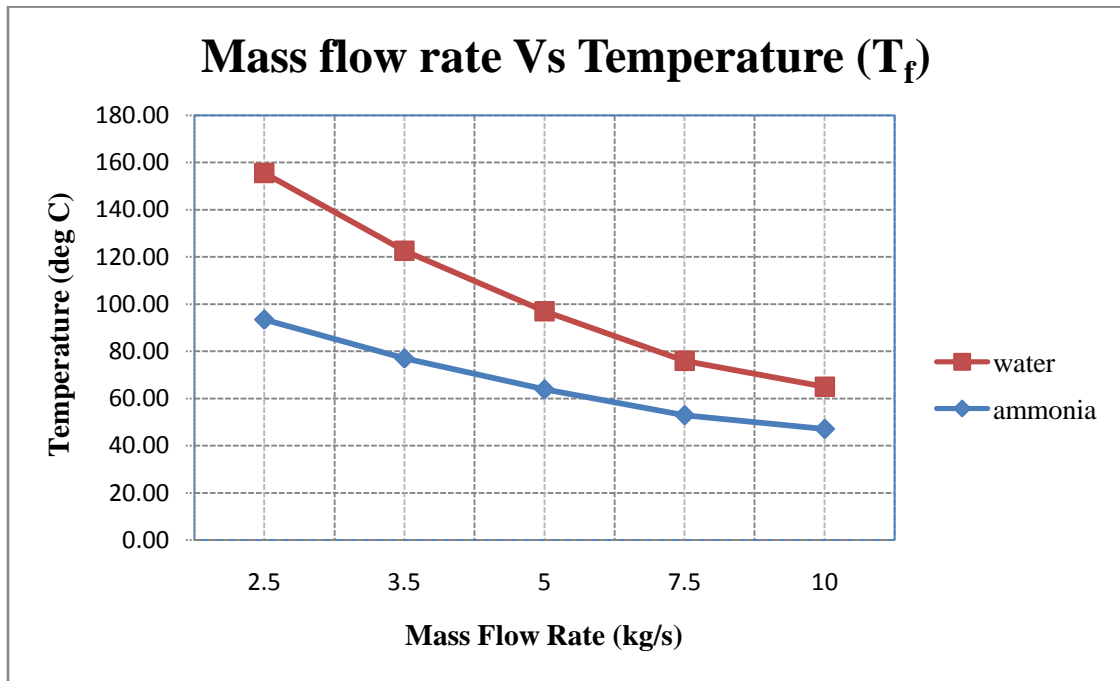


Figure 23: Steady state temperature T_f from the theoretical model of HT design

4.3 Wind energy calculations

Wind power is a measure of the energy available in the wind. It is a function of the cube (third power) of the wind speed. If the wind speed is doubled, power in the wind increases by a factor of eight. This relationship means that small differences in wind speed lead to large differences in power.

The amount of power available in the wind is determined by the equation

$$\text{Wind Power } (W) = \frac{1}{2} * \dot{M} * (\text{velocity})^3 \quad (\text{eqn 4.10})$$

Where,

\dot{M} = mass flow rate over the rotor with area A_{rotor} .

Velocity = velocity of air in the wind tunnel onto the turbine rotor

Now,

$$\dot{M} = \gamma * A_{\text{rotor}} * \text{velocity}$$

Therefore from equation 4.10 we get

$$\text{Wind Power } (W) = \frac{1}{2} * \gamma * A_{\text{rotor}} * (\text{velocity})^3 \quad \dots \dots \dots (\text{eqn 4.11})$$

Where,

Wind power is measured in watts; A_{rotor} is the area swept by the rotor of the turbine; velocity of the air onto the turbine is measured in m/s.

Assuming at sea level the density of air is 1.24 kg/m^3 we get

$$\text{Wind Power (W)} = 0.62 * A_{\text{rotor}} * (\text{velocity})^3$$

This is the maximum power available in the wind. The maximum electrical energy the rotor can extract out is limited by the Betz limit factor of 59%. In practice the conversion efficiencies of wind turbine rotors are much less than the Betz limit. Optimally designed rotors reach levels slightly above 40%. Energy is also lost in transmission, generators, and power conditioning. When running at their rated output – where they are designed to operate best – generator efficiency can be above 90%. But wind turbines drive their generators at the rated output infrequently.

The overall energy conversion efficiency can be summarized by the equation below:

$$(Overall)_{\text{eff}} = (Rotor)_{\text{eff}} * (Transmission)_{\text{eff}} * (Generator)_{\text{eff}} * (Power\ conditioning)_{\text{eff}}$$

$$(Overall)_{\text{eff}} = 0.4 * 0.9 * 0.9 * 0.9$$

$$(Overall)_{\text{eff}} = 0.2916$$

Hence the amount of electricity generated will be

$$\text{Wind Power (W)} = 0.62 * A_{\text{rotor}} * (\text{velocity})^3 * (Overall)_{\text{eff}}$$

$$\text{Wind Power (W)} = 0.62 * A_{\text{rotor}} * (\text{velocity})^3 * 0.2916$$

$$\text{Wind Power (W)} = 0.1808 * A_{\text{rotor}} * (\text{velocity})^3 \quad (\text{eqn 4.12})$$

To use our set up as a wind energy harnessing device, the air flow would accelerate through the system, generating power. In section 6.3 we perform the simulations to validate this accelerating effect. We work from our concept system presented in this section towards a refined model based on the simulation results and recent developments found in literature.

4.4 Economic calculations

Levelized cost of energy

The Levelized unit cost of energy (LCOE) can be expressed in the following manner

$$LCOE = LRR / \text{Annual energy output} \quad (\text{eqn 4.13})$$

Where,

LRR is the levelized annual required revenue.

$$LRR = LCC + LAE + O\&M \quad (\text{eqn 4.14})$$

In this expression, LCC is the levelized cost of capital (initial capital multiplied by the fixed-charge rate (FCR); LAE is the levelized annual operating expenses (including fuel, variable operational and maintenance charges); and O&M is the fixed operation and maintenance charges. The initial capital is the investment cost, as laid out at the time of construction or installation of the energy plant.

$$LCC = \text{Initial Capital} \times \text{Fixed charge rate (FCR)} \quad (\text{eqn 4.15})$$

The FCR is customarily levelized using a discount rate, either market derived for private sector projects or a social discount rate for public projects. If taxes are not included the FCR reduces to the capital recovery factor (CRF) used in standard financial formulae.

$$CRF = \frac{i(1+i)^n}{(1+i)^n - 1} \quad (\text{eqn 4.16})$$

Where, i , is the annual interest rate or rate of return and n , is the depreciation lifetime in years. A detailed calculation and analysis for the proposed system based on the LCOE method is shown in section 6.4.

CHAPTER V

RESEARCH METHODOLOGY

The objective of this work is to validate the techno-economic feasibility of using the proposed concentrator system described in section 1.2 in two modes; to function as a solar collector in solar energy mode and as wind speeding device in wind energy mode. To this end we used 3D modeling software to design the concept system. The concept system was then researched using simulation software for optical, heat flow and air flow analysis. The economic analysis of the system is presented with a levelized cost of energy (LCOE) calculation. Being a validation study of the new concept, as well as the first step towards designing a refined system, it was necessary to follow design, analysis and improve methodology. Figure 21 shows the tools and iterative process used for the concept refinement and validation. The study herein presents a first order analysis of the system using the optics and CFD software. The critical components of the system

studied were the power available by optical concentration for solar energy harnessing, heat to be rejected by the VMJ cooling system and the air flow through the system and the wind turbine.

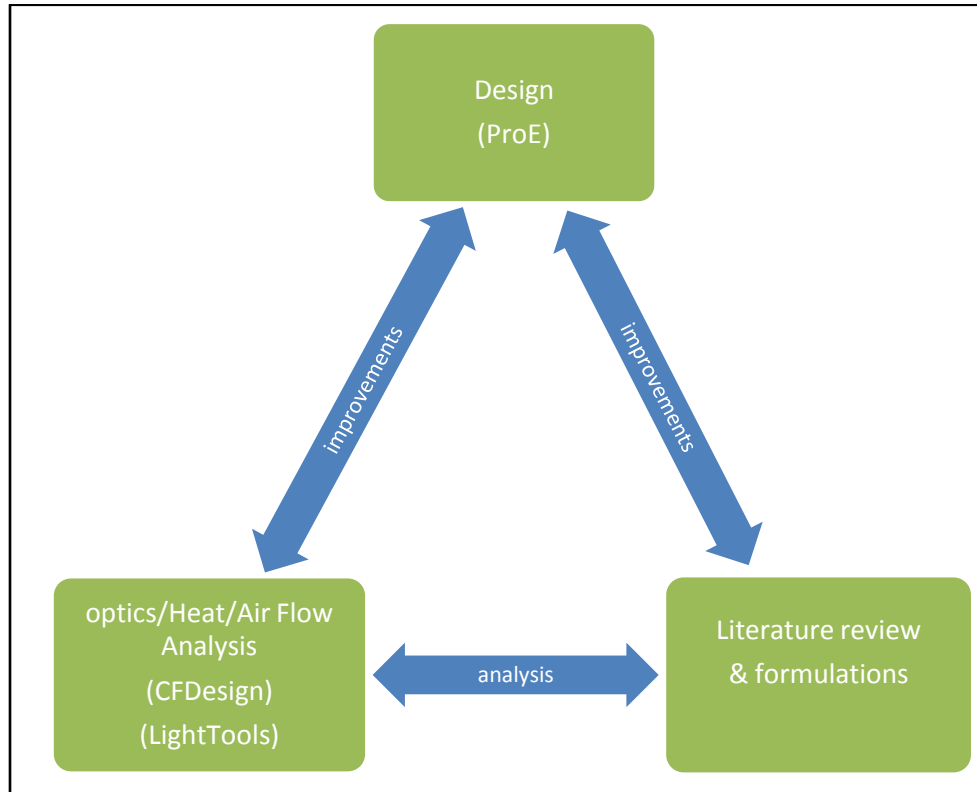


Figure 24: Concept refinement Approach

The basic concept system was first designed in ProE. To study and analyze the different components of the system, their design was modeled in ProE and then exported to the simulation software. The simulation software selected was able to import the modeled assembly and we could analyze the components using the capabilities within the software. To study the optical concentration achieved, the vanes designed in ProE were exported to the LightTools 5.40 optics software. The effective shape formed from the

vanes was analyzed using simulations. The results of simulations showed the power density distribution at the receiver. It was also used to verify the results from theoretical calculations of the power available from the concentrator. The calculations gave the heat that need to be rejected from the receiver to maintain lower temperatures.

For analyzing heat rejection designs, we used CFdesign software. We ran simulations for different flow rates and made necessary design changes to obtain lower temperatures. Design changes were performed by observing the heat rejected in the simulations. First a copper plate was used as the receiver and the temperature achieved was observed. CFdesign imports the 3D model from ProE and creates the fluid volume and the mesh required for analysis. We then apply the boundary conditions to the model and perform the simulation. Upon observing the results, we made modifications to the design in the ProE model of the receiver and follow the iterative process. As a second design 10 fins, 5mm thick and 3.8cm high were added to increase the heat transfer area. Upon reviewing the results it was necessary to create a third design in which a total of 24 fins, each 2mm thick and 4.8 cm high were added to the plate. This increased the heat transfer area between the heated surface and the cooling fluid. We present the analysis of the three receiver designs. Simulations were performed for two types of cooling fluids, water and ammonia. Water being the most commonly used cooling fluid was used in this work. Ammonia is one of the most commonly used industrial solvent. Using ammonia to cool VMJ cells can be thought of as a primary heating process of the solvent using solar energy and could be part of a process plant. We present the results of simulations of the three designs in section 6.2.

To study the air flow through the system, a similar approach to the one used in heat transfer simulation is followed. The model is imported from ProE into CFdesign, an air volume is created and the simulations are performed. The boundary conditions are then set on the model for the simulation. The shape of the tunnel allows the air to accelerate as it passes through the system. The airflow simulations are shown in section 6.3. The concept refinement took place with an iterative design analysis and improvement method, based on inputs from the simulation as well as theory related to the matter found in the literature. Finally in evaluating the cost of energy of the proposed system, a levelized cost of energy method is used. The total amount of energy that can be generated by the system during the year and the levelized annual cost of operating and maintaining the system over its life period is computed in section 6.4.

The methodology adopted for analyzing the system in the simulation software is presented in the sections to follow. We first look at the 3D modeling approach adopted for the system and then look at the method of setting up simulations in LightTools and CFdesign.

5.1 3D Model of the system

ProE is one of the most advanced 3D modeling software used in the industry. One of the aims of this work was to work towards a manufacturing model. One of the few constraints imposed while making changes to the model based on the study work was to have a modular design. The earlier schematic of the proposed system in which the solar concentrator was formed by individual vanes and a wind turbine housed in a wind tunnel is shown in Figure 25.

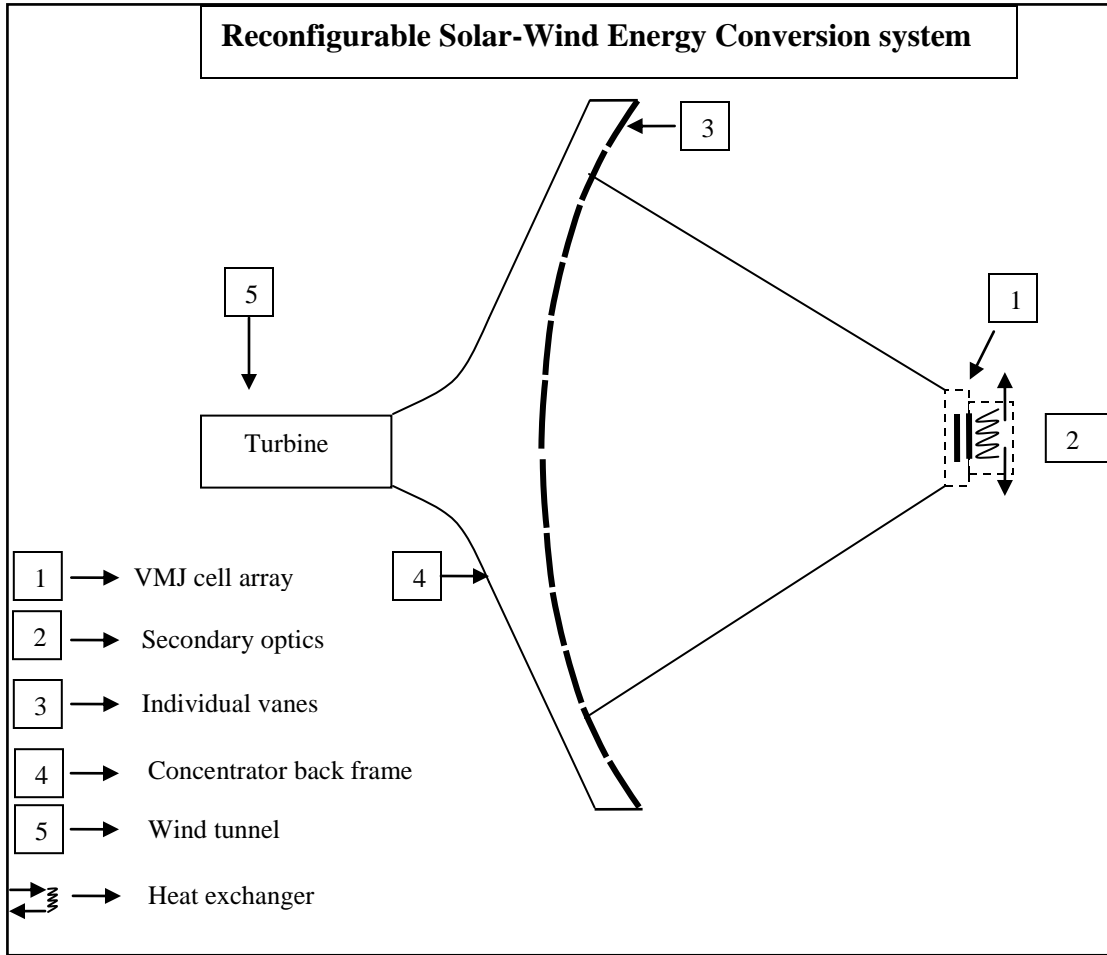


Figure 25: Schematic of the concept system

The study was to refine this concept and analyze for its technical feasibility. For this we would to import individual parts into the LightTools and CFdesign software for optics and CFD analysis. The three main components to be analyzed were the concentrator formed with the individual vanes, the heat transfer mechanism and the air flow through the system.

The methodology adopted while designing was that of top down designing where in the overall outline of the system components were defined by a skeleton model in ProE. This approach helped to make any changes in the individual parts of the system without affecting the dependencies. The outline was primarily the 10 m² of vane area, the rectangular frame that housed it, the funnel transition for airflow into the system, the tunnel housing where the turbine was to be placed. We defined sketch planes as the external limits for the overall system. The individual parts were then created by using these planes as reference. Figure 26 shows the skeleton model of our system. Any changes to be made in the model for instance, changing the diameter of the tunnel, the length of the tunnel, the transition shape, etc could be done easily without affecting the overall system outline. This helped in incorporating the design changes that were based on the simulation results.

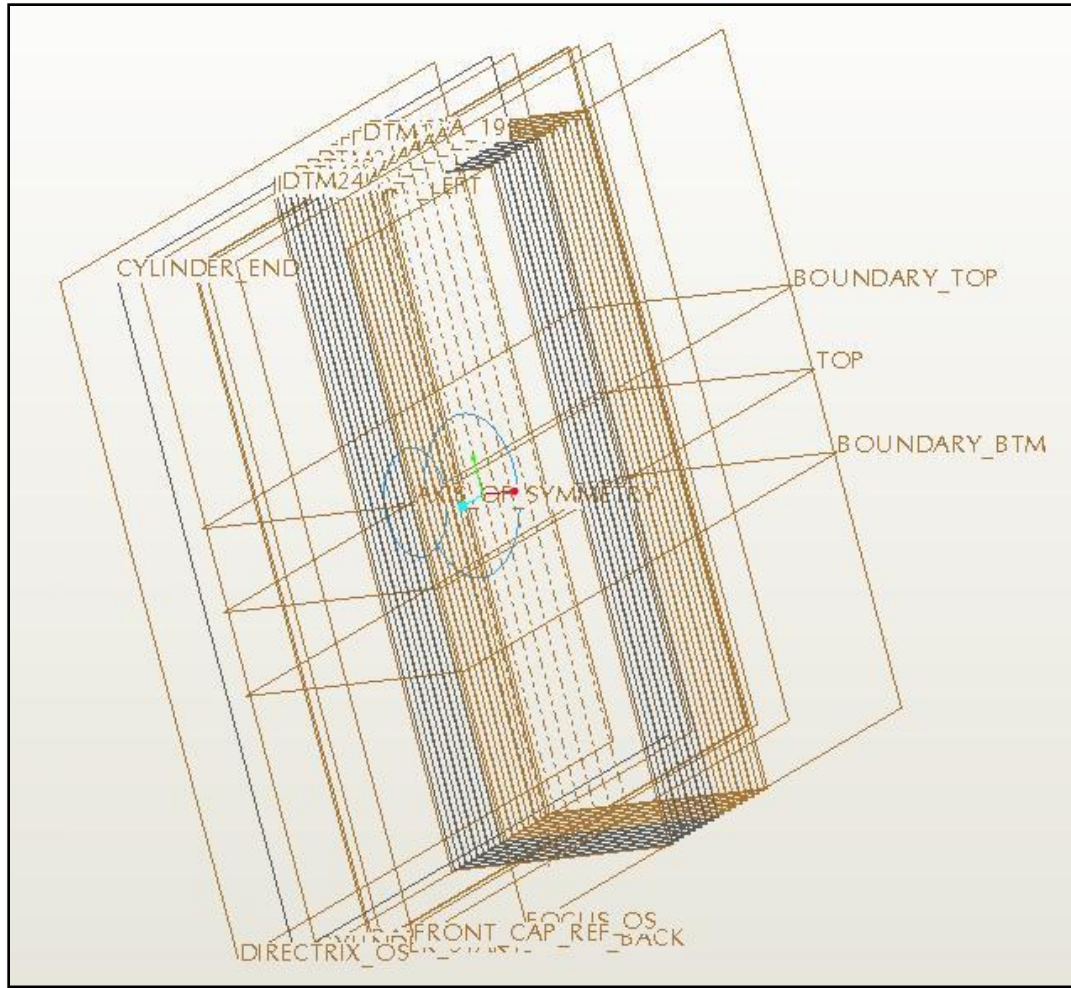


Figure 26: Skeleton model in ProE

The three main components of the system that were studied were the concentrator formed with individual vanes, the funnel transition and turbine housing and the heat transfer mechanism. The vanes and the funnel parts were designed as part of a single assembly. The concentrator vanes were modeled so that they could be rotated along their axis while importing into CFdesign for airflow simulations. The vanes were created using a complex parabolic surface and extruding individual mirror elements. The total

area of the vanes was 10 m^2 . The heat transfer system was designed as a separate assembly. The receiver was an individual part. We could make the necessary design changes to the receiver after analyzing the heat transfer simulations. The concentrator vanes were exported to the optics software for optical analysis. The receiver for the optics analysis was placed at the focal point and was designed in the LightTools software. To analyze the airflow through the system, all the parts except the heat exchange mechanism was exported to CFdesign. To analyze the cooling of the receiver, the heat exchange mechanism was modeled separately and exported to CFdesign.

5.2 Optics Simulations Methodology

The aim of the optics simulation was to validate the design of a parabolic concentrator with individual vanes to give the desired concentration. In addition, we want to observe the flux distribution on the receiver. We also performed a validation experiment for the accuracy of the tracking system. To perform these simulations the components imported into LightTools from ProE were the vanes, through an IGES data exchange module. Once in LightTools we were able to give individual vane surfaces mirror properties. Figure 27 shows the window of vane model imported into the software.

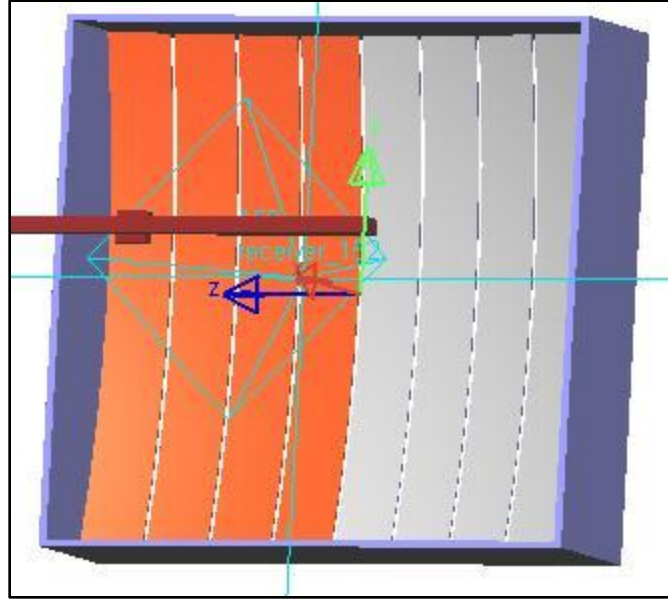


Figure 27: Vane assembly imported in LightTools

Once the vanes are in the LightTools software, we give the curved surfaces optical mirror properties. We use 90% reflectance for the mirrors. We assume the tracking system to accurately follow the sun. Hence, it was assumed that the light source was a collimated source. The light source is a rectangular block 3.3m by 3.3m area, with one of the surface given the light source properties. This assures that the light is incident on the entire vane surface. The light source is collimated. We use radiometric units to configure the power of the source so that we observe the W/m^2 incident at the vane surface.

We insert two cylindrical blocks that represent the receiver (VMJ) mounting and the heat transfer tubes of the system. This was necessary to observe the shadow effect of the receiver mounting on the concentrator. A block of 20cm by 20cm is added as the

VMJ receiver and a rectangular block 15cm wide and 3.2m in length is added to obstruct the incident light simulating the obstruction caused by a solar load in concentrator systems. For simulation set up we placed two surface receivers in the model for the illumination simulation results. One was on a dummy surface at the reflecting vanes and the other was on the 20cm by 20cm receiver block. The components used in simulation are shown in Figure 28.

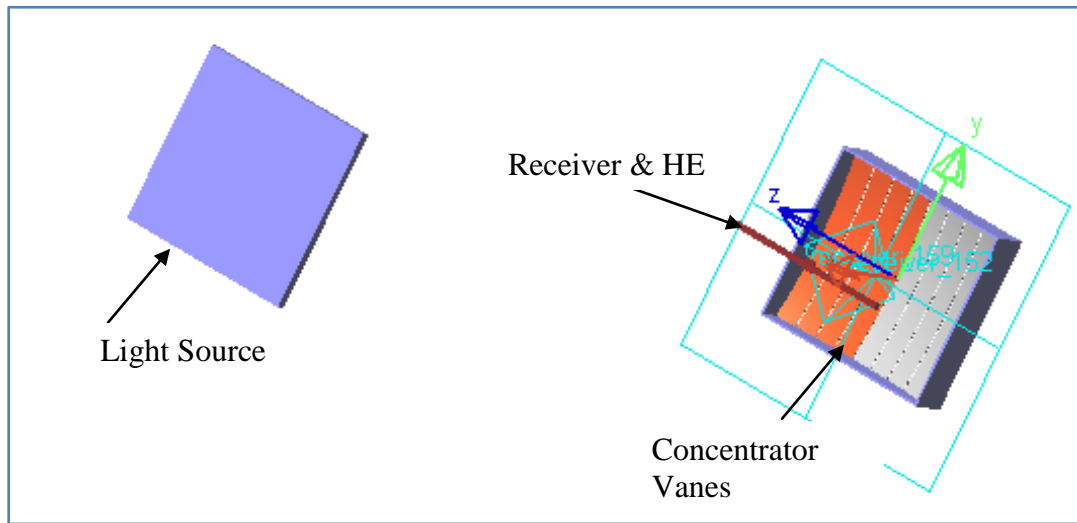


Figure 28: Components for simulation in LightTools

To simulate the solar irradiance at earth's surface

The receiver and the heat exchange block were placed near the focus. The exact distance of the light source was found out by the first experiment, which was to stimulate the solar irradiation at the earth surface. For this experiment, the distance and the radiometric intensity of the cylindrical light were varied to find the distance at which we

get AM0 (1000W/m^2) and AM1.5 (850W/m^2). Figure 29 shows the schematic of the elements used in simulation and parameters to be varied in the optics software.

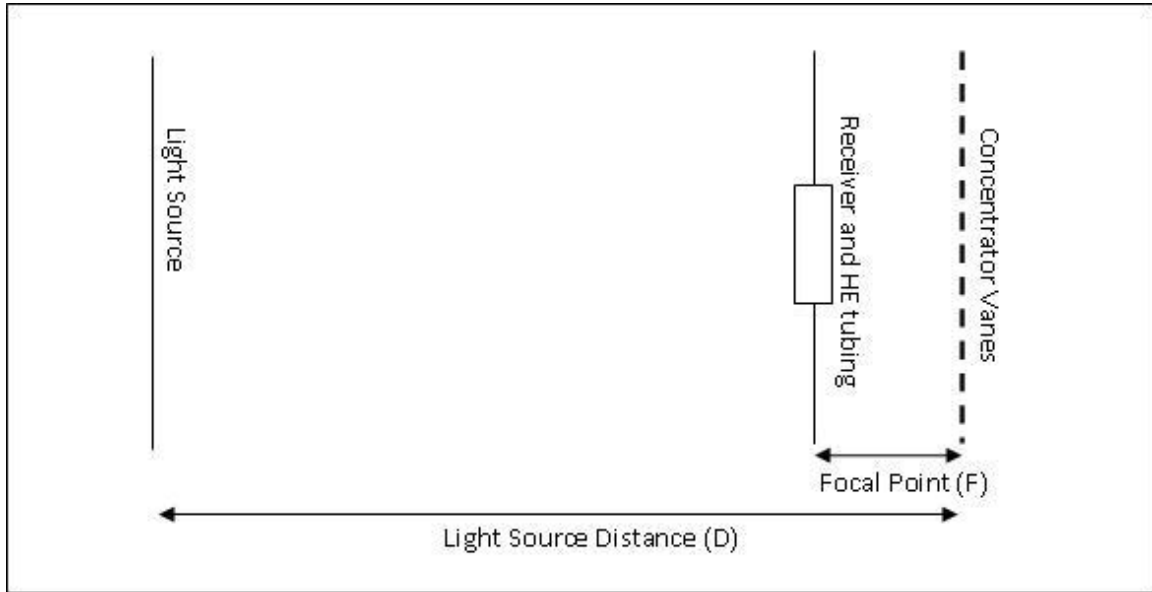


Figure 29: Schematic of experimental setup in LightTools

To find the optimal receiver distance from the focus

The objective of this simulation was to find the possible placement of the receiver in the concept system. In these simulations the receiver block was moved away from the focus at a distance of 25 mm, for each simulation. The focus of the parabola formed by the vanes was at 3.20 m. We performed analysis for the receiver located at a distance of ± 10 cm around the focal point.

To verify the accuracy required by the tracking system

Traditionally in concentrator systems, high cost tracking system is looked upon as one of its drawbacks. But over the years with the development of the drive technology, it has no longer being looked upon as a cost disadvantage. However with even small errors lead to a significant reduction in ability to harness power. The objective of this simulation was to validate the effect of tracking system errors. This experiment was aimed to view the distortions in the optical concentration achieved at the receiver, due to the errors and also observe the tolerances within which these systems need to operate. To simulate these effects, we change the angle of the incident light source with the concentrator at 0.5° intervals. The receiver is placed at a constant location for all simulations which is selected from experiment 2.

5.3 Heat Transfer Simulations Methodology

The objective of these simulation experiments was to achieve temperatures at the receiver which are within the operating ranges for the cells. Although VMJ cells have performed well at really high temperatures, the nominal operating temperature for the cells is 25 C. After this temperature there is degradation in the efficiency of the cells. In order to operate at higher efficiencies it is therefore needed to maintain lower temperatures at the receiver. In the optical calculations mentioned in section 4.1, we saw that the temperatures at 1000 suns concentrations were about 450 C. We had calculated the heat flux incident at the receiver surface that needs to be dissipated. We use 55 W/cm² as the heat flux incident on the receiver. These heat transfer simulations present a first order analysis of achieving this heat dissipation.

The simulations were carried out in CFdesign software. The methodology adopted was to simulate a heat exchange mechanism between a cooling liquid and the copper plate acting as the receiver. It is at this receiver, the VMJ cells would be mounted. The fluid pipe was a rectangular aluminum tube. The assembly modeled was the rectangular pipe with the copper plate in the center. The inlet dimension for the rectangular duct is 0.16m by 0.06m. The length of the pipe was 1.2m. The copper plate was a separate part in the assembly. Figure 30 shows us the assembly model of the heat transfer mechanism. The figure shows the first design of a simple copper plate used as a heat exchanging surface.

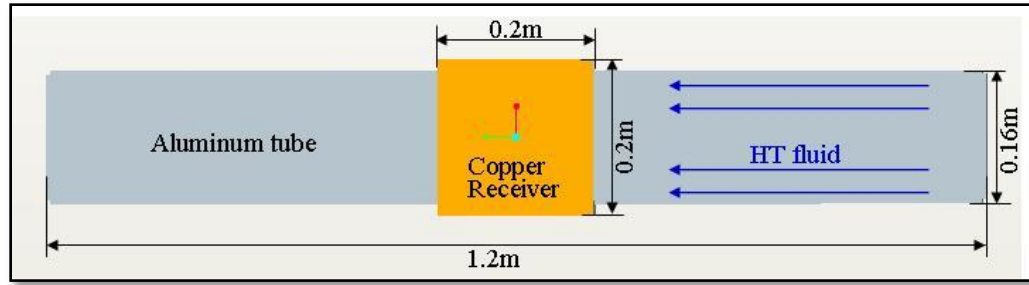


Figure 30: Heat transfer mechanism assembly

The model was imported from ProE and CFdesign created the fluid volume for analysis. Based on the results of temperatures achieved at the receiver we made changes to the copper plate part and repeated the process. To attain the desired temperatures we underwent an iterative process to get results from three different receiver designs. Using the simple heat exchanger principle of adding more heat transfer surface area for heat exchange, we added fins to the copper plate. The three designs are shown in Figure 31. In addition to the changes made at receiver, we also use ammonia in addition to water as the heat exchanging fluid. The results are shown in section 6.2.

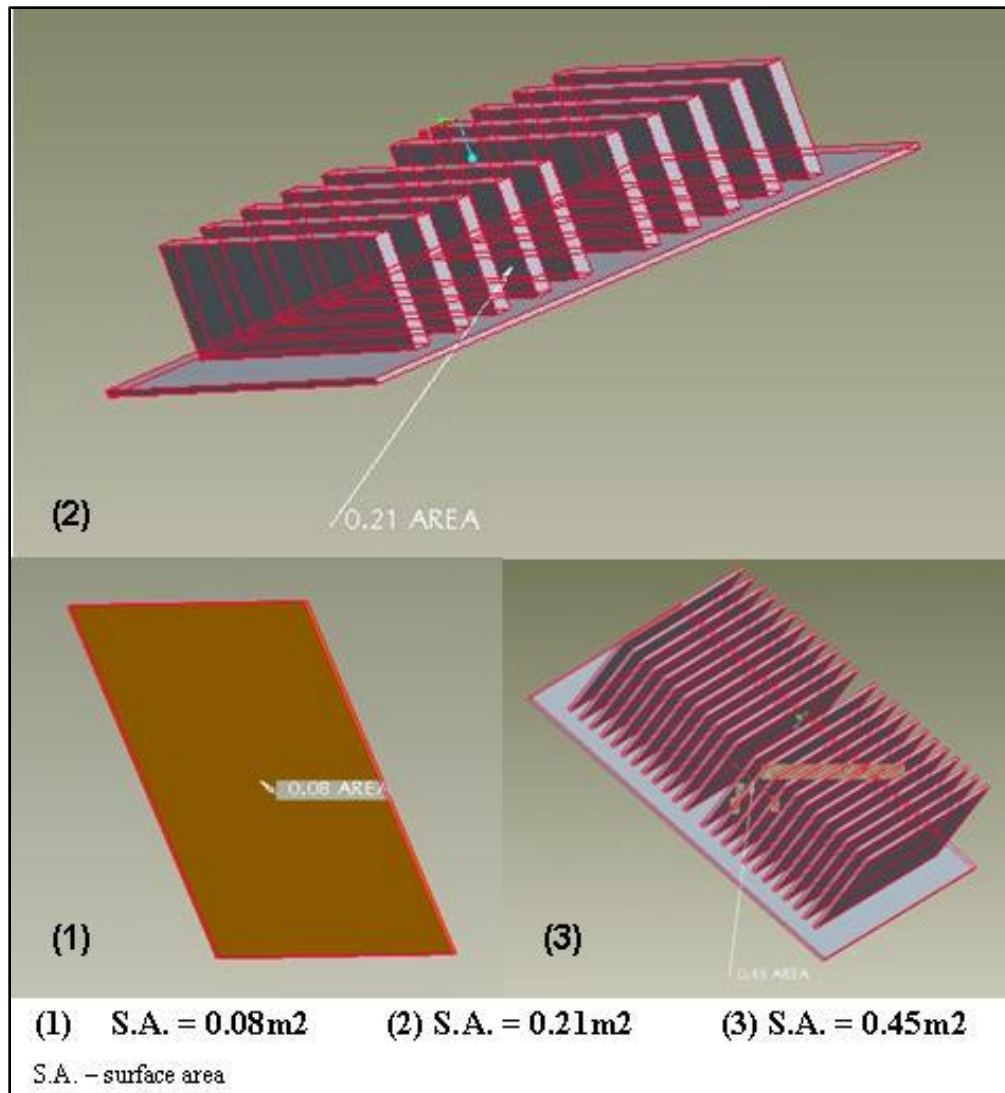


Figure 31: Three receiver designs used for HT simulations

We now go through the procedure for setting up a simulation in CFdesign. CFdesign was also used for airflow analysis, and the procedure mentioned below was followed while performing the simulations.

Step 1: Importing from ProE

Once the modeling is complete we select the CFdesign tab from the Applications menu in ProE as shown in Figure 32, to export the model into CFdesign. One of the important steps while modeling and exporting is to have consistent units in both the software. In our simulations we use MKS system.

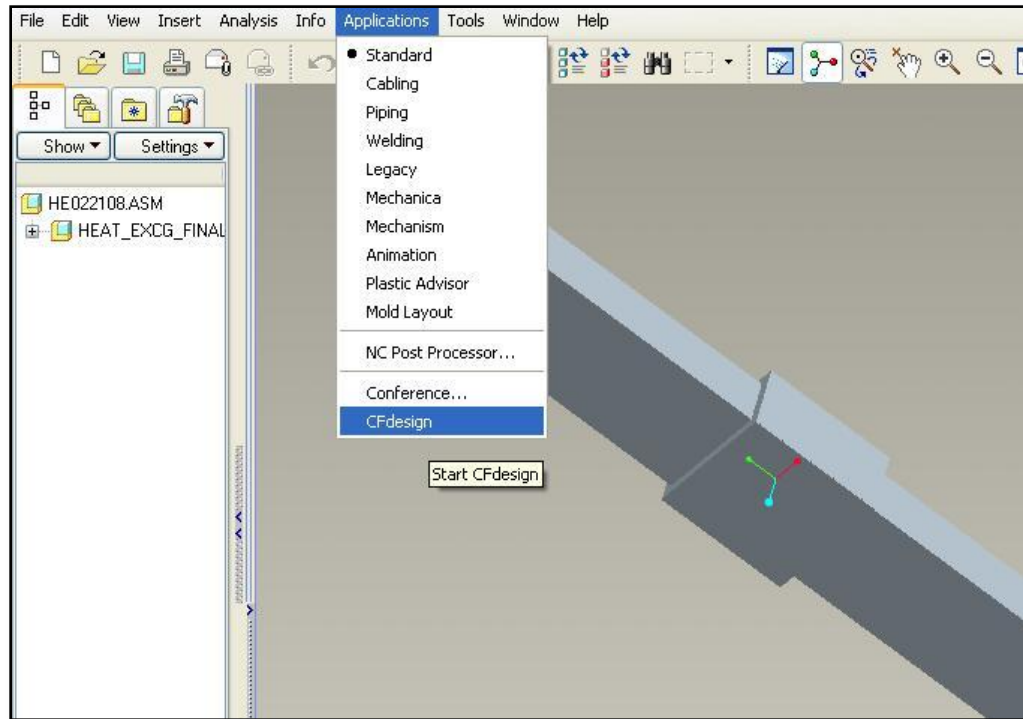


Figure 32: Exporting model from ProE

The total model is divided into different solid parts. The fluid volume is generated in CFdesign and it forms another part of the model. We can select and hide individual parts. Figure 33 shows the imported model into CFdesign. In the heat transfer mechanism model shown, the receiver and the fluid volume are currently hidden. This

enables the user to hide the individual parts and assign materials, boundary conditions and investigate the model post analysis.

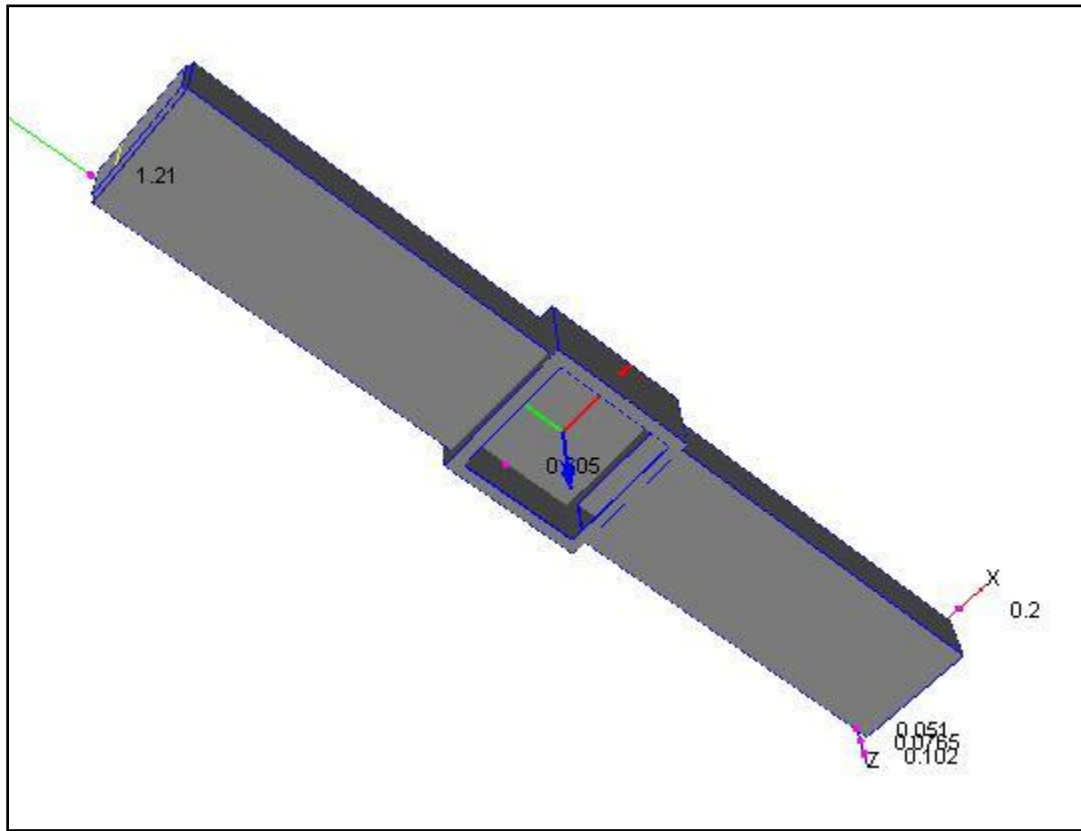


Figure 33: Imported model in ProE

Step 2 : Meshing the model

By using the mesh tab all the different volumes get meshed. We can also refine the mesh using the various functionalities in mesh tab. Meshing tab also helps in investigating any geometry issues associated with the model. If there are any irregularities in the imported model, CFdesign flags the issue. In order to investigate the

mesh, we then run a single iteration of the simulation and look at the meshing quality. Figure 34 shows a meshed heat transfer model.

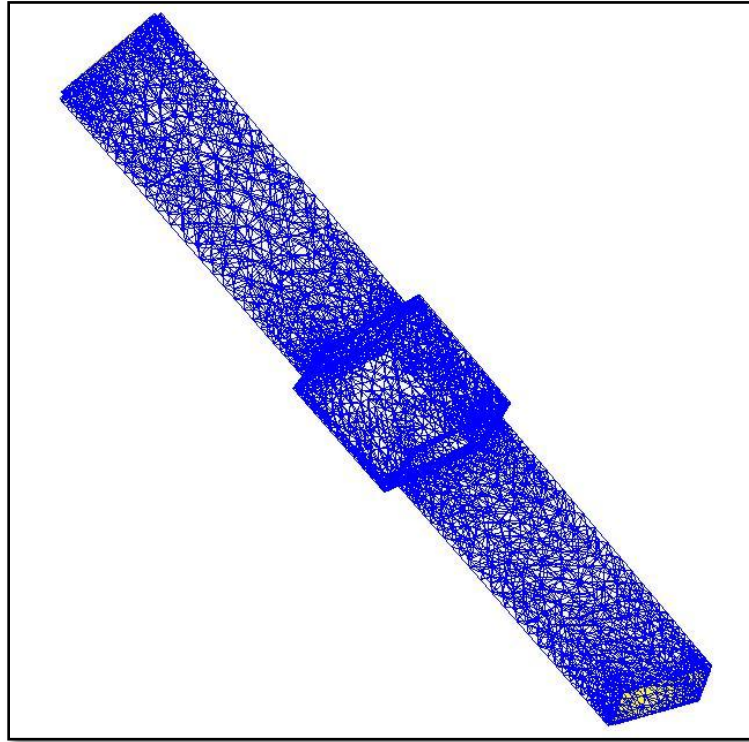


Figure 34: Meshed model in CFdesign

Step 3 : Assigning boundary conditions

In this step we select the individual surface where we want to assign the boundary conditions. We assign the inlet fluid temperature and mass flow rate, the heat flux incident on the receiver and the pressure boundary condition at the outlet. Figure 35 shows the boundary condition of 3 kg/s of mass flow rate being applied to the inlet. The

figure also shows the boundary condition task dialogue and the various options available in the tab.

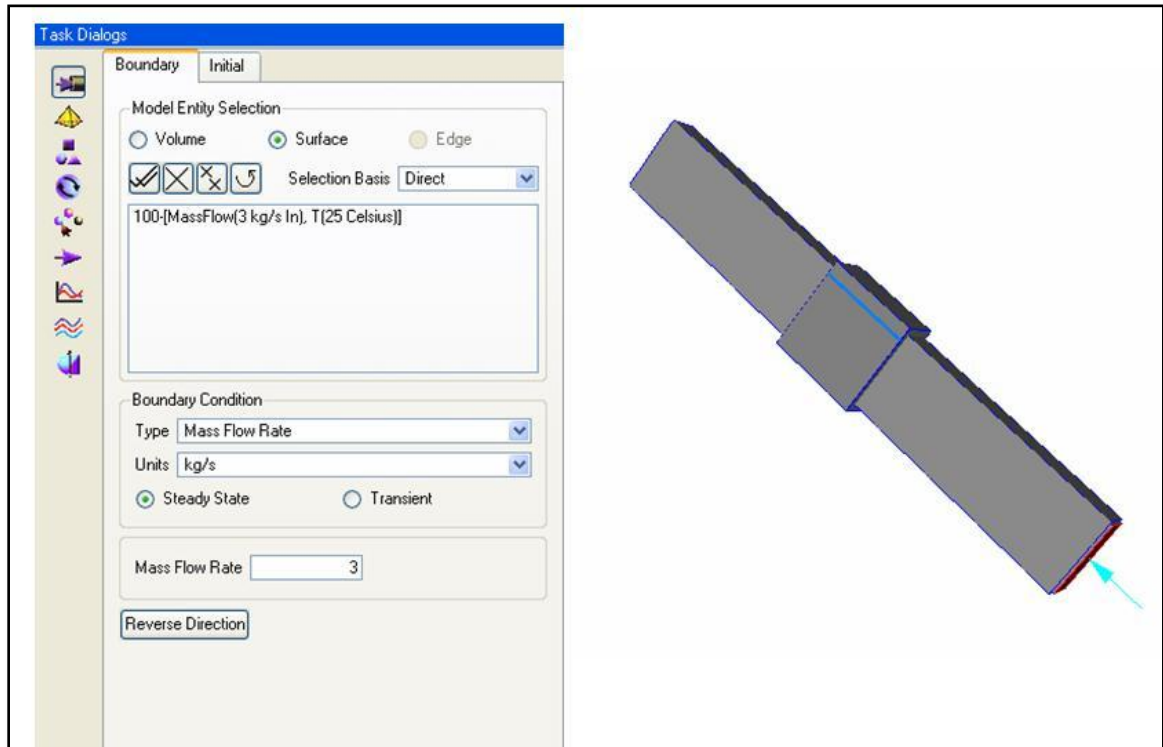


Figure 35: Assigning boundary conditions in CFdesign

Step 4: *Assigning materials*

The next step for the simulation is to assign materials to the different parts in the model. As the imported model in CFdesign is composed of discrete parts we assign the materials to them from the available database. We could also create custom materials but within our scope of work, it was not necessary. A selection of solid, fluid and gaseous

materials is available. Figure 36 shows the model with the materials tab. In the figure, we see the blue water column for heat exchange fluid and the brown copper material for the receiver.

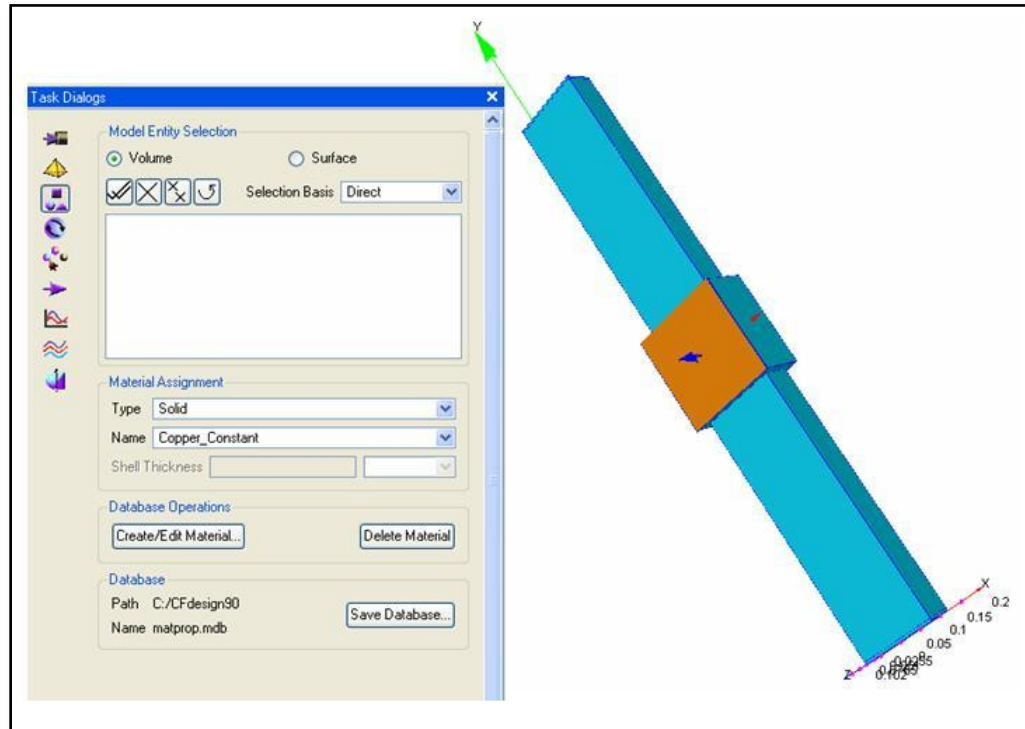


Figure 36: Assigning materials in CFdesign

Step 5: Options for the simulations

In the options tab, we set the type of analysis we want. We opt for incompressible flow for our simulations and also turn the heat transfer on. An option for staged forced convection is also available. Using this option the software first runs the simulations for

the fluid flow and once the flow is steady or solution converged, it then runs additional 10 iterations for the heat transfer calculations. We have used this setting for most of our simulations as they help to reduce the simulation time. Figure 37 below shows the options selected for one of the simulation

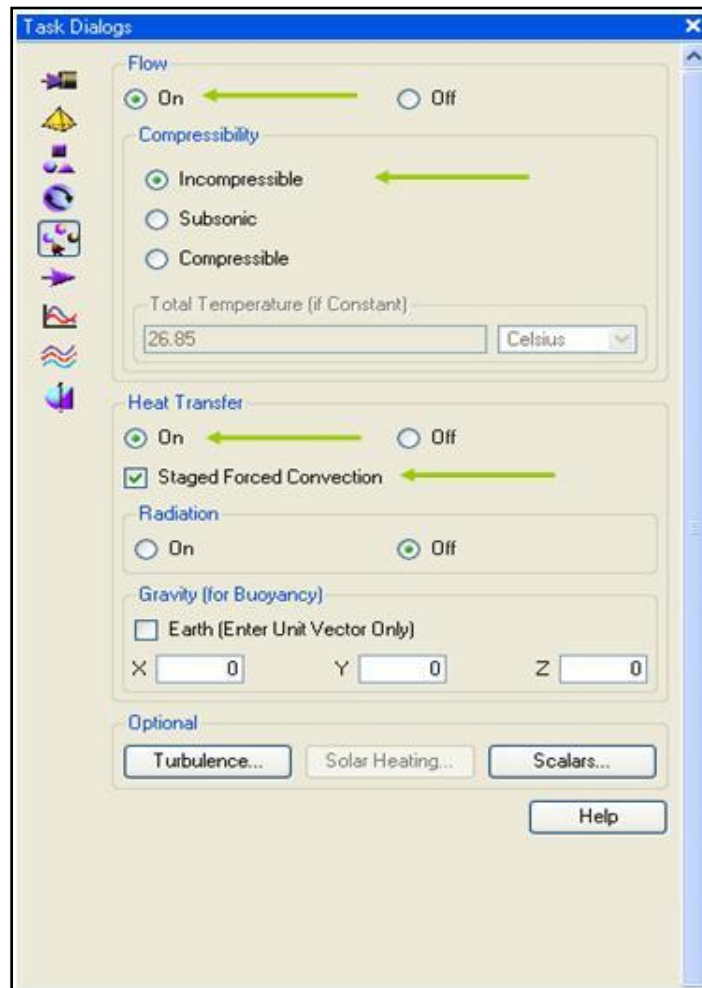


Figure 37: Simulation properties in CFdesign

Step 6: Starting the simulation

In the analyze tab we set the number of iterations for the analysis to take place. Since the software has an auto convergence detection algorithm the method adopted for our simulation was to run the simulation for 600 iterations. Most of the heat transfer simulations converged before 600. We also set the number of results we want to save. We save the simulation results every 50 or 100 iterations to get the animated view of simulation. They were useful to view the airflow analysis once the simulation was over.

If we use the staged forced convection option, the last 10 iterations perform the temperature analysis. In this case the temperature visualization is ineffective for heat transfer simulations. While the simulation is running we look at the convergence plot that runs on the bottom part of the screen. We can observe the convergence of various parameters of the CFD simulation. The analyze tab with the settings for the simulation is shown in Figure 38. Figure also shows the convergence monitor at the bottom of the screen.

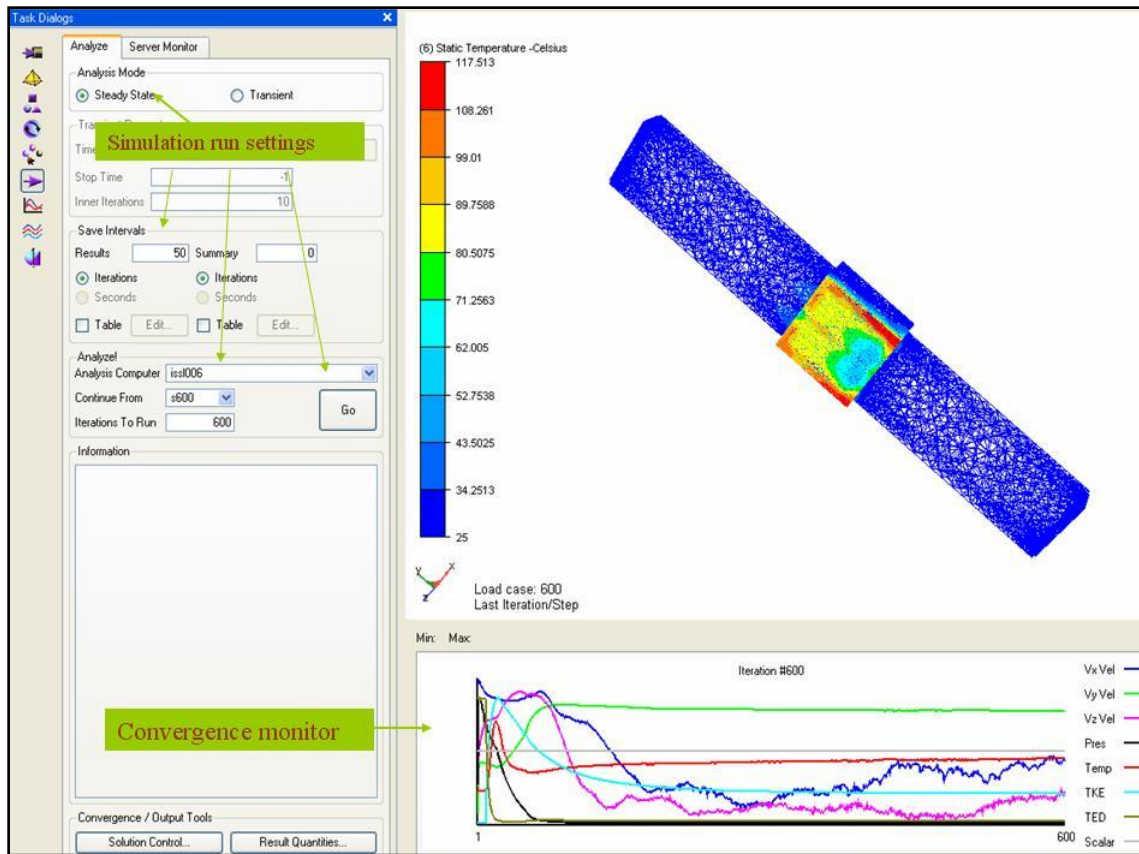


Figure 38: Analyze tab in CFdesign

Step 7 : *Reviewing results*

Once the simulation is complete we look at the results tab and review the results. There are two task dialogues available for analyzing the results. In the first dialogue box we can look into the summary of the analysis as well as see animations from the saved results. Various text and excel files are also created with the data. In the summary tab we get the summary of the analysis. In the second task dialogue we can add cross-section planes on the parts and investigate the various parameters like temperature, velocity etc.

We can also add trace to observe the flow of the particle in the design. The two dialogue boxes are shown in Figure 39.

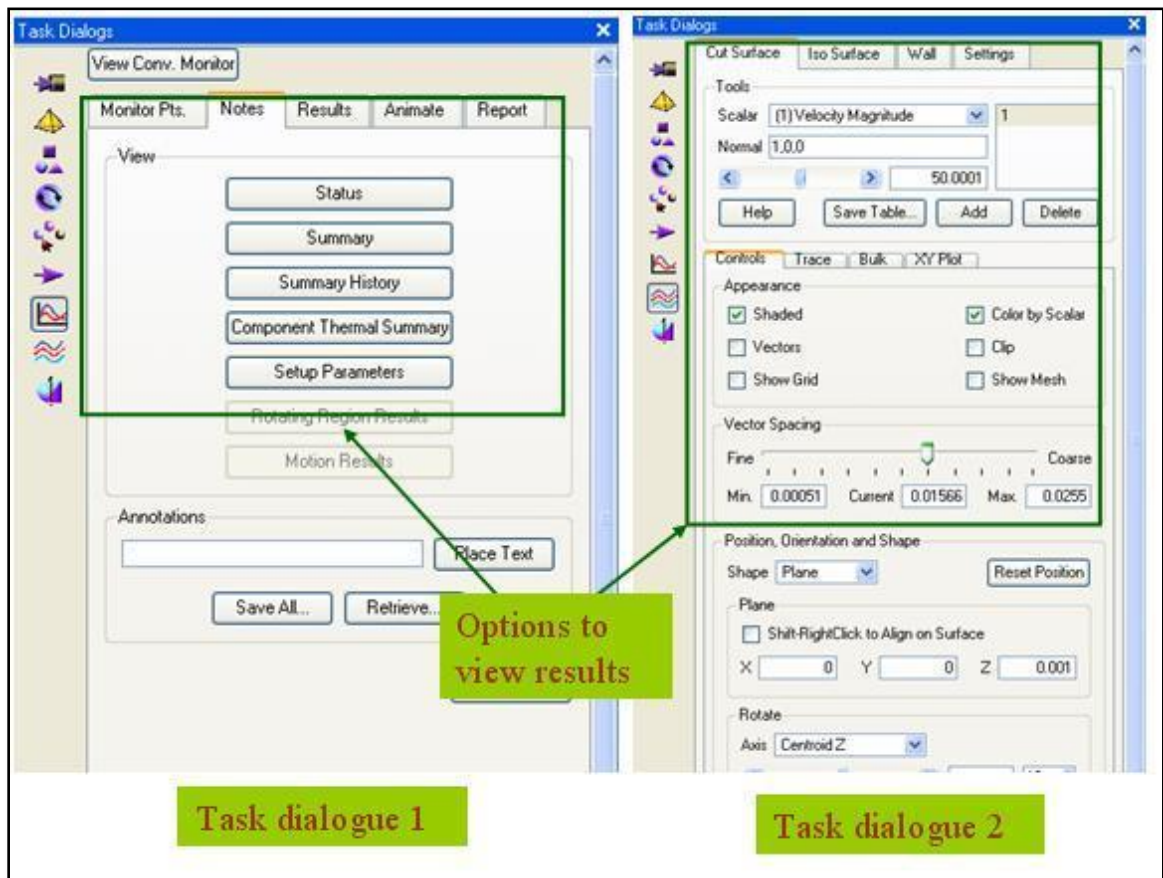


Figure 39: Results task dialogues in CFdesign

5.4 Airflow Simulations Methodology

The first step for simulations was to model the concept design compatible for importing into CFdesign. As CFdesign creates the fluid volume for analysis, it is necessary to add necessary features in ProE to accommodate for it. Hence any model designed had to have an enclosed volume for analysis. For our analysis we did not include the receiver design, as it was not necessary for simulations and also would add computation time for what wasn't needed. For the fluid volume generation, we created a rectangular hollow block that would house the entire assembly. As such, in CFdesign, a fluid volume was generated subtracting the assembly from the hollow block. A wireframe image of a model exported to CFdesign for analysis is shown in Figure 40. The rectangular block was designed generated a fluid volume, enough to have an upstream and downstream air flow. The boundary conditions for inlet wind speed and outlet pressure were applied depending on the direction of air flow.

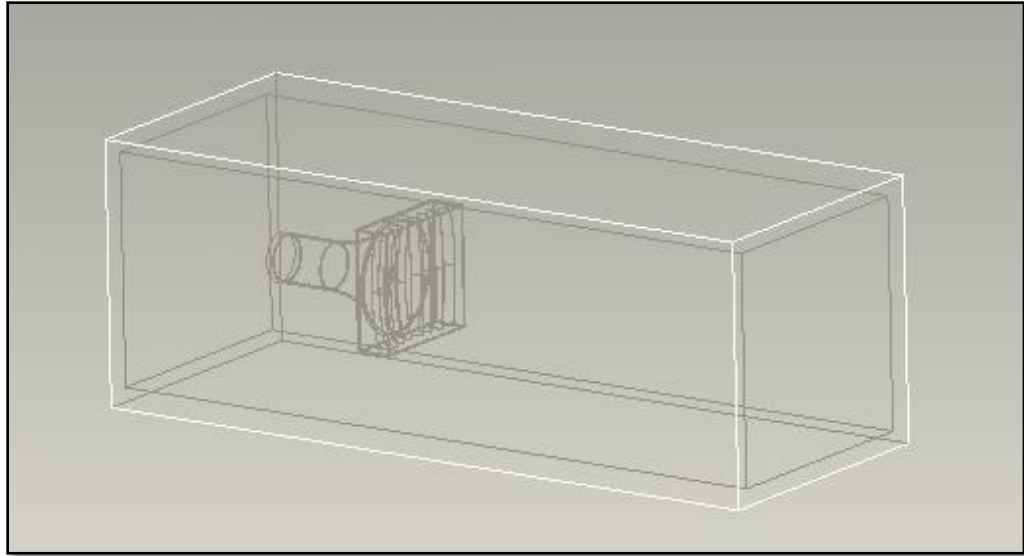


Figure 40: Model exported to CFdesign

In our first analysis observed the effect of the vanes for airflow. For this we imported only the vanes in CFdesign. The vanes were rotated by 80 degrees and offered minimum obstruction to airflow. The analysis observed any obstruction in flow caused by the vanes. The results of the simulations are shown in section 6.3.

Once the flow through the vanes was analyzed, the next important component in the system was the funnel transition and the tunnel. It was important to observe the flow of air through the system. The airflow through the concentrator back frame and the tunnel housing for the turbine were analyzed. We investigated the airflow from both sides; from the vanes side and the tunnel side. The reason for investigating airflow from the tunnel side, was to use the system as a diffuser following the ideas of references [1-7]. The simulation results of airflow from the back frame and tunnel and the current development of the multistage turbine [14] found in literature it became clear that it was

necessary to design a small wind turbine. Also a smaller tunnel length decision was based by taking into consideration the overall system design manufacturability. With longer lengths it would be problematic for the tracking system to rotate the system while tracking the altitude axis of the sun. Hence we designed the small length, larger diameter tunnel with a small turbine housed in it. We also added air diffusing slots in the concentrator back frame, to facilitate the air flow through the system. The reason for this was primarily, the stagnation achieved in the previous simulations and also the reason that, the air flow was observed occurring around the system. Figure 38 shows the design and dimensions of the small turbine. The turbine was not optimized, and was created using simple features in ProE. A small hub and six turbine blades were designed in the baseline model of the turbine. The tip of the hub was placed to face the oncoming wind.

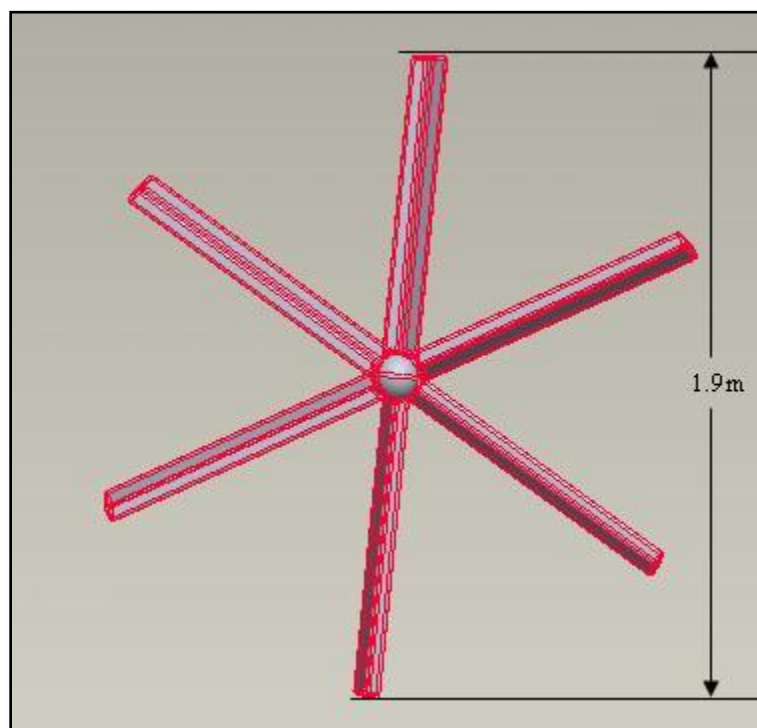


Figure 41: Turbine modeled in ProE

For the simulation with the wind turbine, the set up is shown in Figure 39. To observe the motion of the turbine, we added the three motion regions in our model. Transient analysis option was selected from the CFdesign options tab. We selected auto time option, as the software calculated, the time step needed for each iteration. However, with the complex design of the system, the transient analysis option and the limited computation power available with the PC, the simulation was stopped after a brief period of simulation time. It resulted in a total of $4.258\text{E}+8$ seconds (5 days) of machine time for the course of the simulation. It was however, necessary to observe the convergence plot and the results available from the simulation.

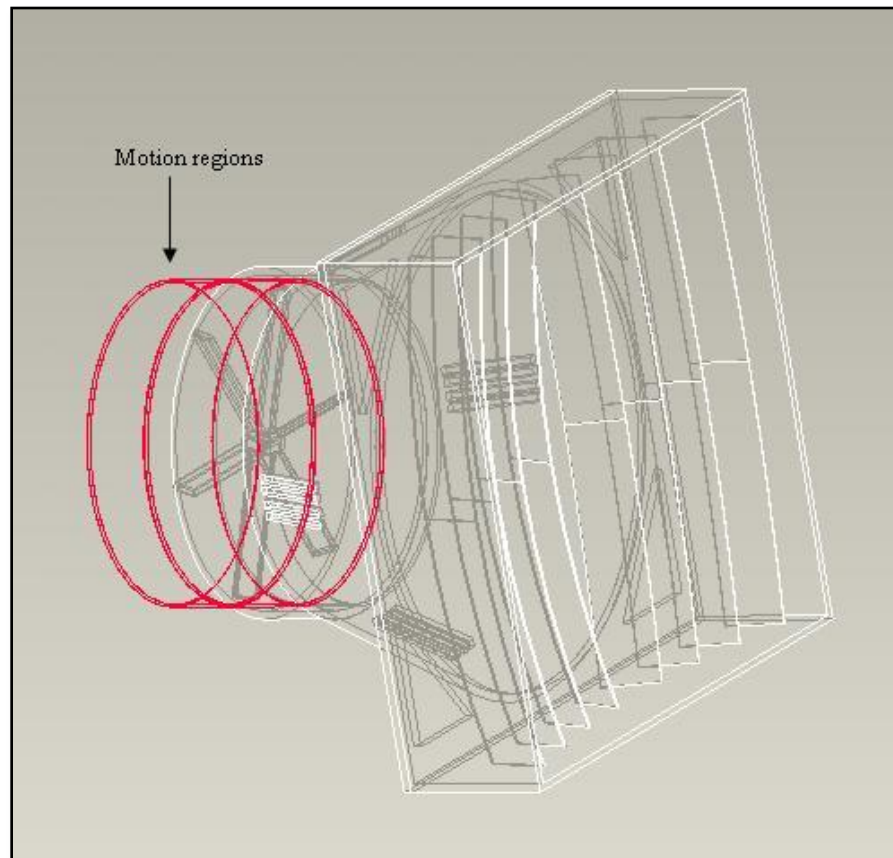


Figure 42: Simulation model with turbine

To investigate the system to be working as a diffuser, the airflow was incident from the tunnel side of the system and flowing out through the vane side. The only simulation setup change for these simulations was the turbine was flipped around, so that the pointed hub faced the incident wind. The boundary conditions were applied on the necessary side. Other parts of the system remained unchanged. Again due to the limited computation power, the simulation was terminated within a brief period of simulation time. The results of wind speed through the turbine were in congruence with those found in literature.

CHAPTER VI

RESULTS

In this chapter we present the results obtained from the simulations. The methodology for the experiments was presented in chapter V. First presented are the Optics, heat transfer and airflow simulation results. We then describe a refined model of the concept system. The results of the levelized cost of energy are shown at the end of this section.

6.1 Optics simulation results

EXP 1 : To simulate the solar irradiance at earth's surface

As the first analysis we wanted to simulate the solar irradiance that is incident on the concentrator vanes. To find the irradiation of AM1.5 at the concentrator vanes we varied the distance D of the light source from the vanes. We varied the power of the light source and its distance from the vanes surface to achieve this. The simulations were carried out using trial and error method so that we get a uniform irradiation at the vane surface of 10 m^2 , comparable to the light incident from the sun onto the concentrator. The uniformity of the incident light falling on the surface can be visualized from the illuminance chart displaying the light intensities falling on the surface receiver. These charts are available in LightTools results. Figure 43 shows the irradiation of AM0 and AM1.5 at the vanes obtained from the simulations. The figure shows a uniform flux of about 1000 W/m^2 at AM0 and 850 W/m^2 at AM1.5 achieved by using a light source at a distance of 35m from the vane surface and with 3600W and 3500W incident power.

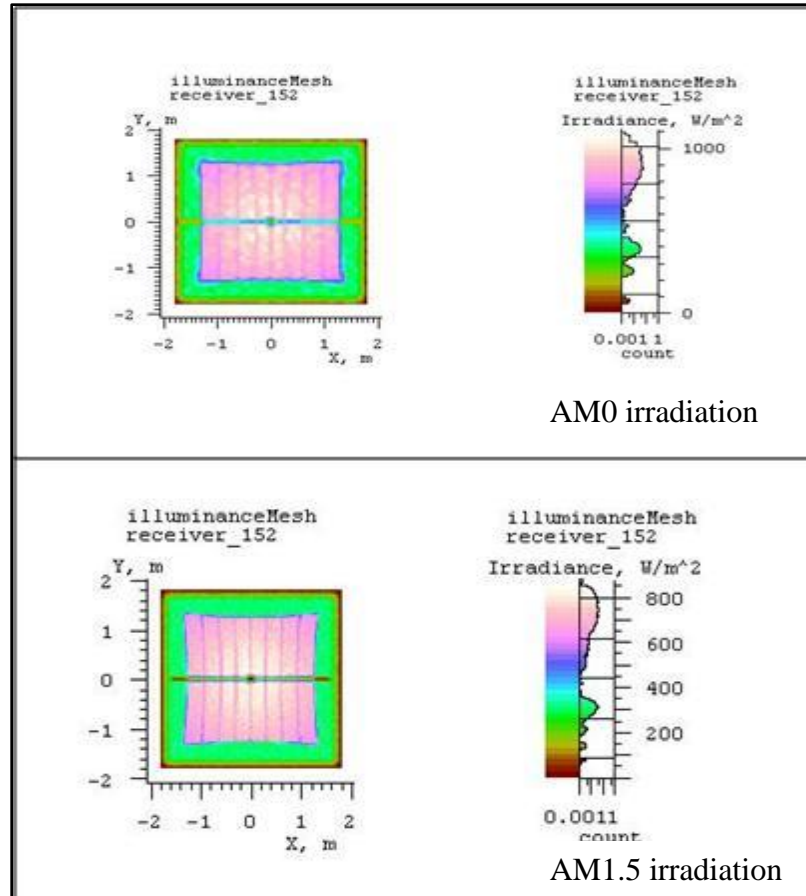


Figure 43: Irradiation of AM0 and AM1.5

The distance for AM0 and AM1.5 are tabulated below. For further experiments the irradiation of AM1.5 was used. This is more in accordance with the solar irradiation available in the northern hemisphere.

TABLE III: SOLAR IRRADIATION RESULTS

	Power of Source	Distance (D)
AM0 (1000W/m ²)	3600 W	35 m
AM1.5 (850W/m ²)	3500 W	35 m

EXP 2 : To find the optimal receiver distance from the focus

The analysis gives an insight into the power distribution of the concentrated light at the focus. This gives us the location for the maximum power incident on the VMJ cells. The incident power radiation also gives us the distribution of the concentrated light achieved by the optical set up. This is important in finalizing the location of the receiver. Figures 44 and 45 show the distribution of the light on the receiver surface as we move away from the focal point. In each of the block in the figure, the light intensities incident at the VMJ receiver is displayed. LightTools creates a mesh on an area of 0.2m by 0.2m where the light rays are collected and are displayed here. On the right, in each of the block, is the color scale which displays the values of light intensities.

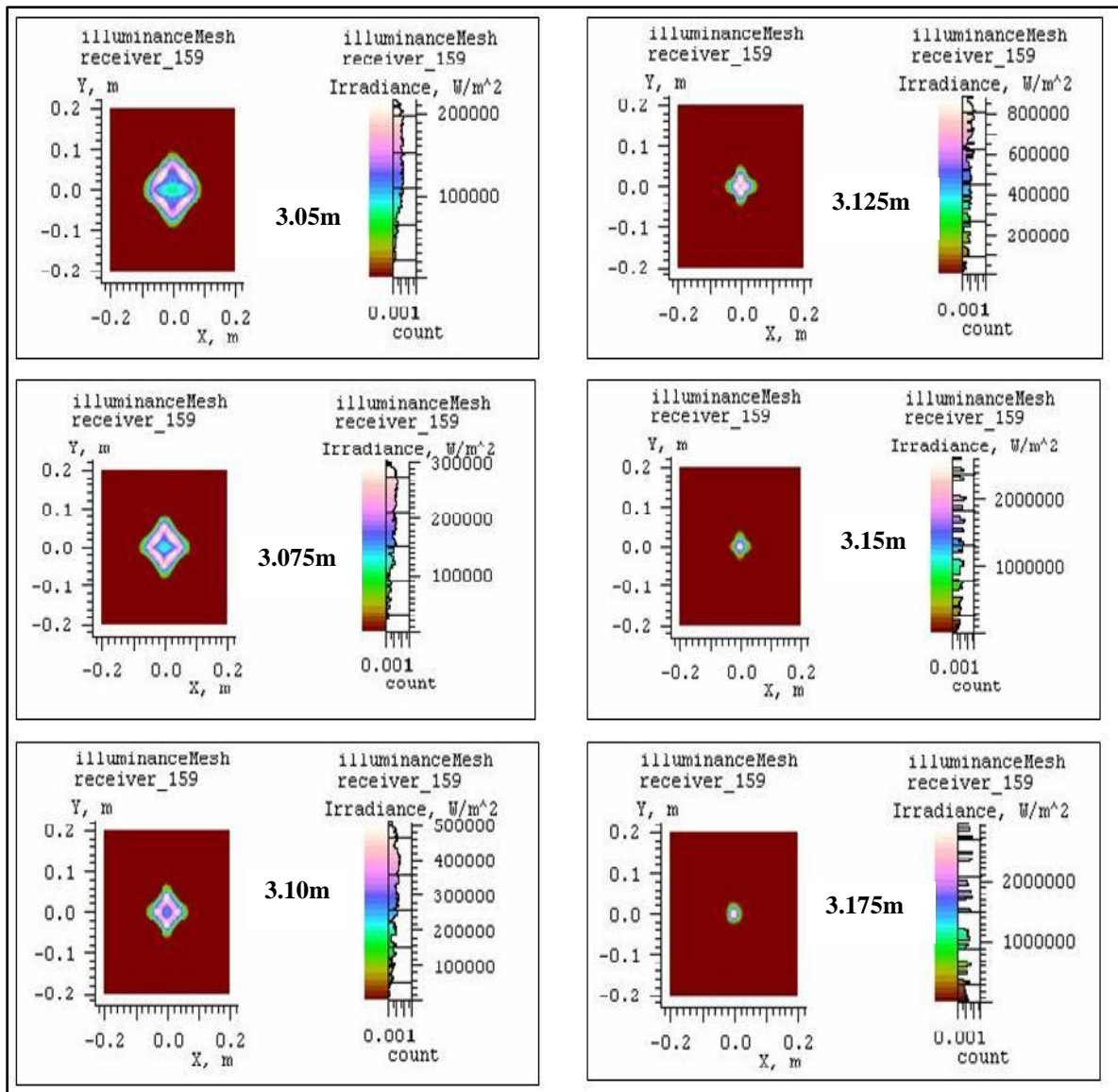


Figure 44: Results for receiver distance 3.05m-3.175m

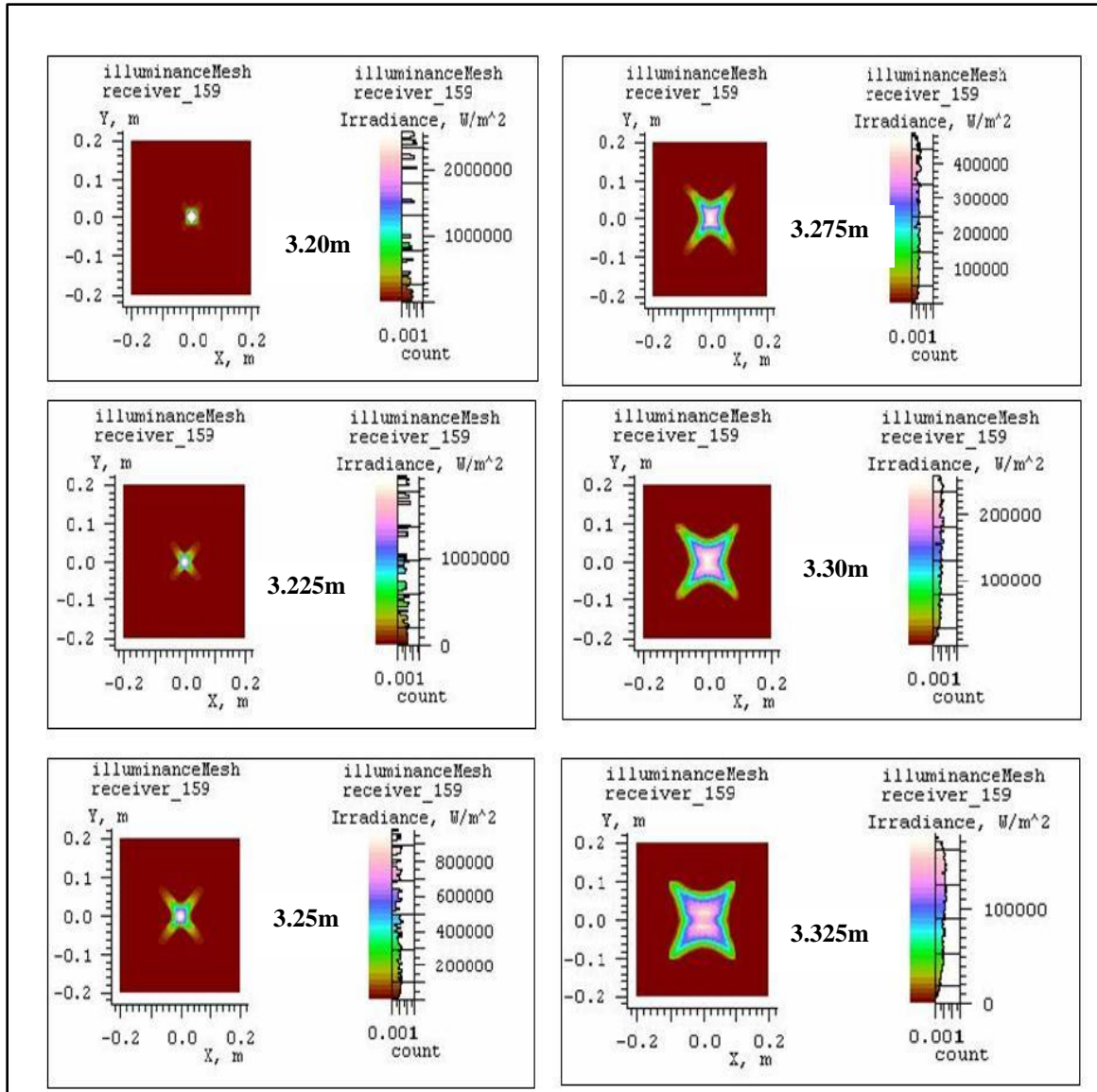


Figure 45: Results for receiver distance 3.2m-3.325m

The focal point of the concentrator is at 3.2m. Figure 44 shows simulation results of placing the receiver at distance ranging from 3.05m to 3.175m. Each block has an increment of 0.025m. Figure 45 shows the receiver being placed at a range of distance

3.2m to 3.325m. Due to the geometric symmetry we find an ideal focal point around the distance of 3.2m. As we move away, we observe the uniform intensity distribution over the area of 10cm by 10cm in the X and Y plane. Observing this we can design the system to have the receiver at a distance of 3.25m where there is an uniform flux distribution of approximately 80 W/cm^2 over an area of 100cm^2 . This helps us understand the distribution of flux on the receiver area. One could also have the receiver placed at a distance of 3.125m, where there is a uniform distribution of around 85-90 W/cm^2 . However at this distance the shape of the lit area is not a perfect square. The VMJ cells will convert part of this into electrical energy, while the rest needs to be rejected by the heat transfer system.

The results from these experiments show the trade-off considerations that need to be accounted while designing the solar load. In this work the solar load a photovoltaic (VMJ) load, and hence the criterion of uniform distribution is used. However, the area is really small and hence a precision in the tracking system and the mounting of the cells is highly desired. If one opts for a solar thermal load, one could select a distance of 3.275m, where, comparably a larger area has a uniform flux, but the light intensities are lower.

EXP 3 : To verify the accuracy required by the tracking system

The simulation is first of its kind, to show the effect of the tracking errors on flux distribution through simulation. In literature it has been mentioned that the tracking systems need to be accurate within ± 0.5 degrees [22]. To simulate these effects, we change the angle of the incident light source with the concentrator at 0.5° intervals. Due to the symmetry in the model, we change the angle of the source with the normal in one direction (+X axis of the vane surface). Similar results are expected if the angle changes in any of the other direction (-X, $\pm Y$). Figure 46 shows the flux distribution at the receiver obtained by moving the receiver away from the normal incidence in intervals of 0.5° . This experiment validates the accuracy required by the tracking system. We see that as the source moves away from the normal, the image is off centered at the receiver and hence will not focus on the VMJ receiver. It is observed that at about $\pm 0.5^\circ$ the system will function with a minimal loss in the intensities. However, if one places the receiver at a distance (from Exp 2) so that we have larger area of uniform flux distribution, a system tolerant to $\pm 1^\circ$ tracking errors can be realized.

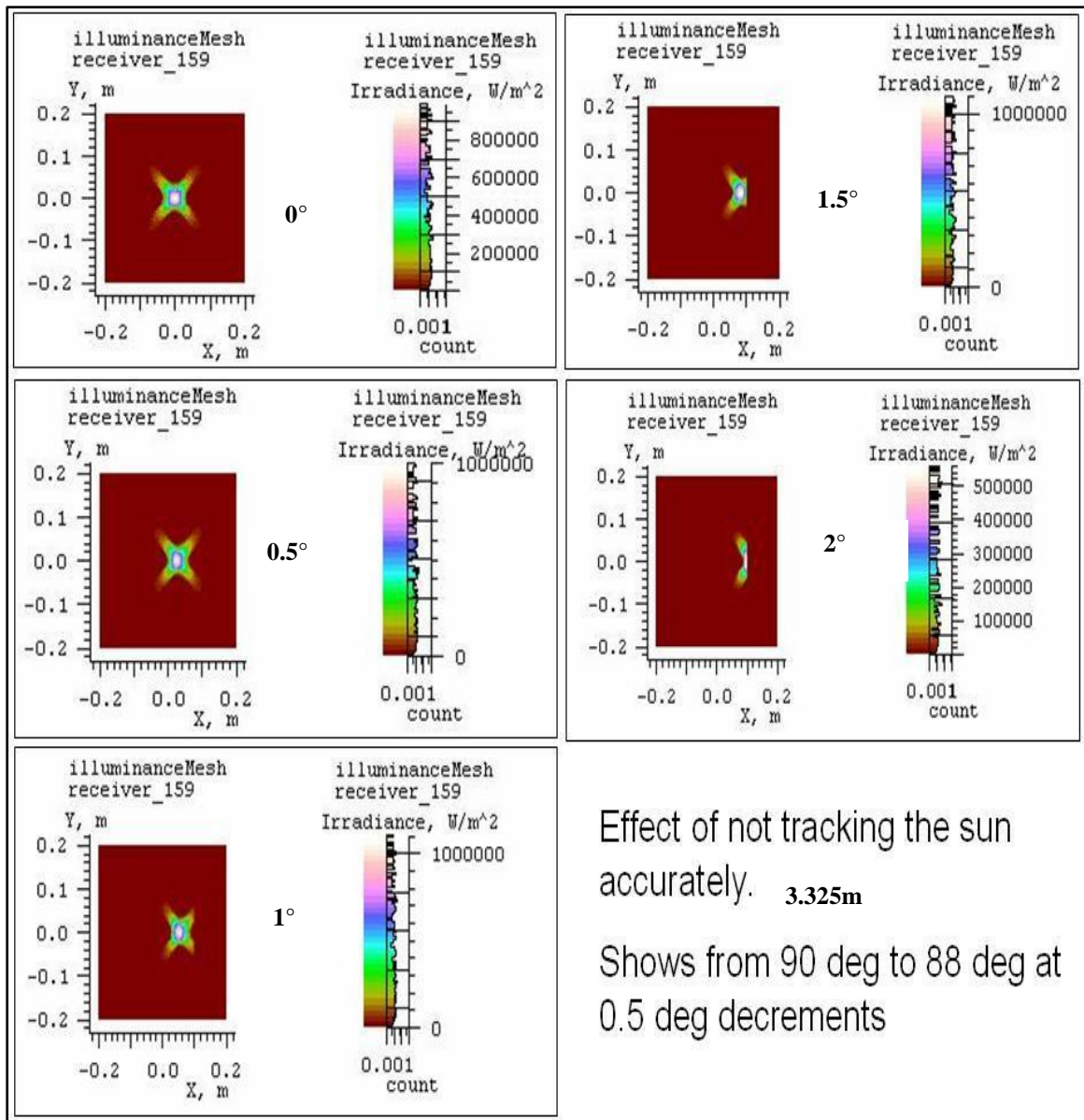


Figure 46: Results verifying tracking system accuracy

The optics simulation experiments validate that the desired concentration ratios are achieved by the concentrator system build of segmented vanes. LightTools gives us the capability to import the design directly from the 3D modeling software and thus

makes the validation of any new design easier. By giving appropriate optical properties to the modeled surface, one can estimate the maximum power that can be harnessed from any designed system. The methodology adopted here gives an approximate measure of the optical concentration and the distribution of flux on the receiver that any concentrator design can achieve. It gives us a good tool to design and analyze new designs of solar concentrators and receivers.

6.2 Heat Transfer Simulation Results

Design 1 simulation

In our first design we used a copper plate as the heat exchanging surface. The size was 20cm by 20cm. The thickness of the plate was 2mm. We assume VMJ cells mounted on an area of 100cm^2 . For simulation purpose the area for the receiver is about 400 cm^2 . Taking into consideration some area to be covered for the wiring and other hardware, area of 200 cm^2 around the center of the plate is the region of interest. Hence, we used 11000 Watts (55 X 200) as the heat input on the surface.

We varied the mass flow rate of the fluid flowing through the pipe. The boundary condition for the flow rate is applied to the inlet surface of the fluid volume. The two fluids used were water and ammonia. Figure 47 shows the temperature profile achieved in simulation for various flow rates of water. The table in the figure shows the maximum temperature on the surface and the average temperature of the receiver. One should note that this is the average temperature of the copper plate volume. The values are obtained from the simulation results tab.

Design 1: Water as working fluid

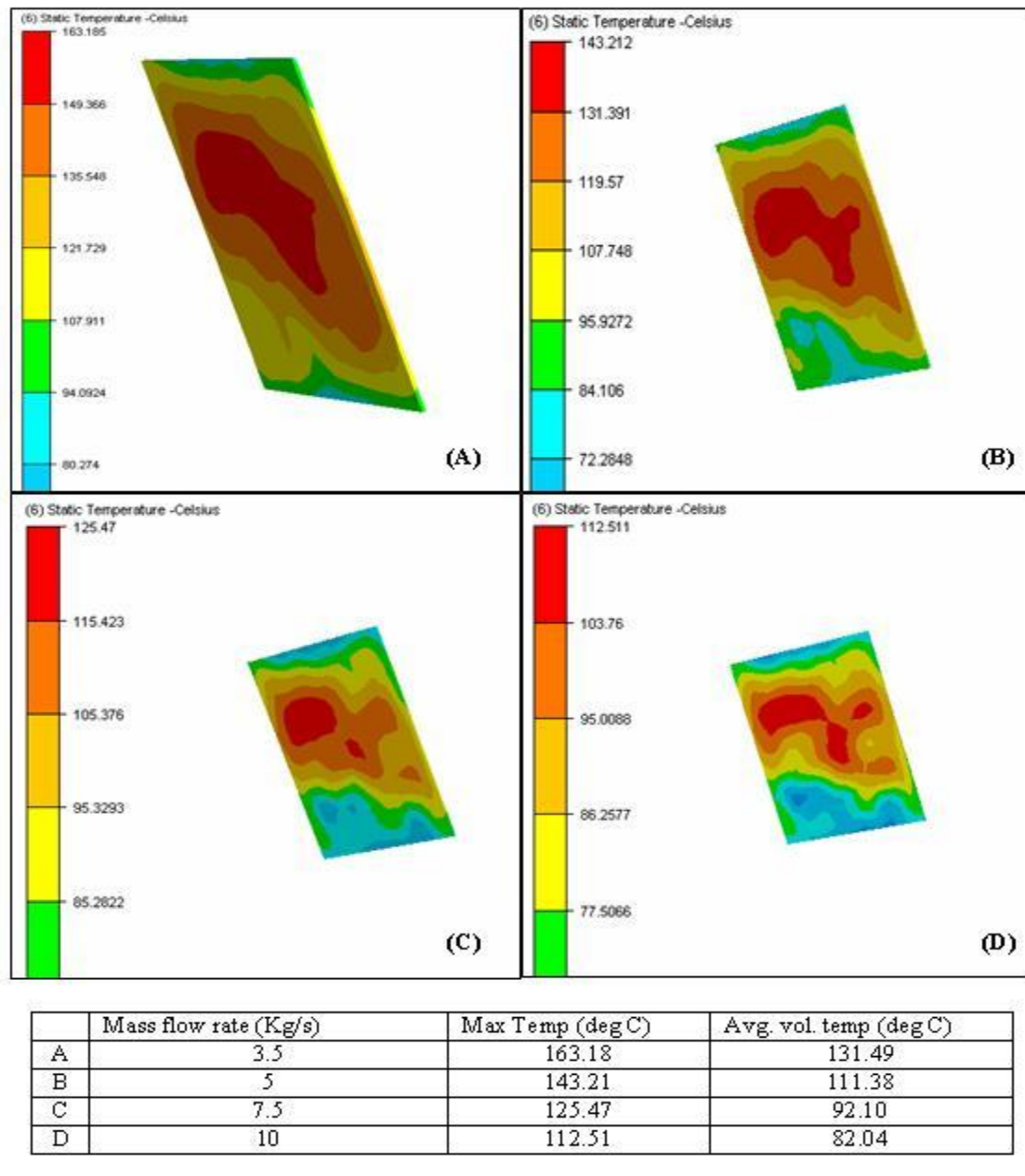


Figure 47: Temperature profile with water as working fluid (Design 1)

The theoretical calculations listed in section 4.2 were then used to compute the temperatures. With the copper plate design, the Heat transfer (HT) model is the closest to

our formulations presented. Figure 45 compares the calculated and the simulation temperatures achieved. The simulation temperatures are the average surface temperatures noted from the simulation results tab.

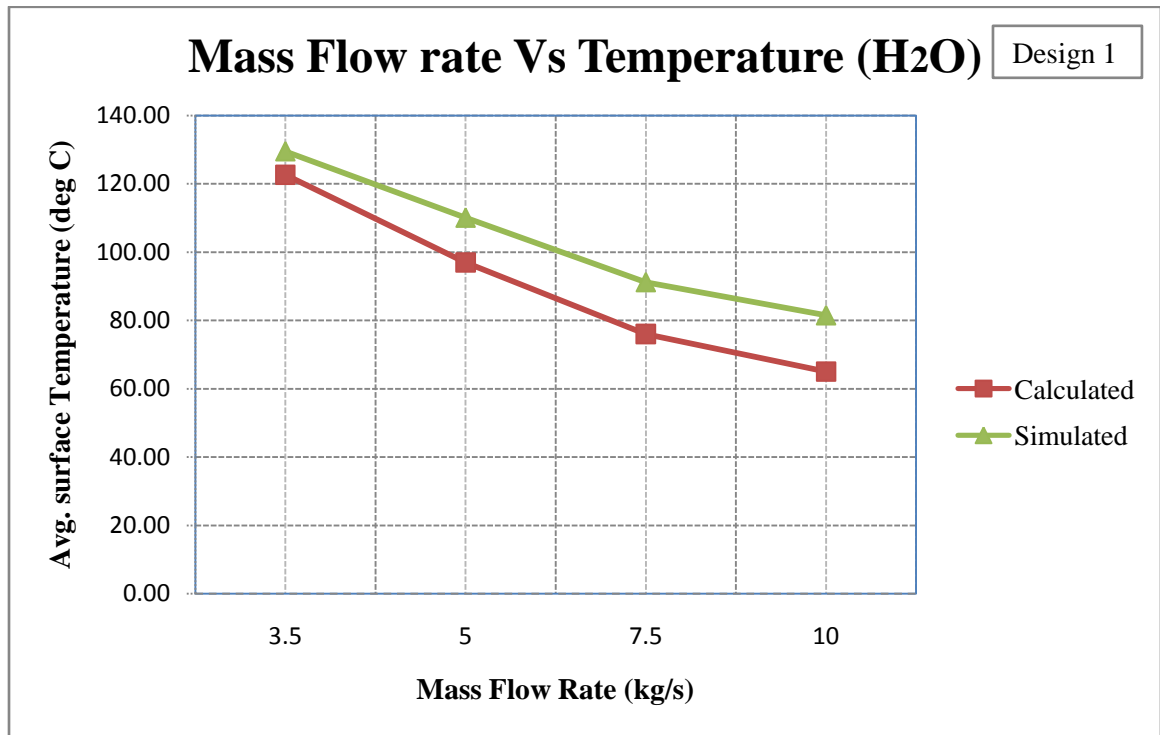
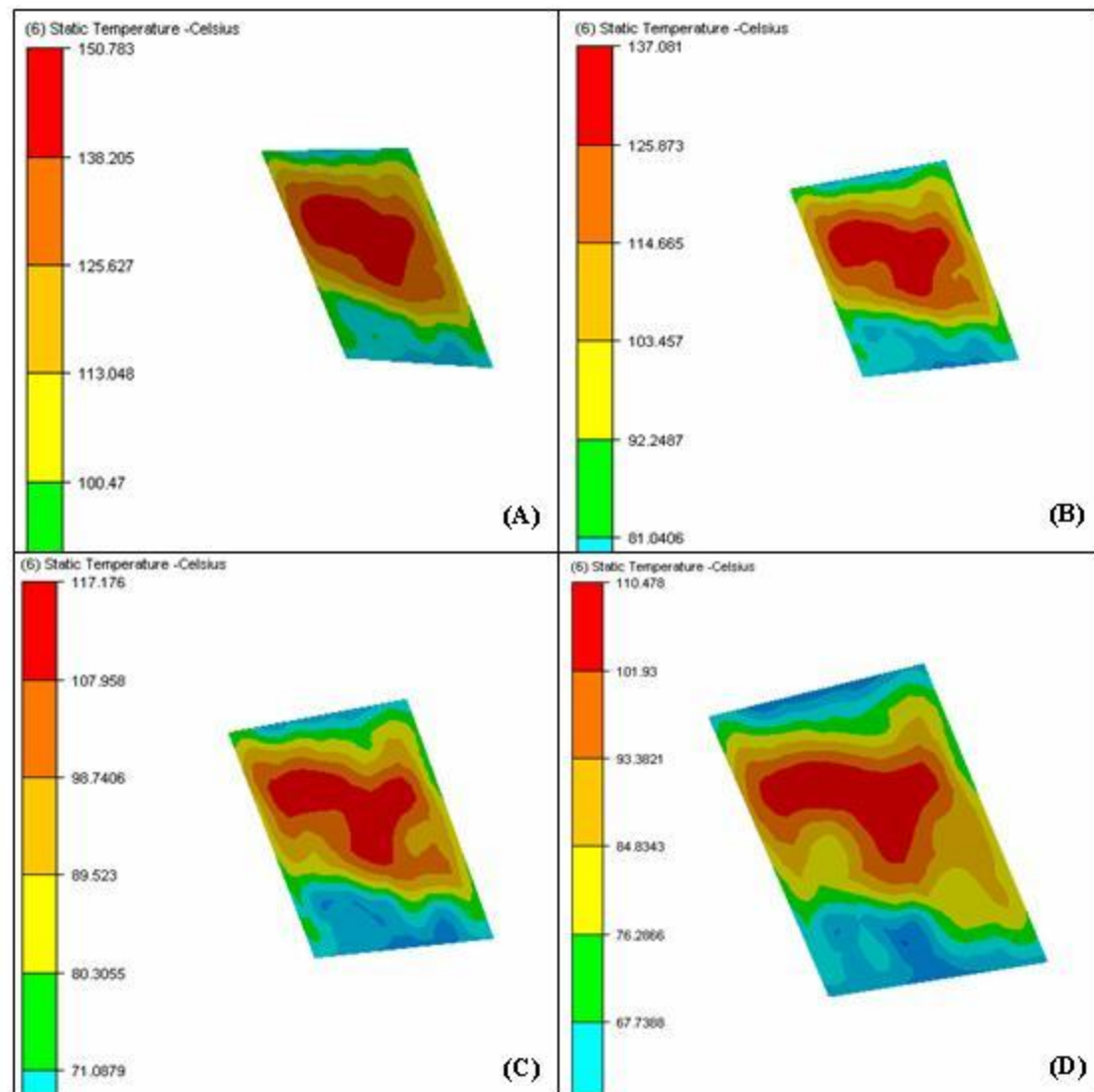


Figure 48: Comparison of theoretical and simulation temperature values HT model (H₂O)

Figure 49 shows the temperature profiles achieved by using ammonia as the heat transfer fluid for various flow rates. The temperatures achieved here are lower than that of water, due to the higher heat transfer coefficient of ammonia.

Design 1: Ammonia as working fluid



	Mass flow rate (Kg/s)	Max Temp (deg C)	Avg. vol. temp (deg C)
A	3.5	150.73	114.29
B	5	137.08	101.28
C	7.5	117.12	85.98
D	10	110.47	79.65

Figure 49: Temperature profile with ammonia as working fluid (Design 1)

We again compare the results from simulation to those from our calculation.

Figure 50 shows us this comparison.

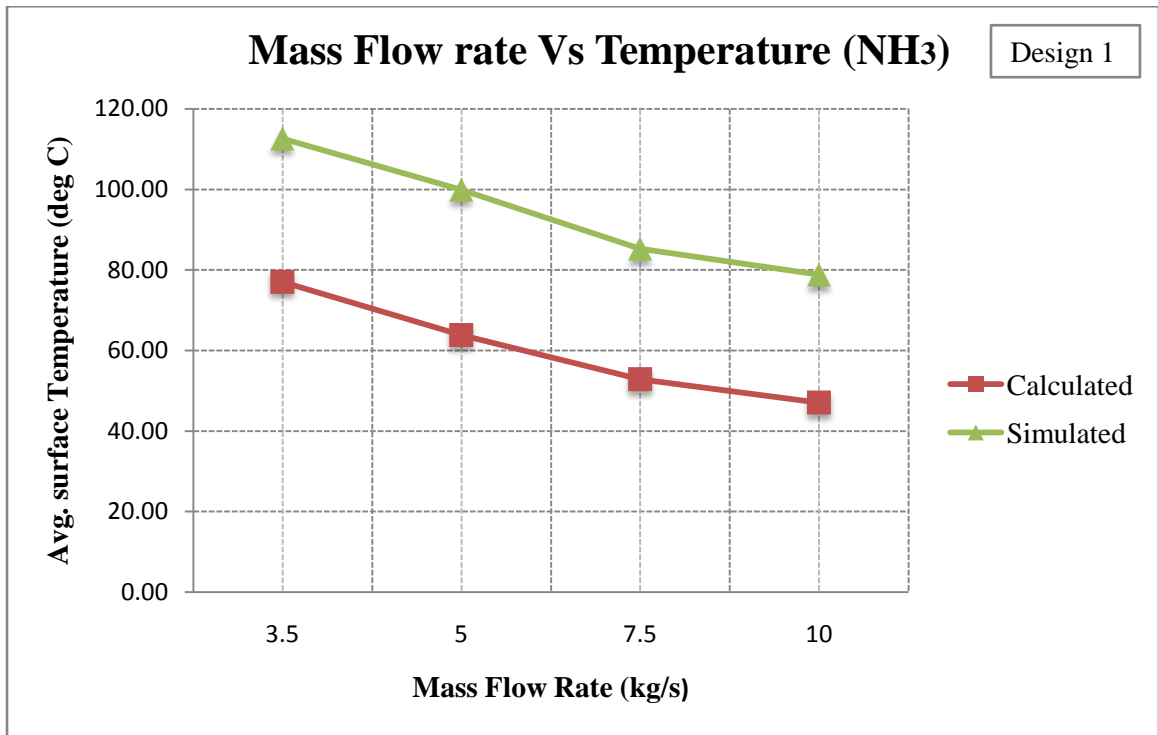


Figure 50: Comparison of theoretical and simulation temperature values HT model (NH₃)

In both the above comparisons we see that there is some error in the theoretical model as compared to the simulations. One of the reasons for this discrepancy is the design of the heat transfer mechanism used and the formulations based on flow through pipes. However, taking into consideration the errors associated with the formulations, the model is fairly consistent.

Even though there is reduction in temperature with increasing flow rate, such high mass flow rates are highly inefficient to the overall system taking into consideration the

immense pump power required to achieve these high flow rates. Hence, we altered the receiver design in order to achieve our objective.

Design 2 simulation results

In design 2 we added some copper fins over the copper plate to increase the heat transfer surface area. We added ten fins to the plate. The fins were 5mm thick and were 3.8cm high. By using these, there weren't any changes to the pipe dimensions. The fins provided more heat exchanging area with the flowing fluid. The total HT area was 0.21m^2 . We performed HT simulations using water and ammonia for various flow rates. Figure 51 below shows the temperature profiles over the receiver design using water. Figure 52 shows the temperatures achieved by using ammonia.

Design 2: Water as working fluid

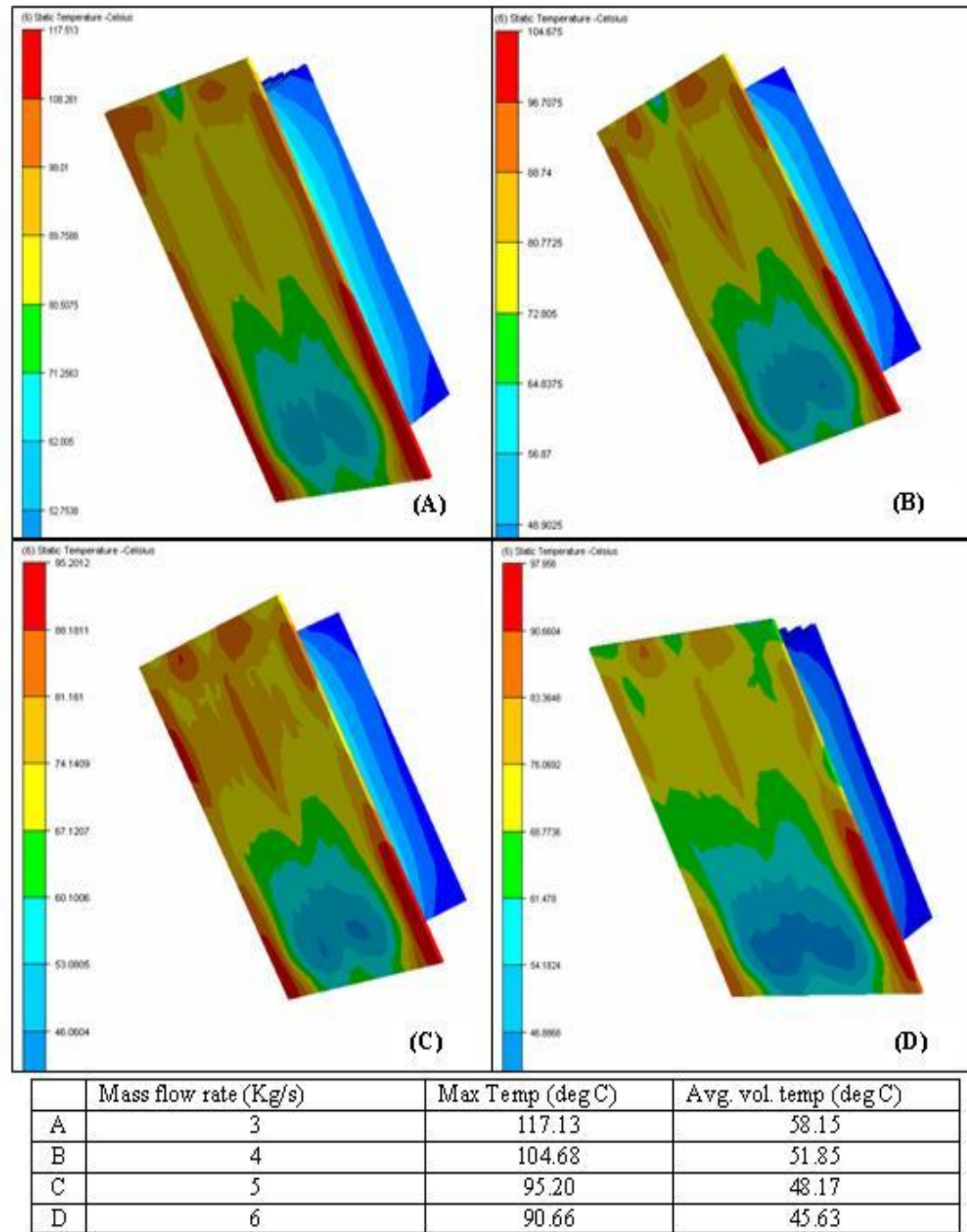


Figure 51: Temperature profiles using water with design 2

Design 2 – Ammonia as working fluid

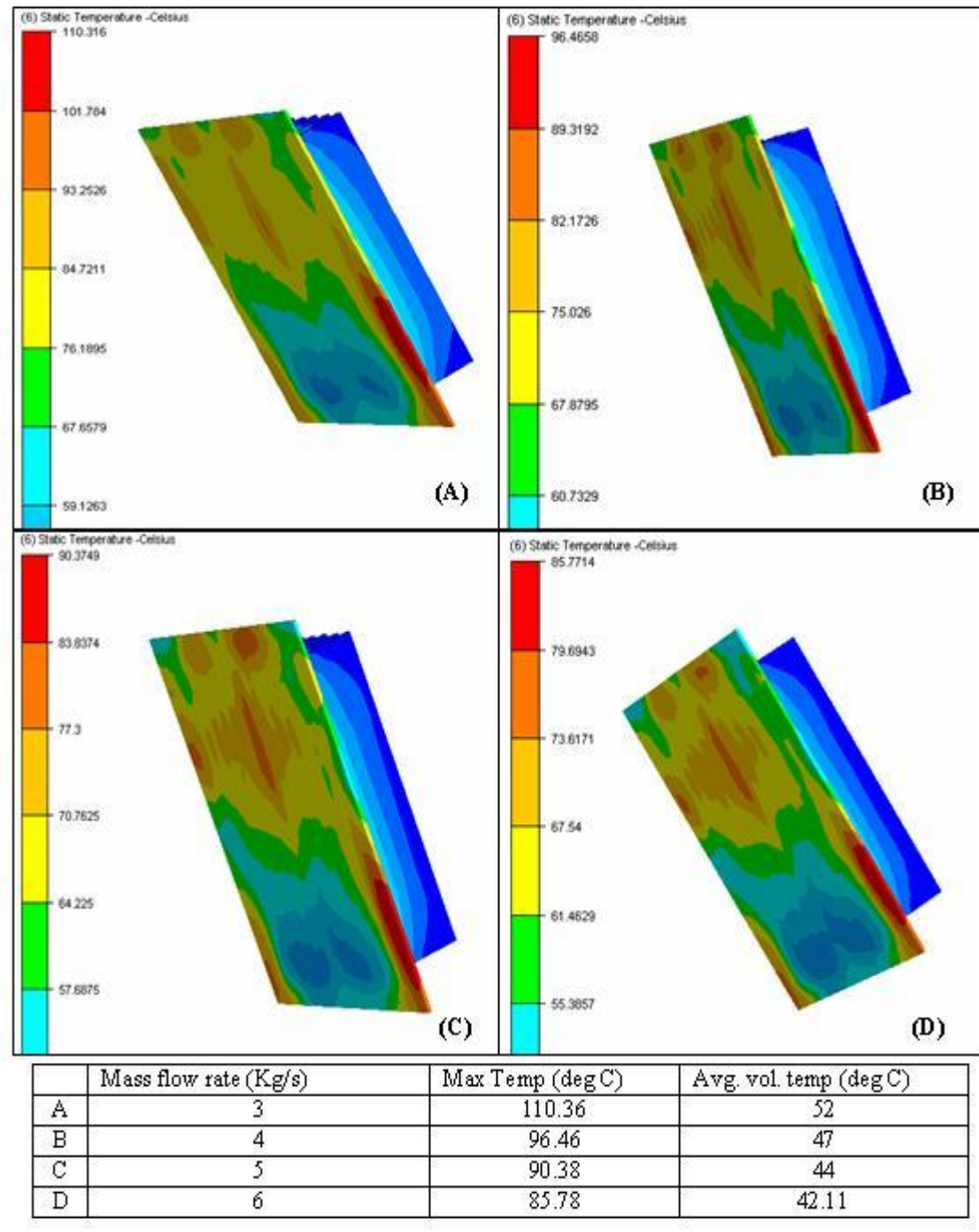


Figure 52: Temperature profile using ammonia with design 2

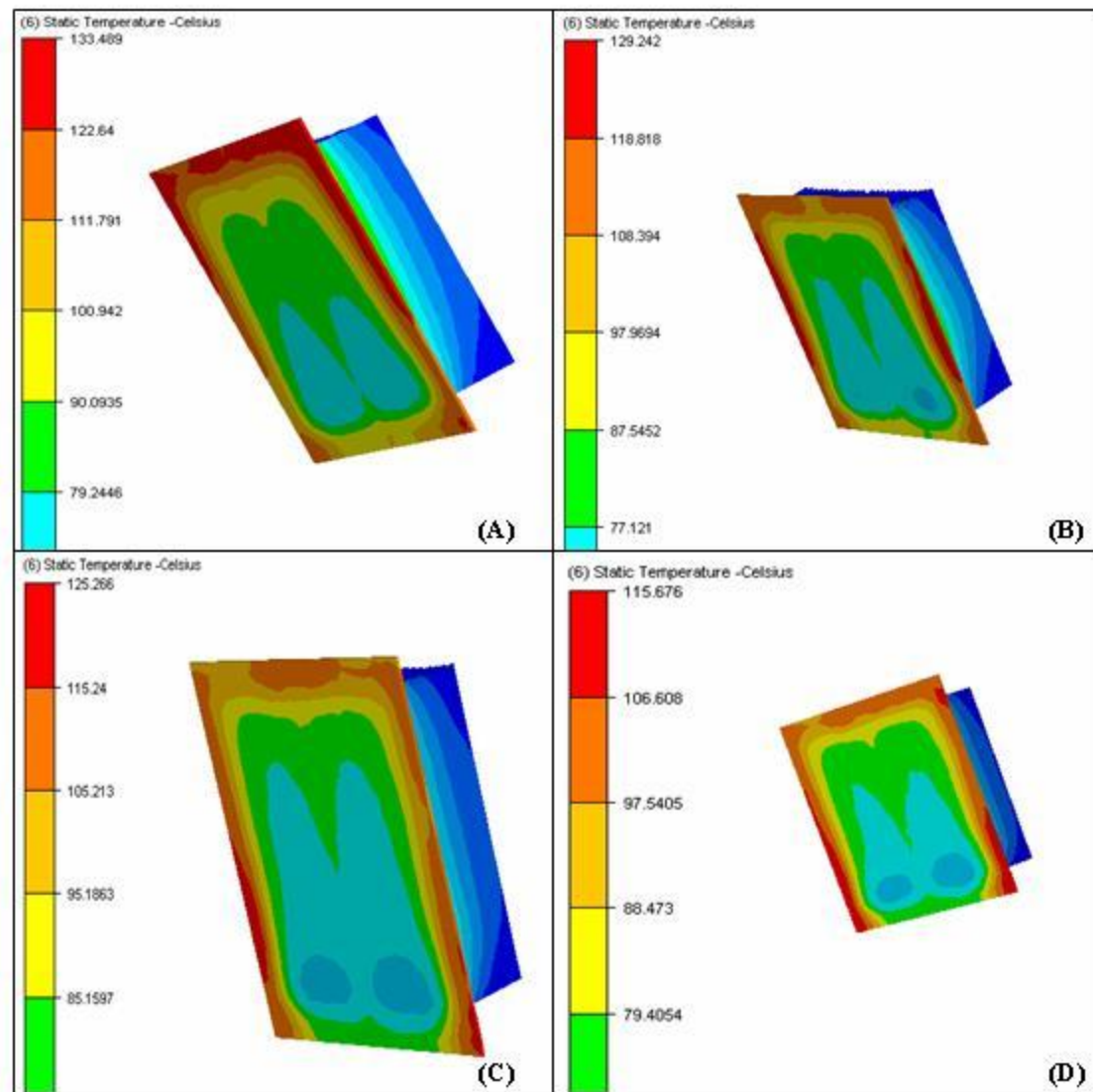
With this design we see that lower temperatures are achieved by using lower flow rates. Although the tables show the maximum temperatures over the surface over 100°C, we see that the average volume temperature for this design is about 50°C. With this design we see that the temperature attained are about 75-85°C around the center of the receiver surface, even with water as a working fluid. We see that with ammonia we have already achieved the desired temperature. However, using ammonia is a hazard in commercial area. It can be used in an industrial setting, but commercially, water is the best alternative. To achieve this objective we added more fins to increase the HT area and performed simulation.

Design 3 simulation results

In design 3 we increased the number of fins to 24. The thickness of each was 2mm and the height was 4.8cm. The total HT area is now 0.41m². Due to more obstruction to flow at the receiver, we have used lower values of flow rates. Figure 53 shows the results obtained from the simulations.

From the results we see that the desired temperatures are attained around the central part of the receiver surface even by using a lower mass flow rate. For water they translate to around 1-2.5 lps which are quite achievable in a residential set up. The higher temperatures shown in the table are mostly towards the edges of the receiver surface. The reason for that is the receiver design, which caused a really lower flow around those zones and also, the more fins caused an obstruction to the flow.

Design 3: Water as working fluid



	Mass flow rate (Kg/s)	Max Temp (deg C)	Avg. vol. temp (deg C)
A	1	133.45	56.43
B	1.5	129.42	52.65
C	2	125.65	49.74
D	2.5	115.68	47.54

Figure 53: Temperature profile with design 3 using water

The simulations performed in this study used a simple receiver design with fins. The objective of the heat transfer simulations was to work towards a temperature range suitable for the VMJ cell mounting. As such that aim has been achieved. We used a rectangular pipe segment for the simulation; however, it is rarely used in real life scenarios. The effective diameter for the design was around 8cm which is about 3.25 inch pipe. However, with a more dedicated effort towards the receiver design, one can achieve the cooling required for the cells, with smaller piping. One can also look into a solar thermal system and extract optimum heat energy from the system. A comprehensive study into the receiver design based on the application is thus required.

6.3 Airflow Simulation results

Simulation to study the effect of vanes

For the first simulation the vanes are imported with the frame holding them to analyze the airflow. The vanes were rotated at an angle of 80 degrees. The inlet boundary condition was air velocity of 2 m/s. The aim was to observe the airflow around the vanes. The simulation result is shown in Figure 54. We have two cut planes in the figure to observe the velocity profile in the system. The ray trace shows the direction of airflow. The results show that the vanes cause the air to flow around the vanes. The air speed is also increased as the air passes around the vanes. The vanes however do not block the flow of air through the system. When using the system in wind energy mode, with the vanes rotated, the air flow through the system will not be impeded by the vanes.

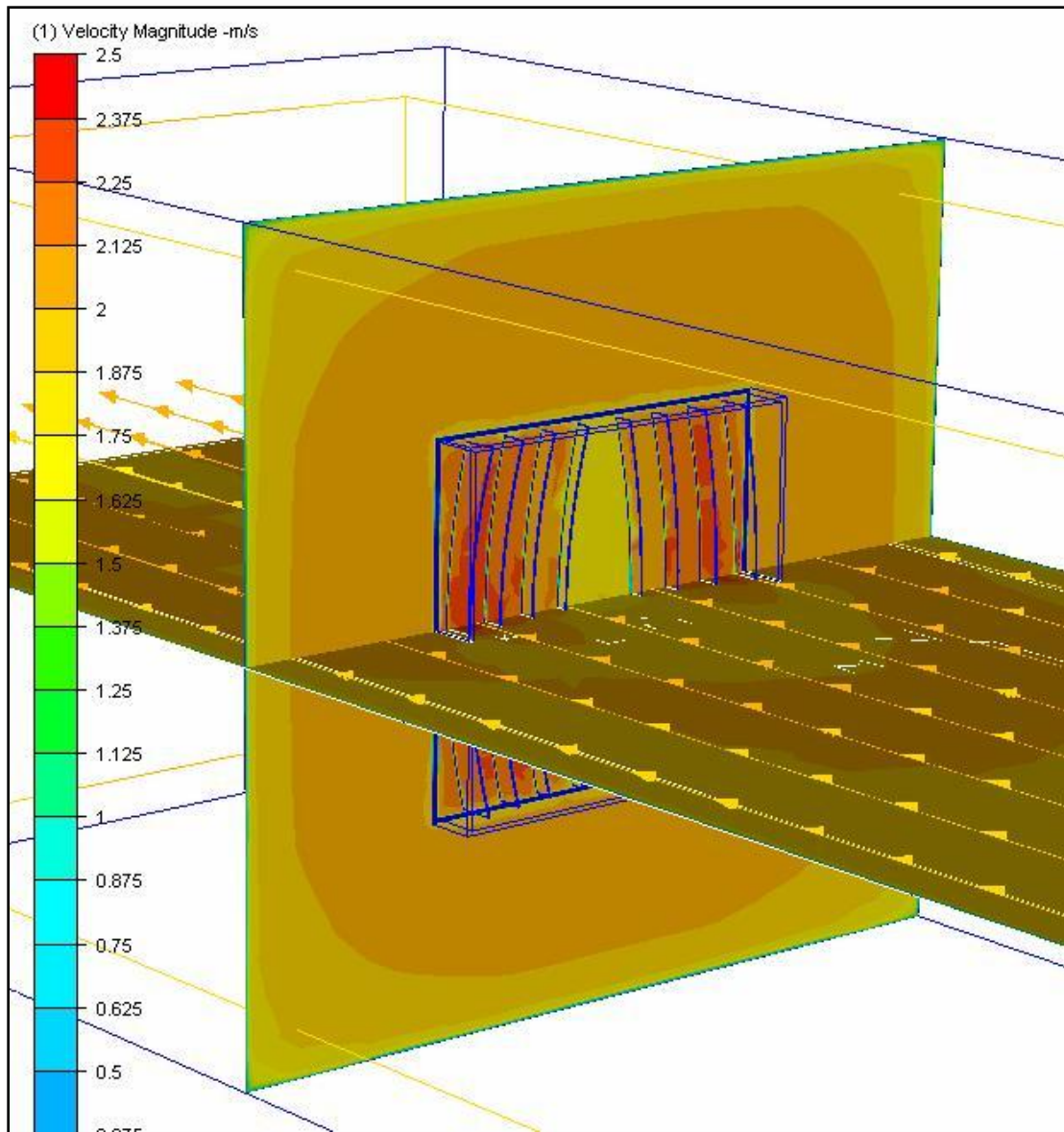


Figure 54: Results of effect of vanes on air flow

Simulations with the early model

In these simulations the entire system was imported into CFdesign. We first simulated for the concentrating effect of the system. The air inlet was from the vanes side. The inlet air speed was set at 3m/s. The simulation results are shown in Figure 55.

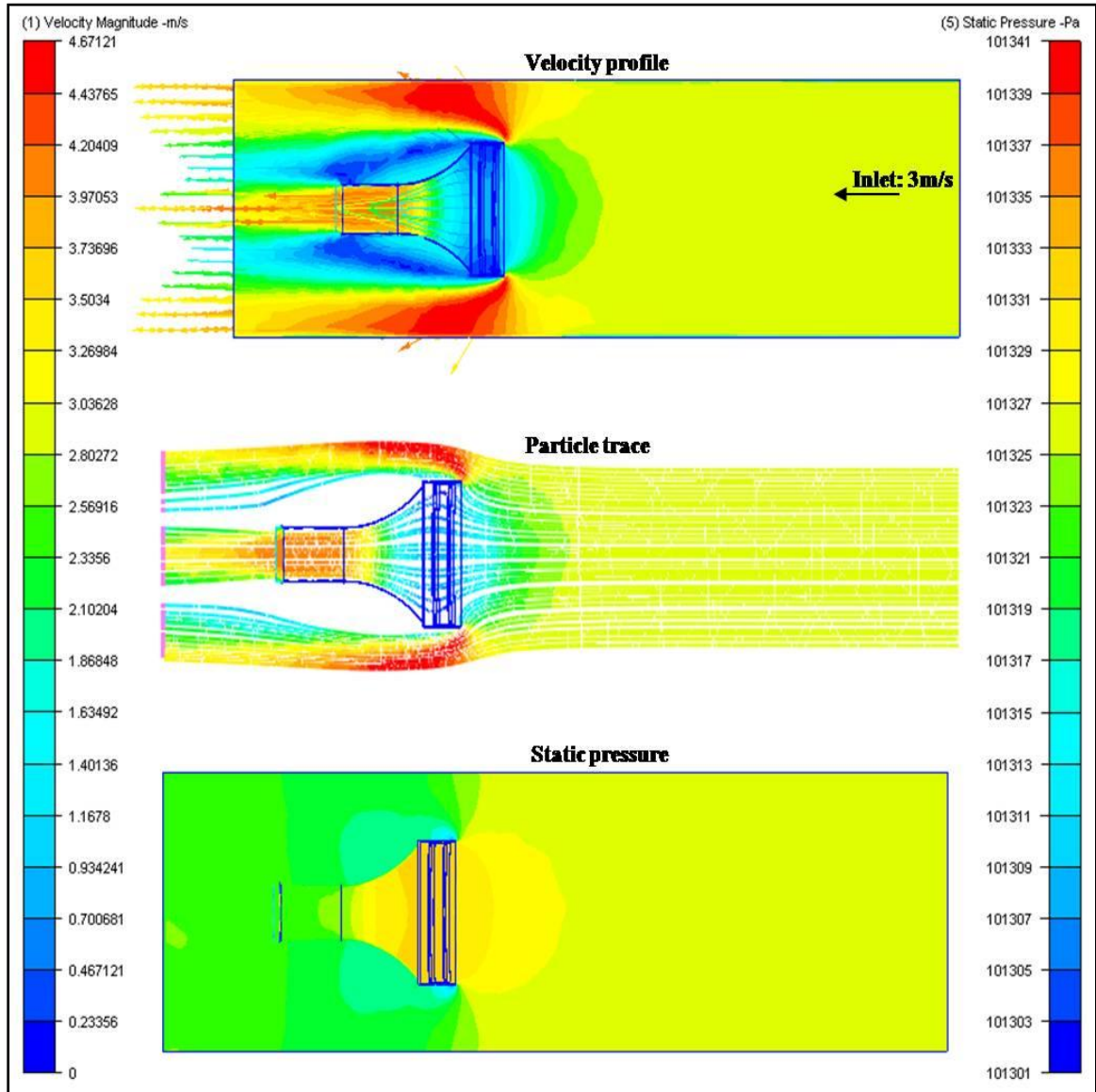


Figure 55: Results from first generation model simulation [concentrating mode]

In the velocity profile we see that there is reduction in the air speeds as it approached the vanes. But due to the funnel shape, the air then accelerates through the tunnel. The air speed in the tunnel reaches about 4.2 m/s. Thus, an acceleration of 1.4 times is achieved. The particle trace shows an example of the air streams that flow through the system. In the pressure profile we observe that there is a drop in pressure behind the rectangle frame with vanes, as it blocks the air. This low pressure causes the air to accelerate more outside the system than through the system. It is observed that the smaller diameter of the tunnel and its length cause this effect.

In the next simulation we analyzed the concept of using the setup as a diffuser. The inlet air was incident on the tunnel side, flowed through the system and then onto the vanes. The inlet air speed was 4m/s. Figure 56 below shows the simulation results.

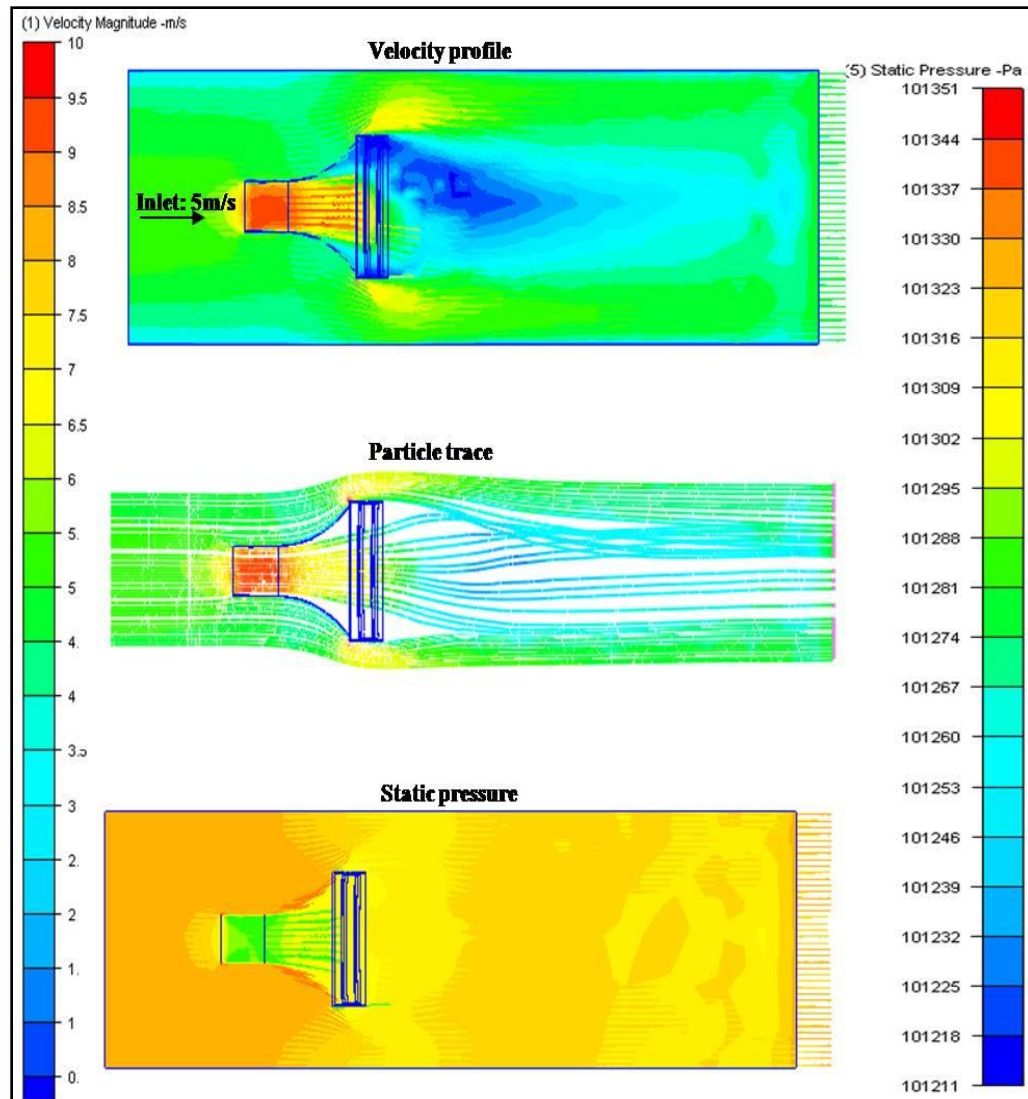


Figure 56: Results from first generation model simulation [diffuser mode]

In Figure 56, we see that the setup used as a diffuser, also accelerates air through the system. There is a significant pressure drop on the side of the vanes and it generates high wind speeds flowing through the system. We see that the velocities achieved are about 2 times the inlet velocity. However, due to the shape of the concentrator back frame, air passing through the tunnel seems to flow towards the lower side of the vanes.

One can relate this phenomenon with the flow along a curved surface. As such, an uneven pressure drop is achieved at the exit side of such a setup and could be detrimental to the stability of the system. The ray trace too shows the reduction in velocities on the upper side of the exit.

The main observations from these simulations was that the concentrator back frame shape and the length of the tunnel and tunnel diameter were causing significant low pressure drops around the system. Although a pressure drop is desirable to accelerate the air flow, that achieved by the simulated setup needed to be addressed. This issue was addressed by changing the shape of the back frame and reducing tunnel diameter and length. Although the feasibility of the system shape causing the acceleration of air speed was validated, its effect with a turbine in the tunnel was to be seen.

Simulation results with turbine

For these simulations, we designed a turbine in ProE. As per the simulation requirements in CFdesign, we added motion regions around the turbine. We also added the air slots in the concentrator back frame, to avoid the flow along its curvature. The concentrator back frame shape was changed too. We used a shape similar to those found in multistage turbine and the diffuser turbine. One of the advantages of this shape is its simple design. Figure 57 shows the results of the simulation where the setup works in the concentrating mode. The inlet velocity of 5 m/s is selected for the simulations.

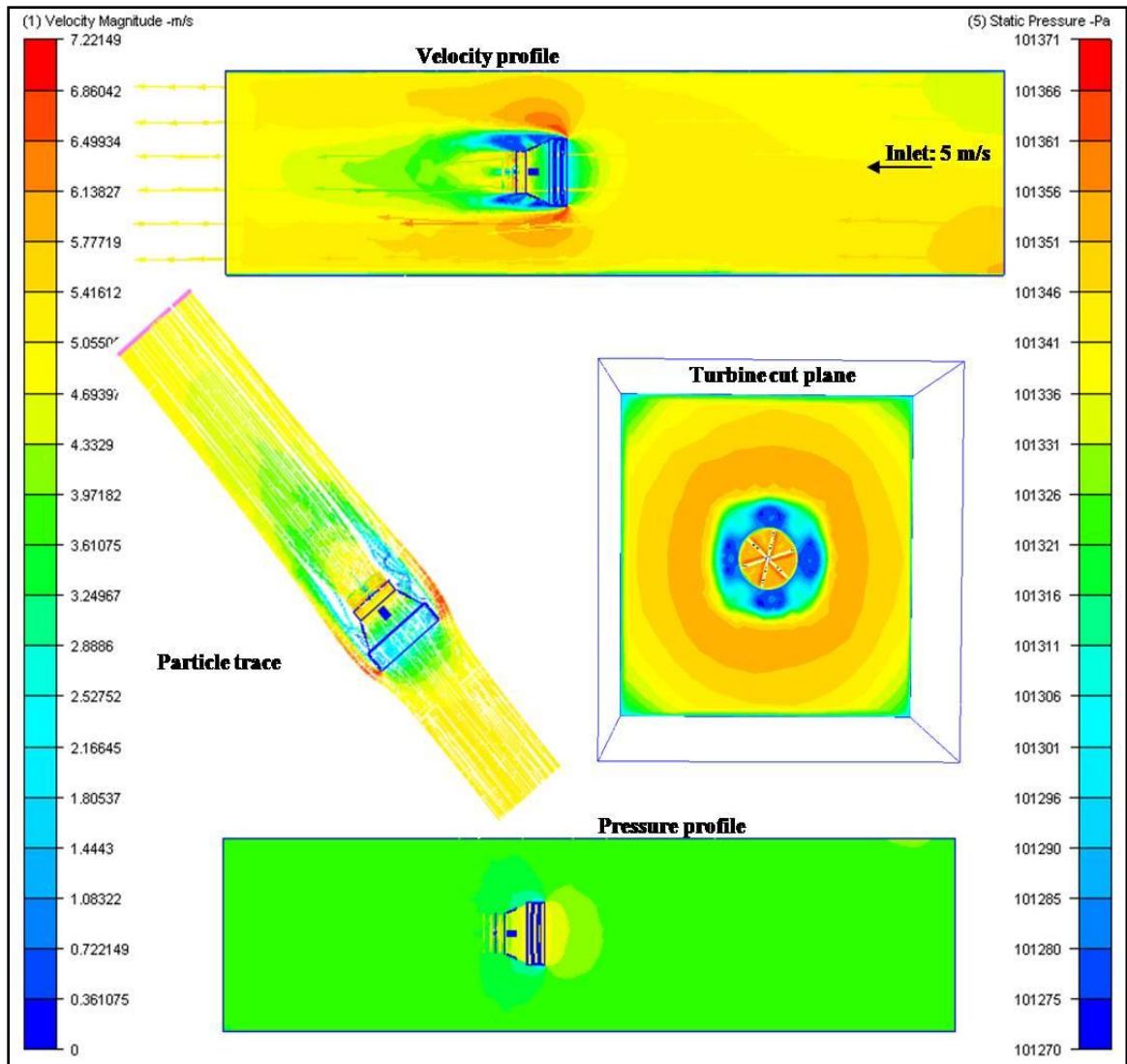


Figure 57: Results with turbine [concentrating mode]

We observe that the air speeds increase as they pass through the system. In the turbine cut plane we can see the accelerated wind velocities. We see that air speeds of about 7 m/s are achieved through the tunnel onto the turbine. There are no significant

pressure drops seen. Figure 58 shows a closer look at the velocities in the tunnel cut plane. The figure also shows us the changes made to the concentrator back frame.

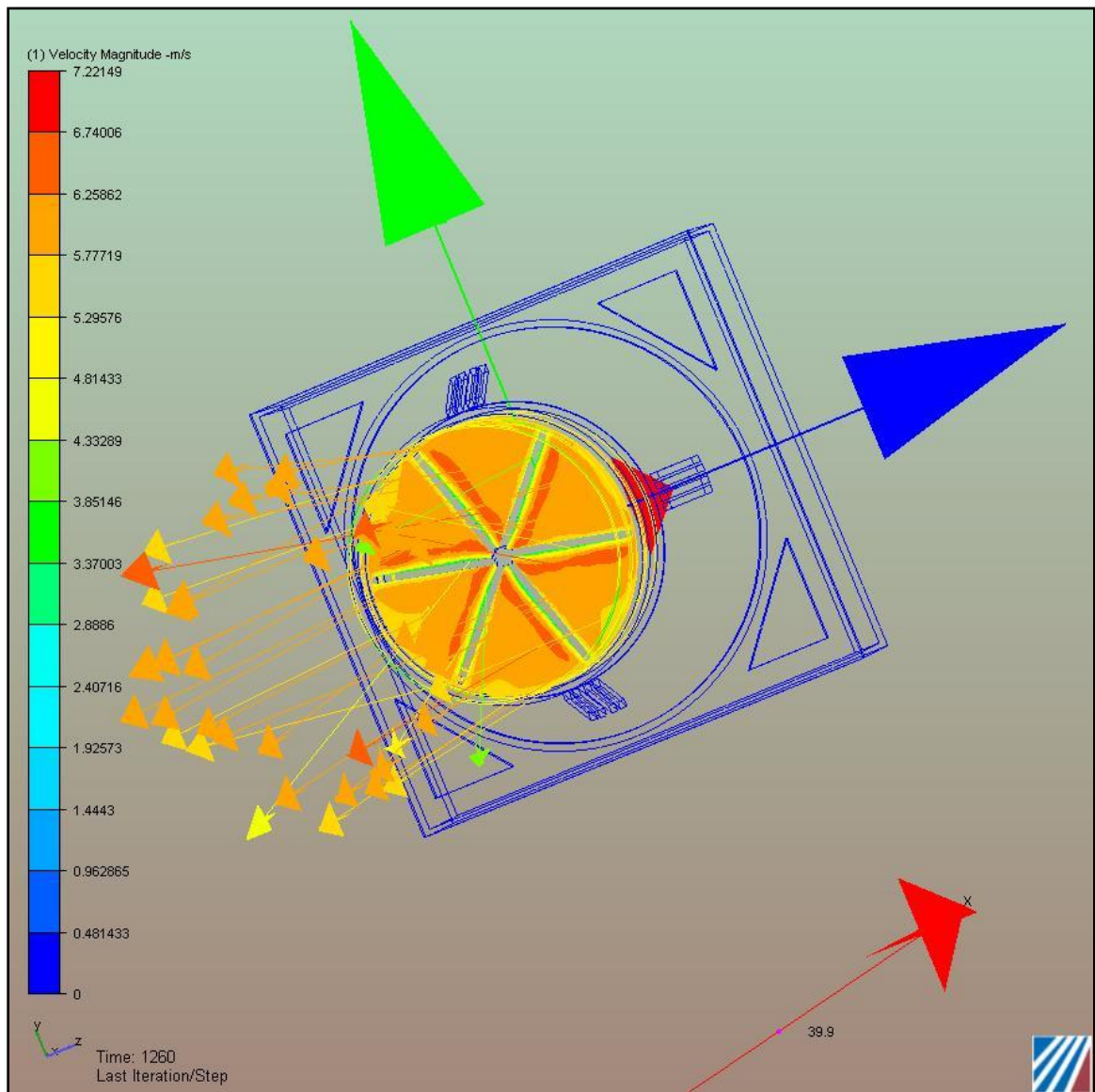


Figure 58: Velocity profile in tunnel cut plane [concentrating mode]

In the last simulation we used the setup in the diffuser mode to observe the wind speeds. Figure 59 shows the results from the simulations. The inlet air speed was set at 5

m/s. We observe that the air speeds achieved in the tunnel are about 8 m/s. The particle trace shows that, there is no obstruction to the flow of air through the system. Figure 60 shows a closer look at the velocity profile achieved at the tunnel cut plane.

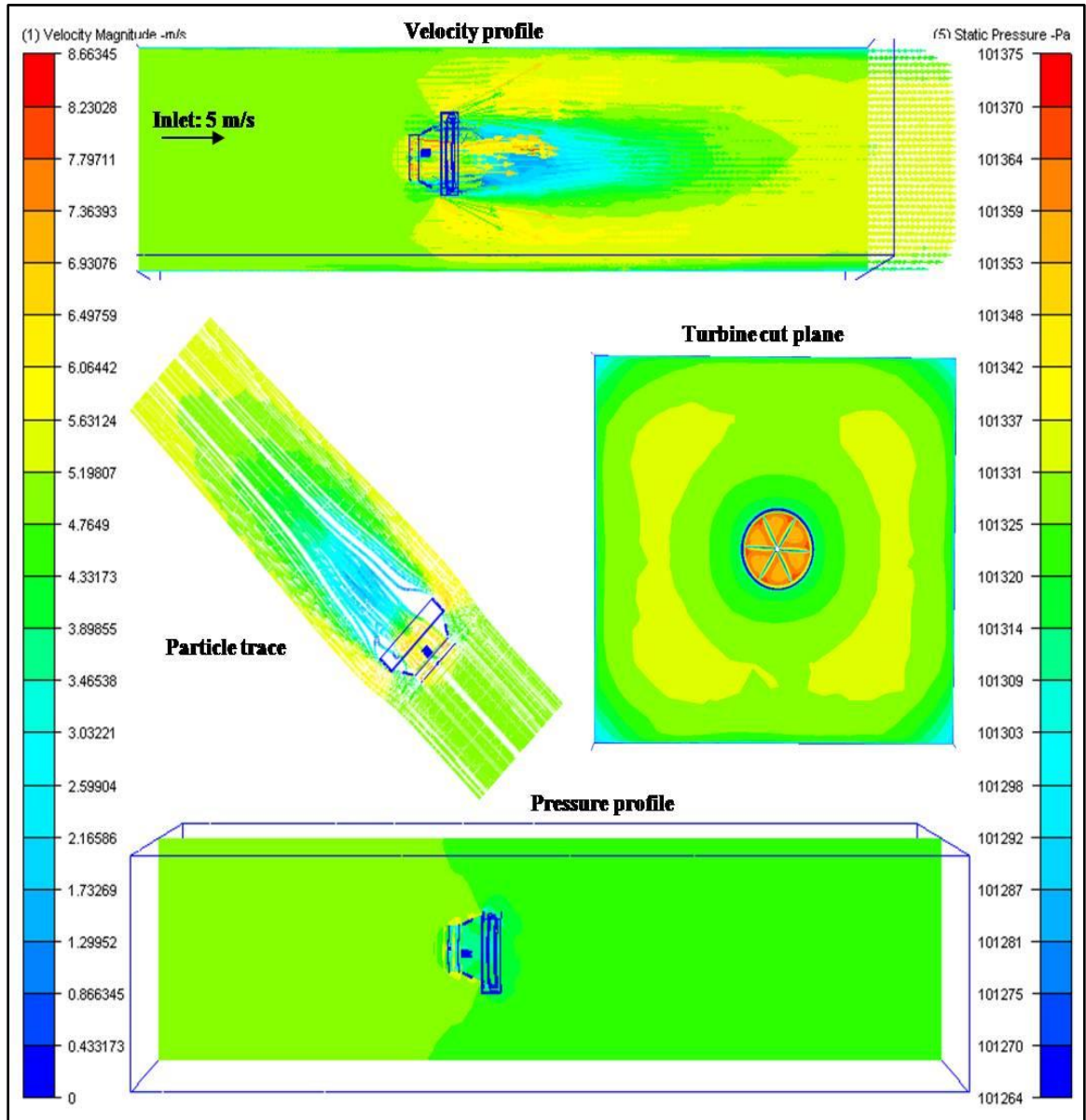


Figure 59: Results with turbine [diffuser mode]

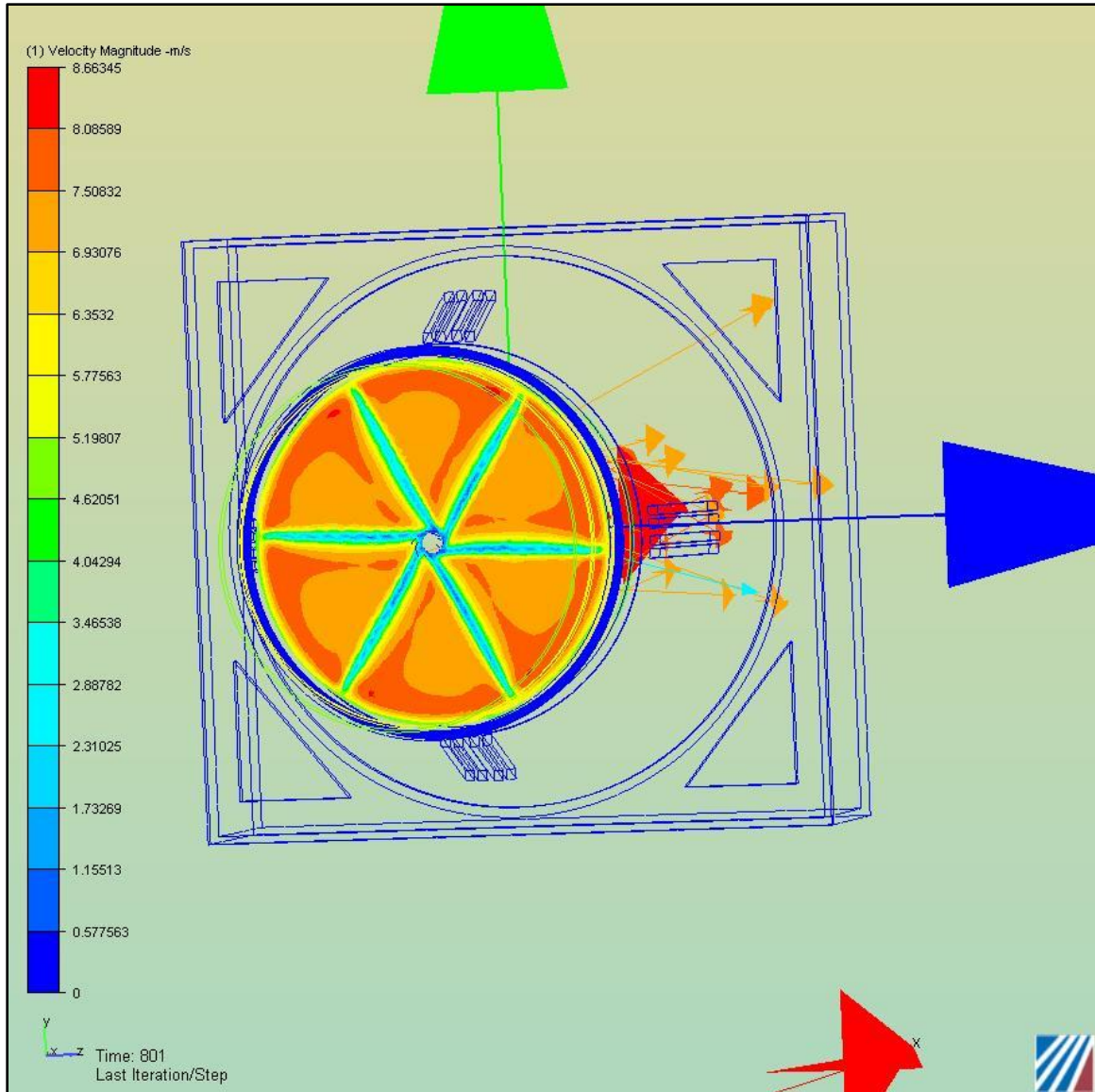


Figure 60: Velocity profile in tunnel cut plane [diffuser mode]

The results shown here are at very early stages of the simulation. The reason for early termination of simulation was limited computer capabilities available to perform transient analysis. Thus we see that the air speeds of about 1.5 times the inlet speeds have been achieved in either mode. . With further investigation into the optimum turbine design and its placement the accelerating factor could be more. But it is out of scope of

the current study and is left for further investigation. The computation limitations did not allow us to simulate for various inlet speeds of air flow. However, similar trend is expected. We now compare the power output from the turbine in the concept system to that of a bare turbine with similar diameter. Figure 61 shows the comparison for a 1.95 m turbine

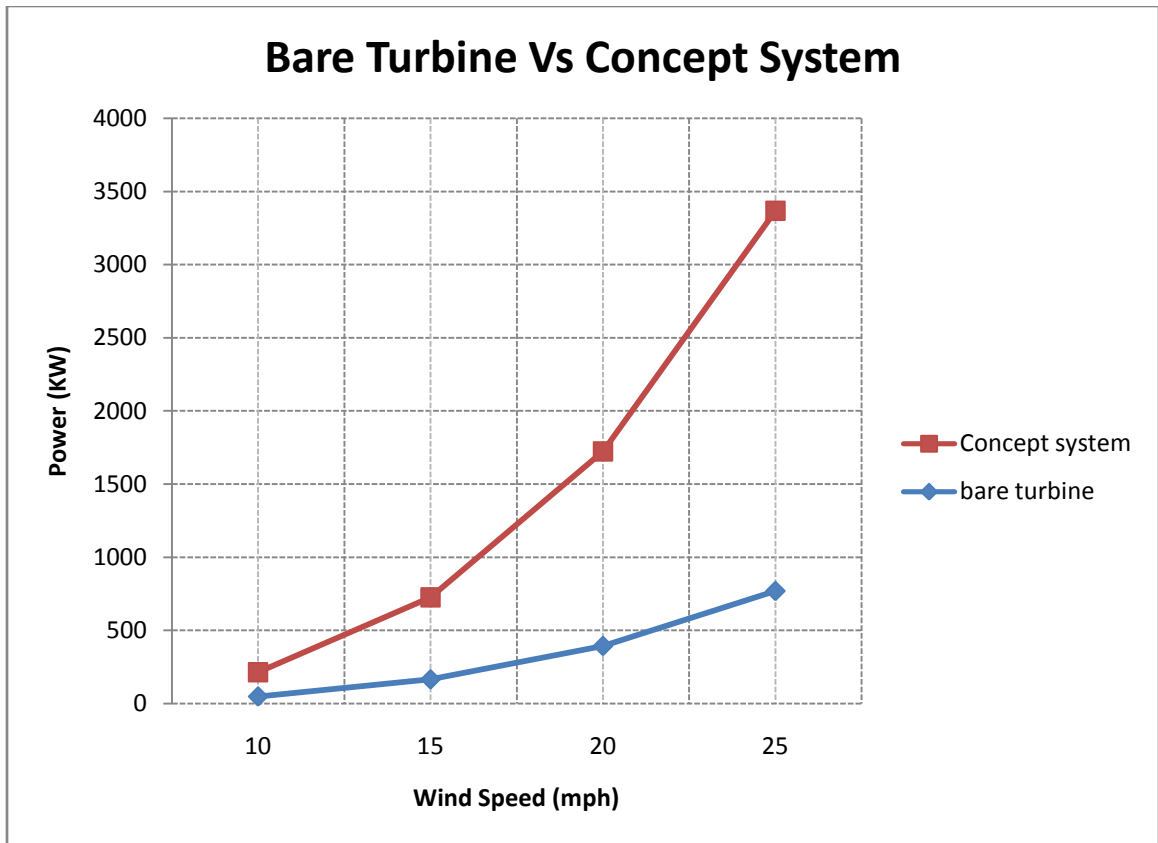


Figure 61: Comparison of bare turbine with the concept system

Figure 61 shows the performance of the concept system to be superior to the bare turbine of similar size. Due to the increase in the wind speeds, the concept system generates power of a higher magnitude even at lower wind speeds.

The simulations performed here do show the accelerating effect taking place in our system. However, the turbine designed, was a non optimized simple model. Also the early termination of the simulations while performing the transient analysis does not give us the entire picture of the phenomenon occurring by introducing the turbine. In literature, with the diffuser turbine accelerating effect of up to 2.5 times the inlet velocities is reported. These speeds can be achieved in our system by working more on the placement of the turbine in the tunnel, the diameter of the tunnel and the turbine. This remains as the task for future research work.

6.4 Economic calculation results

The formulations to calculate the economic feasibility of the system were listed in Section 4.4. In this section a levelized cost of energy for the proposed system is presented.

Annual Capacity of the system

Our hybrid system is based on two types of energy resources; solar and wind. The sun and wind energy available on daily basis depends on the site selected. However,

we use the four seasons in a year for the availability of sun and wind. With global climatic changes, these seasons to have witnessed changes to their pattern, however for calculation purposes we can have four categories of days within a year into which these resources can be divided. The ratings for our system used are as follows:

Concentrated Photovoltaic 1.3KW (@1000suns)

Wind turbine 1.3KW (@20mph)

We tabulate the seasonal energy output below. The numbers are from the average sun and wind hours available in the northern hemisphere. These numbers are site specific and will vary at different parts of the globe.

TABLE IV: ANNUAL CAPACITY OF THE SYSTEM

	Summer High Solar	Fall Moderate Wind	Winter High Wind	Spring Moderate Solar
Sun Hrs.	6	3	2	5
Wind Hrs.	2	5	6	3
Days/yr	90	90	90	90
KW/day	10.4	10.4	10.4	10.4

Annual Energy Output : 3744 KWhr

Levelized Unit cost of energy (LCOE)

We compute the LRR using equation (4.14). We first need to find the LCC, LAE and O&M cost components. Since the learning curve involved with the refinement of the technology and the mass production costs that can be attained will depend on the

prototype production and eventual process improvements, we assume some baseline numbers for estimating the cost of energy.

We calculate LCC using equation (4.15) and assume a fixed cost for LAE and O&M

The following table tabulates the numbers used for calculations

TABLE V: SYSTEM COSTS

Initial Capital	\$10000
Levelized annual operating costs (LAE)	\$500
Annual Operating and maintenance costs (O&M)	\$500
Discount rate	8%
Lifetime of the system	25 yrs

With these numbers and using equation 4.16 we get the levelized unit cost of energy as **\$0.51 per KWhr**. According to [2] the levelized cost for PV is now around 30 cents/kWh. At this price, PV is cost effective for residential customers located farther than a quarter of a mile from the nearest utility line. The proposed system would perform better taking into consideration its technological learning curve. Using the same formulations, for a solar-PV system alone, using VMJ cells, and with a capital of \$5000 and the remaining parameters assumed to be the same, the levelized cost per KWhr is about \$1.21. The cost advantage of the concept system is more profound, if we take into consideration that the trend of increase in electricity prices will remain.

The cost analysis presented here is for a standalone system, without taking into consideration any tax incentives. Often, for renewable energy projects there are rebates,

tax incentives and subsidies provided by the state governments. These incentives will further reduce the cost per unit of electricity. These calculations can be done comprehensively, by taking into account all the parameters once the site for the system is finalized. Although the cost of energy achieved for the proposed system here are relatively high in comparison to the conventional electrical supply, but they are comparable for a standalone energy system away from the grid.

Another point to note on the capacity side is that generation levels are assumed from the results of this study. With optimized wind turbine for higher rated wind speed, there will be an increase in the capacity of the system, ultimately driving down the cost of electricity. Also for a utility installation by replicating these systems, the total cost of electricity will be driven down.

6.5 Prototype system model

As a final task the concept system was designed in ProE to form the first generation of the prototype model design. This included all the necessary parts for a prototype model. Figure 59 below shows all the system components of a first generation concept prototype. We include the mounting, the tracking mechanism and the vane

rotation mechanism. One of the important design considerations while building the prototype design was the modularity in design.

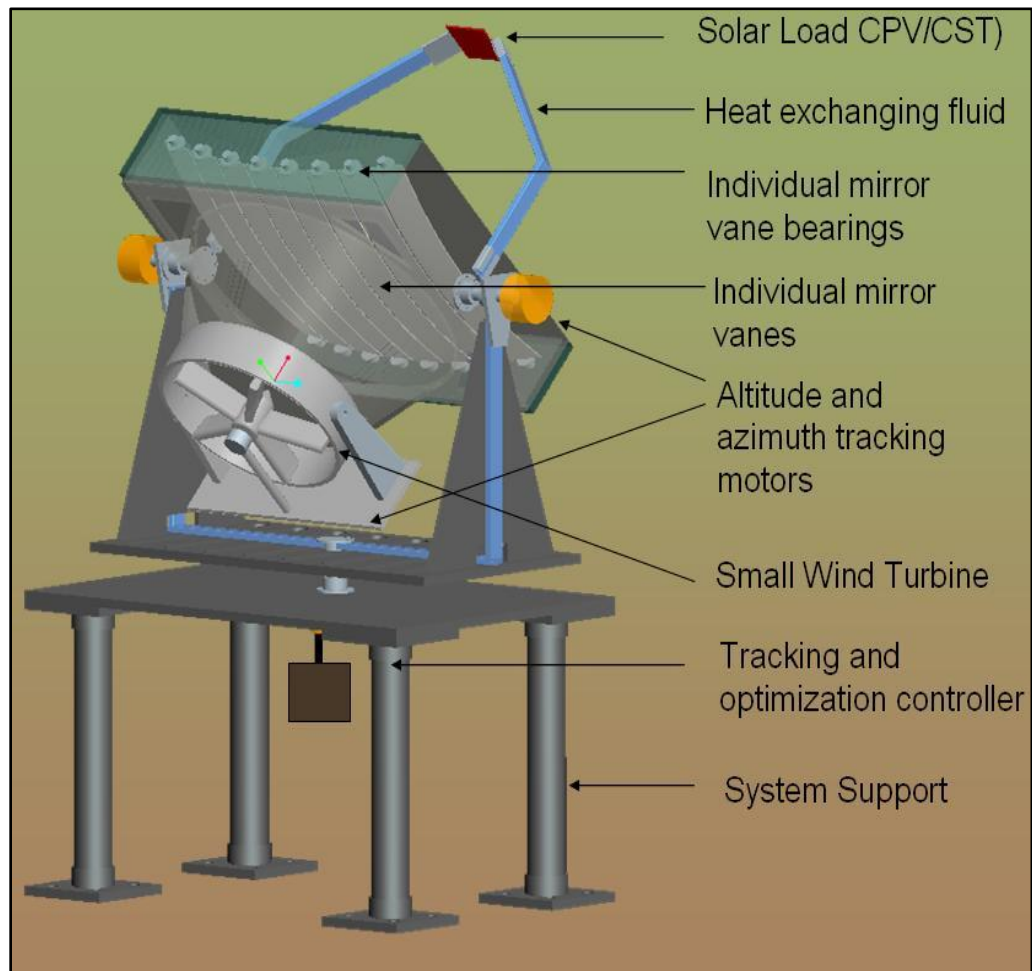


Figure 62: Prototype model design

Advantages of the system

1. Independent of single source

The system will be able to harness from both solar and wind energy resource. As compared to individual systems which heavily rely on the high availability of a

single resource, the concept system shall function in the optimized mode, utilizing the best resource available in either mode.

2. Distributed generation

Utility plants build away from the point of use and long transmission lines add to the cost of electricity. The concept system will address that concern by functioning near the point of use of the electricity.

3. Shared infrastructure

The system uses a single set up to function in either mode. As such, any land, built-up area and necessary infrastructure is shared. This is a great advantage if we take into account regions with high real estate prices

4. Shared storage and distribution

Both the solar-PV and the wind energy modes, being electricity generation devices, the storage system and the electricity distribution is common. Intelligent power management and distribution algorithms can be incorporated in the system based on the site demand.

5. Useful for grid isolated and grid tied applications

For locations located remotely the system presents a sustainable power source option. The remote location could be as simple as a water pump or a small remote housing. One can also use the system to work during the utility peak hours through the system storage capacity. Excess generated electricity could be diverted back to the grid.

6. Shared electronics and tracking systems

Both solar and wind systems require tracking systems. The solar-PV system requires dual axis tracking and the wind system requires a single axis tracking to turn in the direction of the wind.

7. Scalability

The system is scalable by replicating such systems. With an increase in demand, the systems can be replicated within the area and meet the demand. A utility scale generation capacity is also possible by replicating these systems in large numbers, and having a centralized storage and control system. However, economics of such a system need to be worked out.

8. Higher utilization

With a solar-PV system alone, the set up is idle during the evenings and during cloudy days. The system can function in the wind energy mode if the conditions are suitable and hence, the overall utilization of the system is increased.

System Options

In this work, we investigated the use of a solar concentrator based system using individual mirror elements to form the concentrator to harness solar energy and using the same set up to harness wind energy by rotating the mirror elements. Although the work presents a solar-PV based system, one can use solar thermal system to utilize the solar energy. This decision shall depend on the type of application the system is to be used. In

the wind energy mode, we validated the system to work in the wind energy mode as a wind speeding device, either using a concentrating effect of wind or a diffuser system. Figure 63 below shows the design options that are possible in the concept system. With the results obtained from this work, the starting point in developing a production model could be a concentrator photovoltaic (CPV) system in the solar energy mode and a diffuser system in the wind energy mode. Although the concentrating wind energy mode has been investigated in this work, with the available literature [10-17] on the diffuser based turbine, it would be a good method to validate the production model. For the concentrator wind energy mode additional investigations with a turbine placed in the tunnel is needed. Also if we include the various tax incentives and externalities [23] for a specified site in the economic calculations will further validate the economic feasibility of the system.

The CFLR [19] method can be used to utilize the solar thermal effect. In such a variant, we can use flat glass mirrors concentrating on a high temperature carrying fluid. One can use this set up as a primary fluid heating device in a process plant. Figure 64 shows one such system.

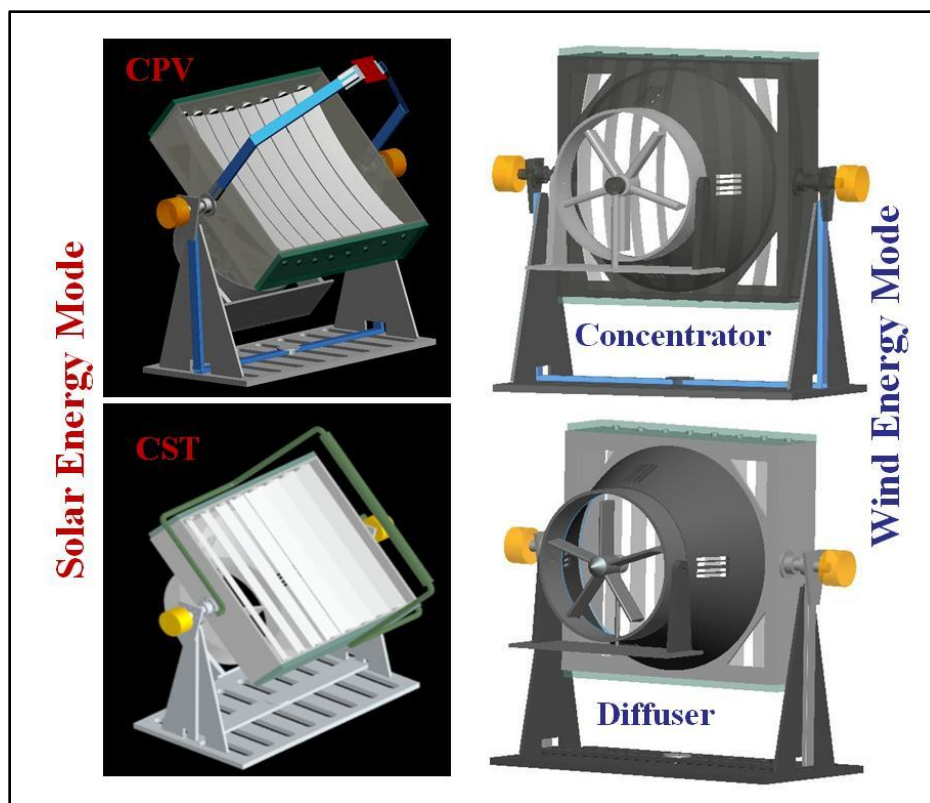


Figure 63: System design options

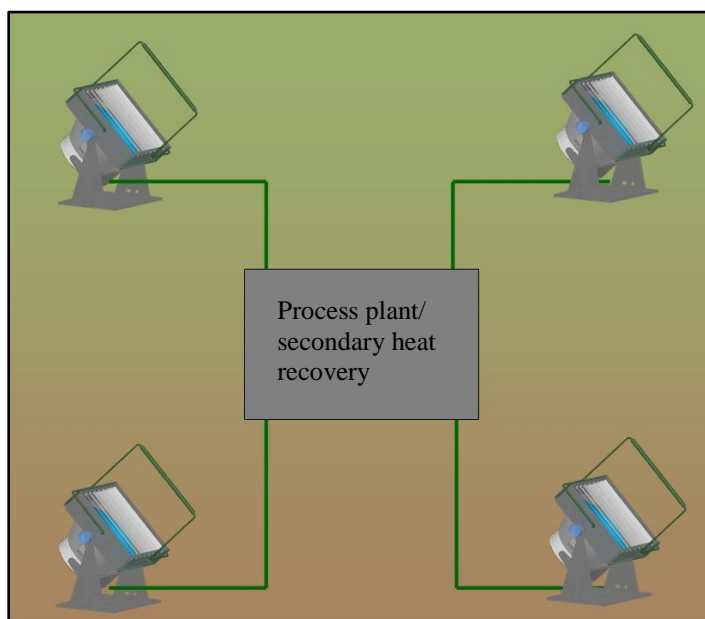


Figure 64: Concentrator solar thermal system

CHAPTER VII

CONCLUSIONS

The objective of this work was to validate the feasibility of a dual use solar and wind hybrid energy system. Simulations to investigate the optics of the system, cooling mechanism for VMJ cooling and airflow through the system were performed. Also a first order of economic analysis for the system was presented. Following are the key findings of the work

- Optics of the system

In our system we use individual mirror vanes to form the parabolic concentrator. We used LightTools software for analyzing the optics. It was found that the individual vanes do not cause any significant loss in the optical concentrations. The light intensity was uniform at the receiver. Although, the focal point of the system was at a distance of

3.2m, it was found that, the receiver placed at 3.25m had a more uniform distribution. Also the tracking system accuracy required for the system was studied. It was validated that the tracking mechanism be accurate within $\pm 1^\circ$. The simulation method using LightTools to study the intensity distribution at the receiver is first of its kind in analyzing the concentrators.

- Cooling of the VMJ cells

It was necessary to investigate the cooling mechanism at the receiver where the VMJ cells will be placed. The aim for these simulations was to achieve operating temperature profiles at the receiver for the VMJ cells to maximize efficiency. Using simulation results we refined our receiver design to achieve the necessary temperatures. Temperatures of about 65-85°C were achieved using water mass flow rates of about 1-2 kg/s.

- Airflow through the system

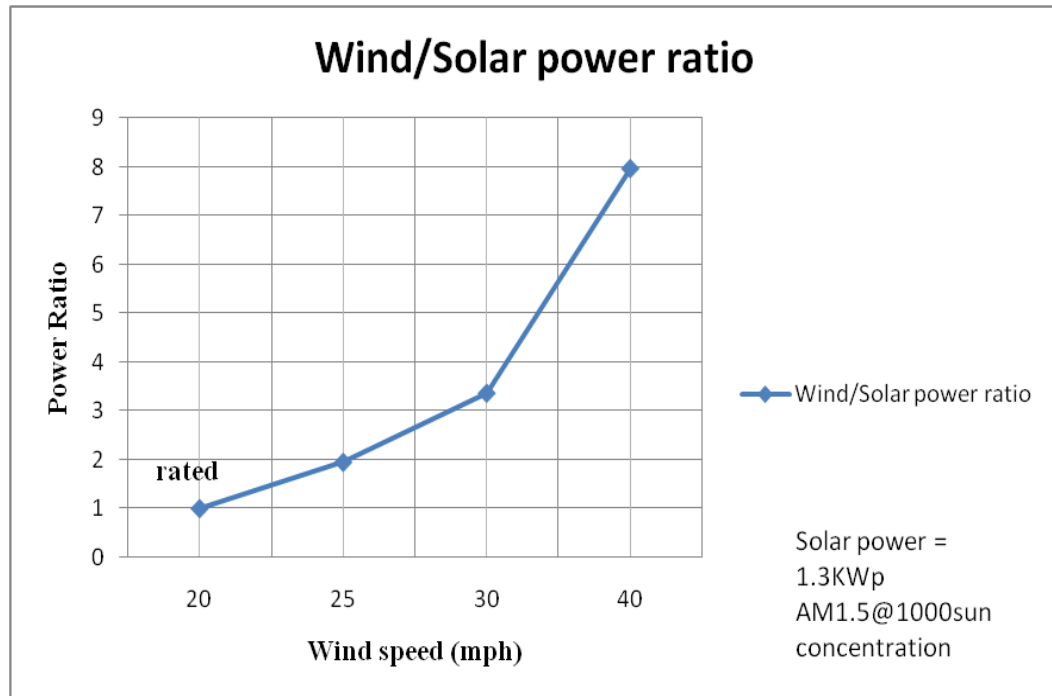
To validate the system to be used as a wind energy harnessing device, we simulated airflow through the system using CFdesign software. We investigated the system to be used as both a wind concentrator turbine or as a diffuser wind turbine system. In either mode wind accelerations of about 1.5 times the inlet air velocity were achieved. Although two different ways to harness wind energy are presented, it will depend on the final design to select either of these mode to function along with the solar

energy mode. A turbine housed in the tunnel of the system can thus be used to harness wind energy during periods of high wind speeds or when there is no sun.

- Economic analysis

A simple levelized cost of energy calculation for the power generated from this system was presented. With few assumptions for the cost of the system it was found that the levelized cost of energy for such a proposed system was about \$0.51/KWhr. Although the cost is significantly higher than the current utility supplied energy, the system is cost-competitive feasible for a standalone system in a remote location or a grid isolated site.

Thus, the techno-economic feasibility of the new type of solar wind hybrid energy generation system was successfully validated. A 1.3 KW system is realized in this work which operates at the peak rating of 1000 sun concentration at AM1.5 in solar energy mode and at a rated wind speed of 20 mph in the wind energy mode. The turbine used in the work is 1.95m in diameter. A similar sized turbine with higher wind speed rating, the peak power generated follows a cubic relation. The figure below shows the wind to solar peak power ratio.



The results reported in here are from simulations of the individual components of the system. The prototype design for such a system has not been developed but there is a need to build a working model of such a system and verify the findings from this work.

CHAPTER VIII

FUTURE RESEARCH

The proposed system is feasible based on the results of the simulations. We also presented the option of system variant that functions as a solar-thermal system. However to achieve this one needs to perform optics simulations for the CLFR based system. The individual vanes for such a system have to be rotated independently to concentrate at a line focus. The vanes in such a system would be flat mirrors.

The cooling system studied in this work was a simple design. However, there is a need to design custom heat exchange surface based on the VMJ layout on the receiver surface. One could also design custom receivers, which can put to use the heat rejected from the VMJ's. Also an entirely solar thermal system could be modeled by optimizing the receiver design.

For the wind turbine, one needs to further investigate the benefits of the concentrating mode and diffuser mode in order to finalize the operation of the system in wind energy mode. As a feasibility study, both the modes were investigated in our work to a limited extent. With higher computation powers available, one can also investigate the rpm's achieved by an optimally designed turbine. The diffuser augmented wind turbine is a relatively new way of looking at small wind turbines. One can use this type of turbine with the system. To use in the concentrator mode the study does validate the concentrating effect of the wind, but more study of the system with an optimally designed turbine for such a setup needs to be done. One can use the multistage turbine shown in section 3.3 too. But the literature available on such a turbine is currently limited.

The economic calculations show us that the cost of energy is competitive for a standalone system. To use the system in utility scale generation a more detailed analysis including the discounts and subsidies available for the site needs to be taken into consideration.

A working model based on the refined design presented in this work would be the first step towards commercializing this technology. An algorithm to switch between wind and solar energy mode needs to be developed. The vane rotation mechanism is a key to the success for the system. The design of such a mechanism is the next priority item.

REFERENCES

1. <http://www.eia.doe.gov/>
2. <http://www.doe.gov/energysources/solar.htm>
3. <http://www.awea.org>
4. <http://rredc.nrel.gov/wind/pubs/atlas/maps/chap2/2-01m.html>
5. Dalal v.L., Moore A.R., “Design considerations for high-intensity solar cells”, *Journal of Applied Physics*, Vol 48, No 3, (1977), 1244-1261.
6. Sater B. L., Sater N. D., “ High voltage silicon VMJ solar cells for up to 1000suns intensities” *IEEE proceedings*, 2002.
7. Illumination module user’s guide, LightTools 5.40, Optical Research Associates, 2007.
8. CFdesign user guide, CFdesign V9, CFdesign, Charlottesville, Virginia, 2006.
9. Cassedy E. S., “Prospects for Sustainable Energy- A critical assessment”, Cambridge press, MA, 2000.
10. Bet F., Grassmann H., “Upgrading conventional wind turbines”, *Renewable Energy* Vol 28 (2003), 71–78.
11. Bet F., Grassmann H., Ceschia M., Ganis L., “On the physics of partially static turbines”, *Renewable Energy*, Volume 29, (2004) Pages 491-499.
12. H. Grassmann H, F. Bet F., G. Cabras G., Ceschia M., Cobai D., DelPapa C., “A partially static turbine—first experimental results”, *Renewable Energy* 28 (2003) 1779–1785.

13. Hansen, M. O. L., Sorensen N. N., Flay R. G., “Effect of Placing a diffuser around a wind turbine”, *Wind Energy*, Vol 3, (2000), 207-213.
14. Matsushima T., Takagi S., Muroyama S., “Characteristics of a highly efficient propeller type small wind turbine with a diffuser”, *Renewable Energy* 31 (2006) 1343–1354.
15. Abe K., Nishida M., Sakurai A., Ohya Y., Kihara H., Wada E., Sato K., “Experimental and numerical investigations of flow fields behind a small wind turbine with a flanged diffuser”, *Journal of Wind Engg. And Industrial Aerodynamics*, Vol 93, (2005), 951-970.
16. Bussel G. J.W., “The science of making more torque from wind: Diffuser experiments and theory revisited”, *Journal of Physics: Conference Series*, Vol 75 (2007)
17. Ghosh D.N, Ghosh S.D., <http://www.multistageturbine.com/index.html>
18. Wood D., US Patent 6485152 B2. “Matrix Solar Dish.”
19. Mills D R and Morrison G L (2000), “Compact Linear Fresnel Reflector solar thermal power plants”, *Solar Energy*, vol. 68 (3), 3 March 2000, pp. 263-283.
20. Pitz-Paal R, “Solar Energy Conversion and Photoenergy systems - High Temperature Solar Concentrators”, UNESCO-EOLSS.
21. Timans P.J., “Emmissivity of silicon at elevated temperatures”, *Journal of Applied Physics*, Vol 74, No 15, (1993), 6353-6364.

22. Kalogirou S.A., “Solar Thermal Collectors and Applications”, Progress in Energy and Consumption Science, Vol 30, (2004), 231-295.
23. Lienhard J V, Lienhard J. IV., “A heat transfer textbook”, 3rd edition, Cambridge press, MA, 2006.
24. Roth I. F., Ambs L.L., “Incorporating externalities into a full cost approach to electric power generation life-cycle costing”, Energy, (2004), 2125-2144.
25. Torchynska T.V., Polupan G.P., “III-V material solar cells for space applications”, Semiconductor Physics, Quantum Electronics & Optoelectronics, Vol 5, (2002), 63-70.
26. Dalal v.L., Moore A.R., “Design considerations for high-intensity solar cells”, Journal of Applied Physics, Vol 48, No 3, (1977), 1244-1261.

APPENDICES

A. Solar Concentrator at Cleveland State University (CSU)

A low cost solar concentrator was built based on the design of Doug Wood. The solar concentrator makes use of low cost materials to form a parabolic concentrator. It uses aluminum tubes to form a parabolic matrix dish. Flat mirrors are then laid atop this matrix to form the concentrator. The raw materials for the dish were shipped to CSU. A group of graduate and undergraduate students built the necessary parts to assemble the dish together. Custom parts designed and prepared by the students included a wheel mounted base for the structure, the pins to put together the dish and the receiver design. A tracking system for the dish was also designed. Figure below shows the dish at CSU. Figure also shows a simple test to observe the concentration achieved was performed on a winter day in March'08 late in the afternoon. Even with low solar irradiation during the testing period a cardboard package tube caught fire within few seconds. The dish presents a testing bed available for future generation receiver designs. The optical concentration expected from the dish is about 1000 suns. The dish can be used to try newer energy harnessing devices based on concentrator technology.



Concentrator dish at CSU

B. One dish per Village (ODPV)

This business model based on the technology presented in this work can be realized for the poor and underdeveloped regions of the globe. It is inspired by the One Laptop per Child (OLPC) approach put forth to fuel computer literacy and learning. The system generates enough capacity to power small rural communities where there is a low demand of energy and providing electricity improves the quality of life. The system also provides the option to increase the supply by replicating such systems. If carried out with the help of local and federal governments of the country such a model could provide growth to the poor population and also help avoid migration to big cities which is a growing concern of any developing country. Figure below is a pictorial representation of the system.



ODPV model concept

C CFdesign Code Validation

Here we present a code validation example to test the CFdesign software. This is necessary to evaluate the accuracy of the software in the simulation analysis. The example here is from Fluid Mechanics textbook, White F.M. (1986). The example measures the pressure drop in a pipe flow. We calculate for the pressure drop at 50m from the upstream from the outlet of a 100m, 1m radius pipe, carrying a fluid with density (ρ) 0.5 kg/m³ and viscosity (μ) of 0.1 Pa-s.

Figure of the model.

The analytical expression for the pressure drop ΔP from White is:

$$\Delta P = \frac{f * 8 * L_{\Delta P} * (\dot{m})^2}{\rho * \pi^2 * d^5}$$

Where,

f is the Darcy friction factor, \dot{m} is the mass flow, $L_{\Delta P}$ is the pipe length across which ΔP is measured. The Darcy friction factor can be computed from the expression:

$$f = 0.316 Re_d^{-1/4}$$

Substituting $L_{\Delta P} = 50\text{m}$, $\dot{m} = 2356.2 \text{ kg/s}$ and (Reynolds no) $Re_d = 15000$, into the expression above the following results are computed. For the CFdesign simulation the intelligent solution control mode was set ON, and the solution auto converged after 434 iterations.

Analytical Solution: 4.02E5 Pa

CFdesign Solution: 4.23E5

% error: 4.9%